

Contents

A1. Factual information	3
A1.16 Tests and research results	3
A1.16.1 Simulation of the flight path and possible options	3
A1.16.2 Metallurgical background information	5
A1.16.2.1 General	5
A1.16.2.2 Properties of Duralumin.....	5
A1.16.2.3 Applied examination methods	5
A1.16.3 Metallurgical examinations.....	5
A1.16.3.1 Fuselage	5
A1.16.3.2 Wing.....	6
A1.16.3.2.1 General.....	6
A1.16.3.2.2 Wing spars	8
A1.16.3.2.3 Joints and rivets.....	17
A1.16.3.2.4 Panelling.....	24
A1.16.3.3 Engine mount.....	25
A1.16.3.3.1 Material analysis.....	25
A1.16.3.3.2 Fracture analysis	25
A1.16.3.3.3 Surface analysis	28
A1.16.3.4 Engine components	31
A1.16.3.4.1 Cylinders	31
A1.16.3.4.2 Propeller bearings	34
A1.16.3.4.3 Supercharger bearings	37
A1.16.4 Corrosion analysis	41
A1.16.4.1 General.....	41
A1.16.4.2 Manufacturer's instructions regarding corrosion protection.....	43
A1.16.4.3 Fuselage	44
A1.16.4.4 Wing.....	46
A1.16.4.5 Engine components	50
A1.16.4.5.1 Cylinder bores	50
A1.16.4.5.2 Propeller bearings	51
A1.16.4.5.3 Supercharger bearings	52
A1.16.5 Forensic examinations.....	57
A1.16.5.1 Instruments	57
A1.16.5.1.1 Tachometers	57
A1.16.5.1.2 Speed indicators.....	57
A1.16.5.1.3 Further examination of instruments.....	58
A1.16.5.2 Warning lights	59
A1.16.5.3 Fuel valve battery.....	59

A1.16.5.4	Engine control elements.....	59
A1.16.5.4.1	Full-throttle limiting mechanism	59
A1.16.5.4.2	Summary	61
A1.16.5.5	Carburetors	61
A1.16.5.5.1	Butterfly valves	62
A1.16.5.5.2	Carburettor accelerator pumps	62
A1.16.5.5.3	Accelerator-pump cylinder	63
A1.16.5.5.4	Accelerator-pump piston.....	65
A1.16.5.5.5	Evaluation.....	66
A1.16.6	Summarised evaluation	67
A1.16.6.1	Material properties	67
A1.16.6.1.1	General.....	67
A1.16.6.1.2	Properties of Duralumin and corrosion protection	67
A1.16.6.2	Aircraft structure.....	67
A1.16.6.3	Engines.....	68

A1. Factual information

A1.16 Tests and research results

A1.16.1 Simulation of the flight path and possible options

Using a simulation, it was investigated as to whether it would have been possible for the flight crew to manoeuvre the aircraft safely out of the valley shortly before the accident. The photogrammetrically determined point F13 was taken as the key point for the simulation and as the last position on the reconstructed flight path of HB-HOT. Before this point, the flight crew initiated a right turn and then steered the aircraft into a left turn to navigate it over the ridge of the Segnes pass. After point F13, roll to the left increased steadily and did not decrease even when there was significant aileron deflection to the right.

The aim of the simulation was not only to examine the flight path options from this key point onwards, but also to approximate the flight path and flight attitude of HB - HOT as closely to the reconstructed conditions before point F13 as possible, in order to verify the assumptions for the simulation (see figure 1).

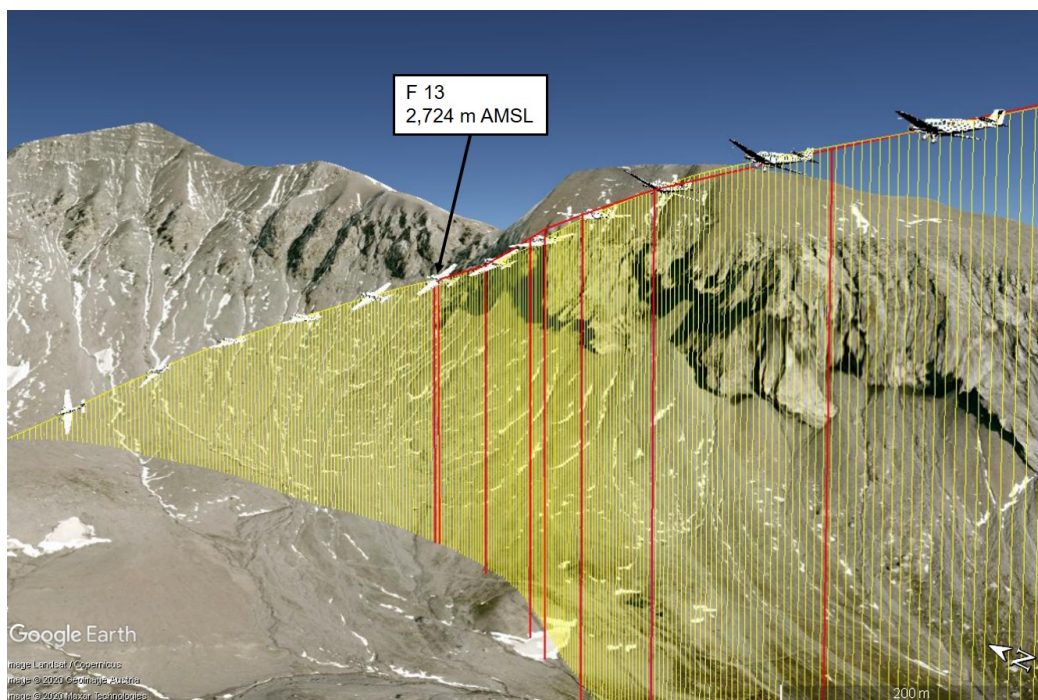


Figure 1: Simulated flight path (yellow) and reconstructed flight path of HB-HOT (red) from 4 August 2018 leading up to the photogrammetrically determined position F13; shown on Google Earth. The enlarged (2:1) three-dimensional models are shown on the basis of simulation results at position F13 and at two-second intervals before and after that point.

The movement of a generic aircraft through a wind field can be approximately simulated using simplified assumptions without having to reproduce all details as required in a full flight simulator. As the flight characteristics of the Ju 52/3m g4e, registered as HB-HOT, are not known in full detail, approximations had to be made. These are primarily based upon the aircraft flight manual and basic physical aerodynamic principles. The most important results are not directly dependent on exact knowledge of, for example, the lift over drag polar curve, but only on correctly selected ratios and the corresponding engine power. These assumptions could be corroborated and adjusted using the precisely known flight path and flight attitude from approximately two minutes before the accident, and idealised flights.

After the above-mentioned aircraft parameters had been determined as best as possible through iteration, it was possible to adjust the wind field based on the assumptions from the meteorological COSMO model (see annex [A1.7](#)), which is to be understood as follows. When the simulated path and speed in a flight phase correspond to the photogrammetrically reconstructed points, but the angle of pitch attitude is too small compared to this reconstruction, the pitch can be adjusted by increasing the downdraught. The same applies to crosswind and its effect on the aircraft's heading. This resulted in a refined wind field with similar characteristics to the wind field from the PALM meteorological flow model (see annex [A1.7](#)): a decrease of headwind and downdraughts towards the north. This refinement is not significant, meaning the analysis is not based on it. Nevertheless, it illustrates that flight path simulation can correctly take into account details in the wind field.

It should be noted that the investigation did not examine the aircraft's behaviour in stall, as this would not have been acceptable using these simplified assumptions and due to missing information. The simulations carried out permitted, however, to provide an answer to the question as to whether, under optimal conditions, the aircraft's envelope would have still allowed for a flight over the pass or for the aircraft to turn around after passing point F13.

Findings from the simulations:

- After several iterations, the simulated flight path and attitudes up to the arrival at F13 corresponded to a large extent with the photogrammetric reconstruction. A conscious decision was subsequently made not to continue this iterative process as the residual uncertainty that would remain as a matter of principle was not relevant for the conclusion.
- The selected wind field adjustments are within the determined possibilities (see annex [A1.7](#)). They even confirm the tendency that headwinds and crosswinds abated in the north-eastern part of the basin.
- For the aircraft to exceed its maximum angle of attack and lose altitude with at least a partial loss of lift before F13 – despite an indicated airspeed (IAS) that is significantly above stall speed – can be conclusively explained by an updraught.
- Based on realistic assumptions, none of the simulation variants showed a course of flight after F13 that would have allowed the aircraft to safely continue over the pass or turn around.
- However, had the area of downdraught continued to exist, a flight over the pass would still have been possible, i.e. the simulation confirms the conclusion that it was not the obviously existing area of downdraught that triggered the fatal course, but a quite plausible updraught in the north-eastern part of the basin.

In order to obtain even more accurate simulation results, an identical Ju 52/3m g4e aeroplane would have to undergo an extensive test-flight programme, the results of which would enable a full flight simulator to be programmed by a specialised team. However, given that the STSB's simulations take into account all of the important environmental parameters and fundamental aircraft characteristics, it can be surmised that the results produced by a full flight simulator up to the loss of control would not be radically different.

A1.16.2 Metallurgical background information

A1.16.2.1 General

The structure of the Ju 52/3m g4e aircraft, consisting of the wing, fuselage and empennage as well as parts of the controls, is of mixed construction. The components are mainly manufactured of aluminium and steel. The steel components are mainly welded constructions fabricated in sheet metal. Most of the structure is made of the high-strength aluminium alloy Duralumin. The components are riveted together, using both Duralumin and steel rivets. The sheets for the panelling and profiles are plated on both sides using thin, more corrosion-resistant aluminium alloy¹. When the aircraft was made, the corrosion-prone components were given a protective coating.

A1.16.2.2 Properties of Duralumin

Duralumin (also known as Dural) is an alloy of aluminium (Al) with copper (Cu) and magnesium (Mg) that was developed at the beginning of the 20th century. This alloy is high in strength and features good plastic elongation values, and – at the time – was used mainly in the construction of aircraft. Its favourable mechanical properties are achieved by solution heat treatment and subsequent natural ageing². The corrosion resistance properties of Duralumin are generally limited.

Prolonged exposure to temperatures above 80 °C can make Duralumin more prone to corrosion, whilst thermal stress above 120 °C drastically increases the material's susceptibility to corrosion; this is referred to as a thermal ageing process.

A1.16.2.3 Applied examination methods

The chemical composition of the investigated parts was determined by optical emission spectroscopy (OES), energy-dispersive X-ray spectroscopy (EDX) and other methods.

The material condition was determined by metallographic microsection analysis. This allows conclusions to be drawn about material properties and the manufacturing process.

Fracture surfaces and cracks were examined using microfractographic analysis under a scanning electron microscope (SEM). Based on the fracture characteristics, the cause of the crack or fracture can be determined.

The mechanical material properties were determined using hardness measurements according to the Brinell or Vickers methods. These test methods do not provide information about the elastic and plastic properties of the material. To determine further mechanical material properties, complex tests such as the static tensile test and impact test, as well as fatigue tests would have to be carried out.

A1.16.3 Metallurgical examinations

A1.16.3.1 Fuselage

Parts of the cabin floor, stringer sections and structural parts from the aft section of the fuselage were examined. According to the OES analysis, the majority of the examined parts consist of an AlCuMg alloy and correspond chemically and materially to the aircraft manufacturer's specification. Individual parts are made of steel and were riveted to parts made of Duralumin. Sheets were found with plating on both sides (see figure 2).

¹ Plating is the process of applying a thin layer of a metal with different properties to a base metal, usually by rolling. In this case, a thin layer of a more corrosion-resistant aluminium alloy was rolled onto the AlCuMg sheet.

² Ageing (natural/artificial): A thermal process used to improve the mechanical properties of a material.

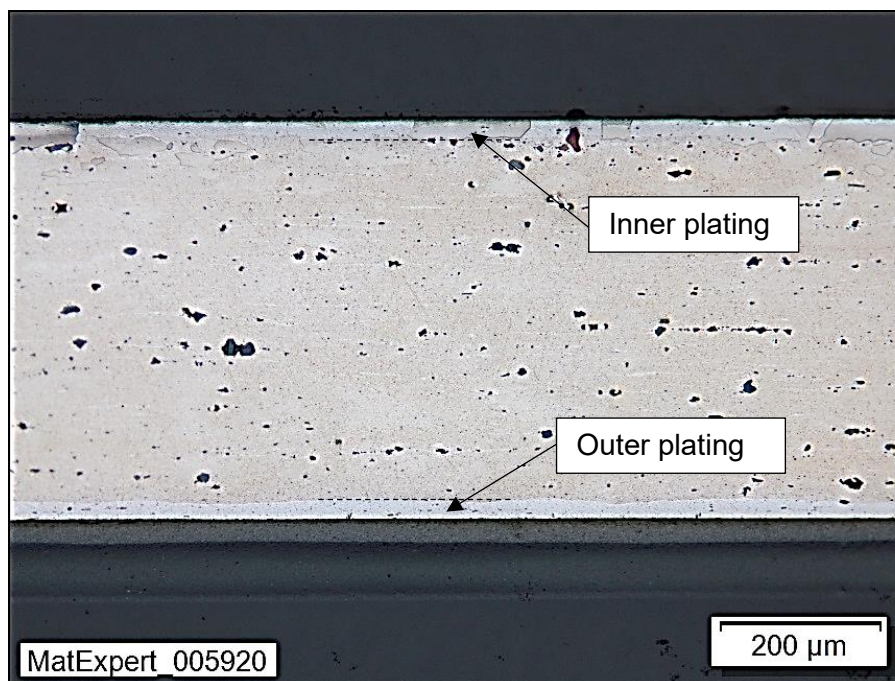


Figure 2: Microsection of sheet with inner and outer plating.

A1.16.3.2 Wing

A1.16.3.2.1 General

The self-supporting wing consists of the centre wing, which is firmly structurally connected to the fuselage, and the two outer wings.

Following visual inspection, the subsequent parts of the wing were subjected to material tests:

Designation in the report	Manufacturer's position numbers
Lower spar section L1	Spar I, left, with joint 89 (mirror image of joint 32, right)
Lower spar section L2u	Spar II, left
Lower spar section 1Ru	Spar I, right, with joint 32
Upper spar section A	Spar I, right, with joints 15, 16 and 116
Upper spar section B	Spar I, left, with joint 85 (mirror image of joint 15, right)
Lower spar section C	Spar I, bottom right, with joint 31 and the fixing for attaching to the centre wing

The joint numbering is based on the Junkers Ju 52/3m aircraft parts list H (see figure 3).

Joints 15 and 32 of the right-hand outer wing and joints 85 and 89 of the left-hand outer wing are part of ribs I. Joints 16 and 116 are part of rib Ia of the right-hand

outer wing. The left or right engine respectively is mounted between those two ribs (rib I and rib Ia).

The lower spar section C comes from the area where the right-hand outer wing is bolted to the centre wing.

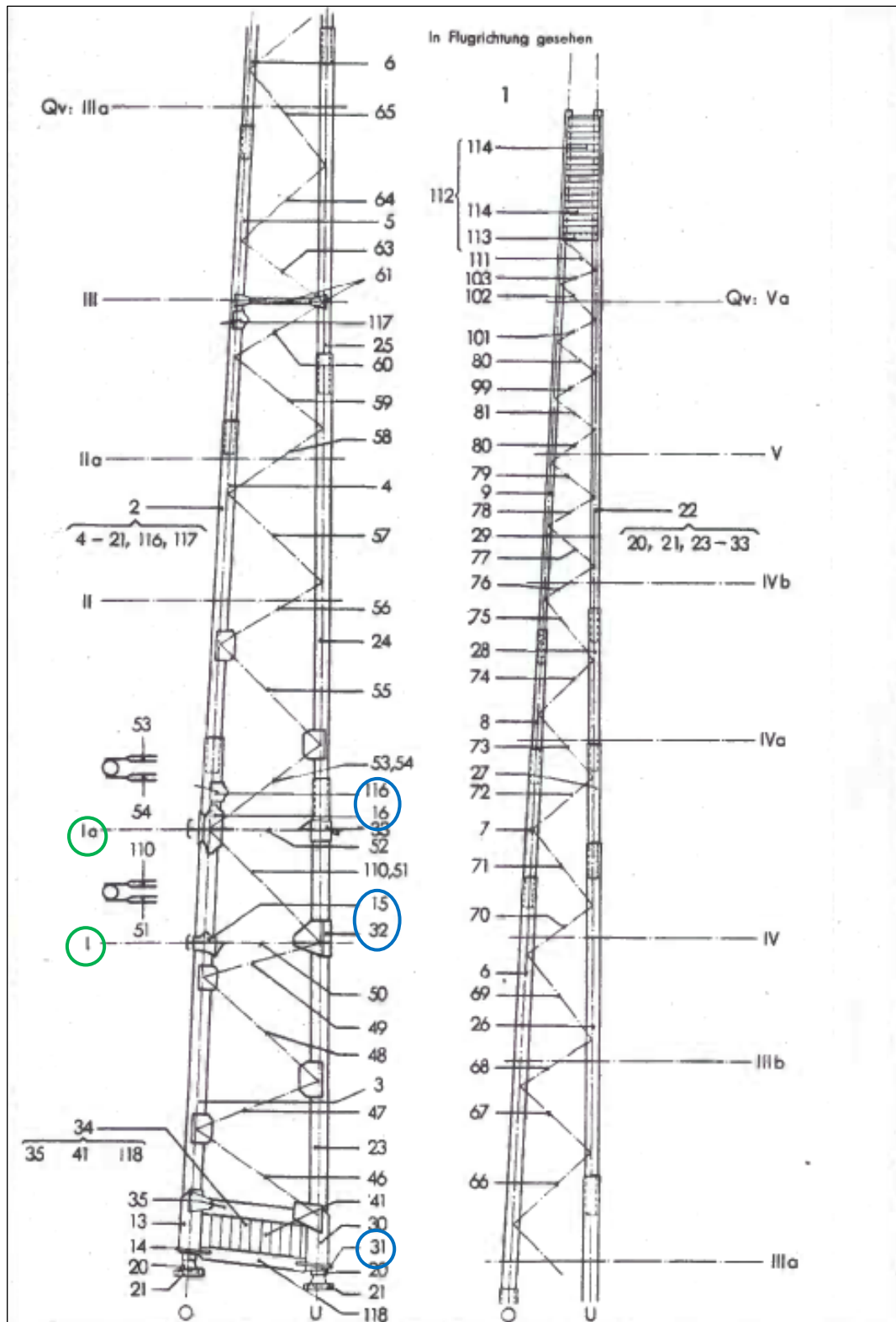


Figure 3: Spar I of the right-hand outer wing – the blue encircled position numbers indicate the examined parts, the green encircled positions I and Ia indicate the ribs. Source: Junkers Ju 52/3m aircraft parts list H.

A1.16.3.2.2 Wing spars

According to the aircraft manufacturer's specifications, the wing's spar tubes are made of the naturally aged wrought aluminium alloy Duralumin Du44 (AlCuMg). When naturally aged, the corrosion resistance of this alloy is very limited due to the presence of the copper used in it. When artificially aged, the alloy is extremely susceptible to corrosion and becomes mechanically brittle.

According to chemical analysis, the material used in the six spar tube sections examined corresponds to Du44.

The hardness of the spar tube sections was measured in microsections according to the Vickers method. The measurements ascertained are usual for the investigated material and correspond to a hardened AlCuMg alloy.

The alloy as it is present in the analysed parts is not in line with the current state of technology.

After removing joint 89 (see figure 4), severe corrosion and cracks were found in the contact area between the joint and the spar tube. This would not have been visible without dismantling the joint or the panelling. After cutting open the spar tube, no damage was visible on the inside (see figure 5). This shows that a borescope inspection cannot detect such damage and is therefore unsuitable (see annex [A1.6](#)).

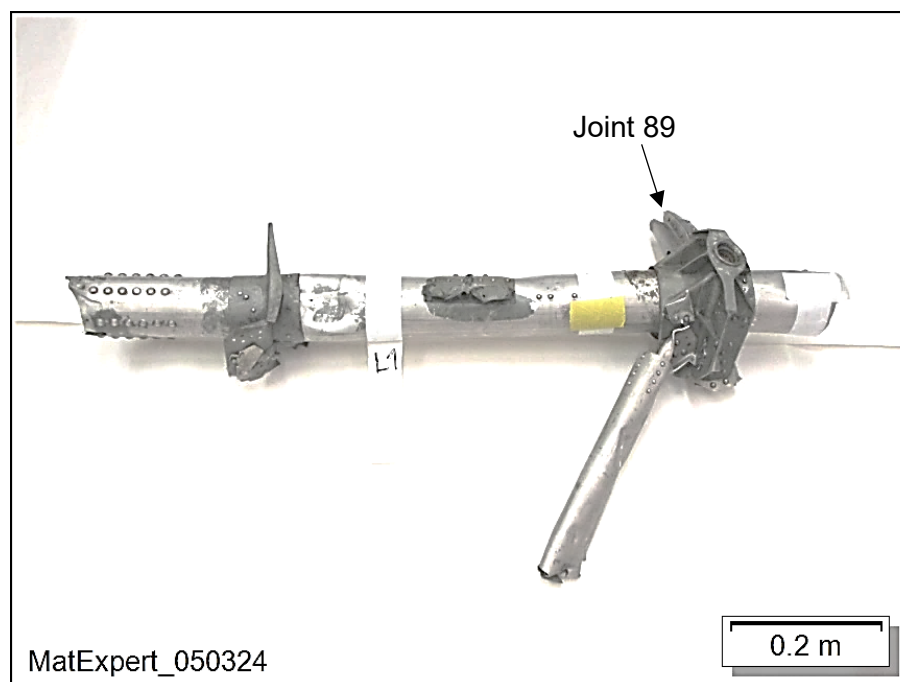


Figure 4: Lower spar section L1 of the left outer wing.

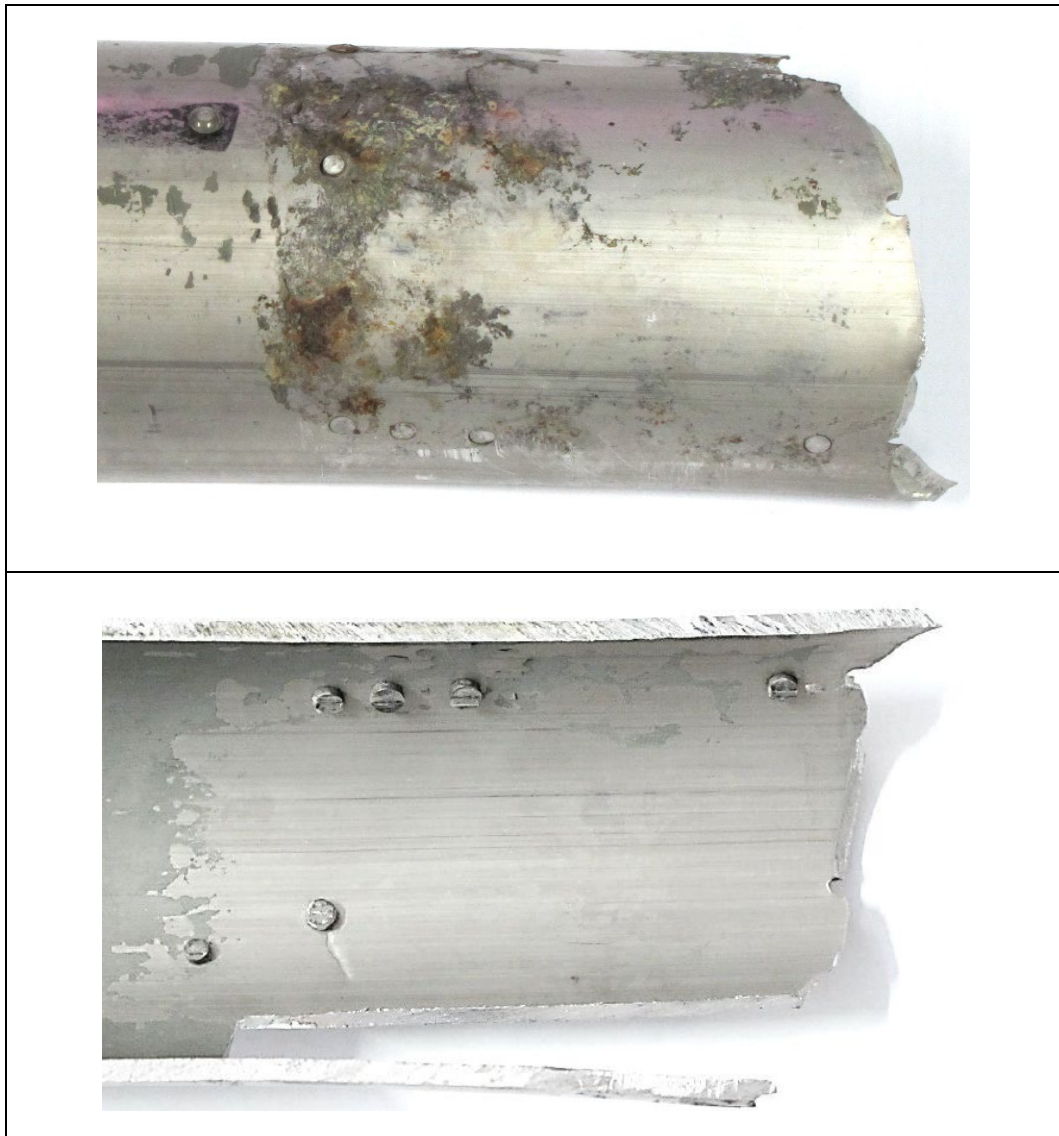


Figure 5: Cut open lower spar section L1 – the outer surface with corrosion and cracks, the inner surface with no signs of corrosion.

Spar section L1 (see figure 4) exhibited grain boundary precipitations (see figure 6). These precipitates were formed either by artificial ageing after solution heat treatment or by a secondary, longer exposure to a temperature of more than 120 °C. This makes the material in question susceptible to intergranular corrosion. Intergranular corrosion can develop along the detected grain boundary precipitates.

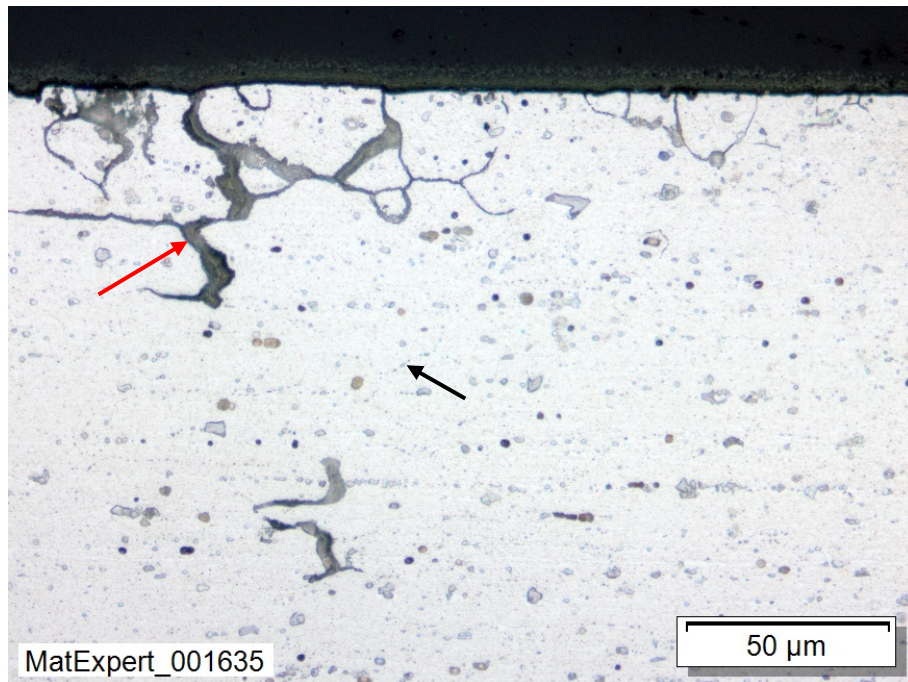


Figure 6: Microsection of spar section L1 – intergranular corrosion attack (red arrow) and grain boundary precipitation (black arrow).

Similar to artificial ageing, thermal stress changes the original microstructure of the naturally aged alloy and has a very negative effect on corrosion resistance.

On further investigation, joint 89 was gently removed from the lower spar section L1, and joints 15 and 16 were removed from the upper spar section A.

The spar tube below joint 89 was broken (see figure 7). The analysis of this fracture surface using SEM showed a ductile spontaneous fracture and a fatigue fracture with typical striations (see figure 8). The fatigue fracture accounted for approximately 10 % of the total fracture surface. Extensive corrosion damage and further cracks were uncovered in the contact area between joint 89 and the spar tube. This corrosion was intergranular corrosion resulting in a loss of wall thickness (see figures 9 and 10). One of the cracks was exposed and fractographically analysed (see figure 11). This crack was an intergranular fracture with striations, i.e. a fatigue crack (see figures 12 and 13).

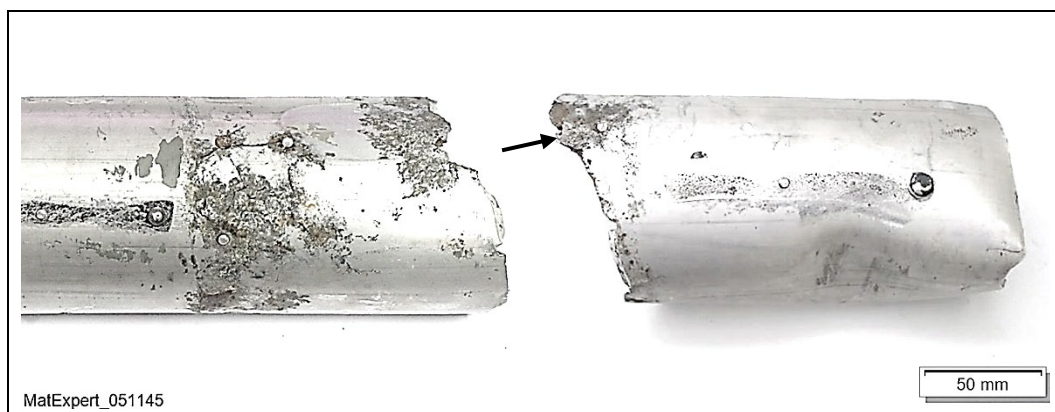


Figure 7: Overview of the broken spar section; approximately 10 % of the fracture surface (arrow) is accounted for by fatigue fracture.

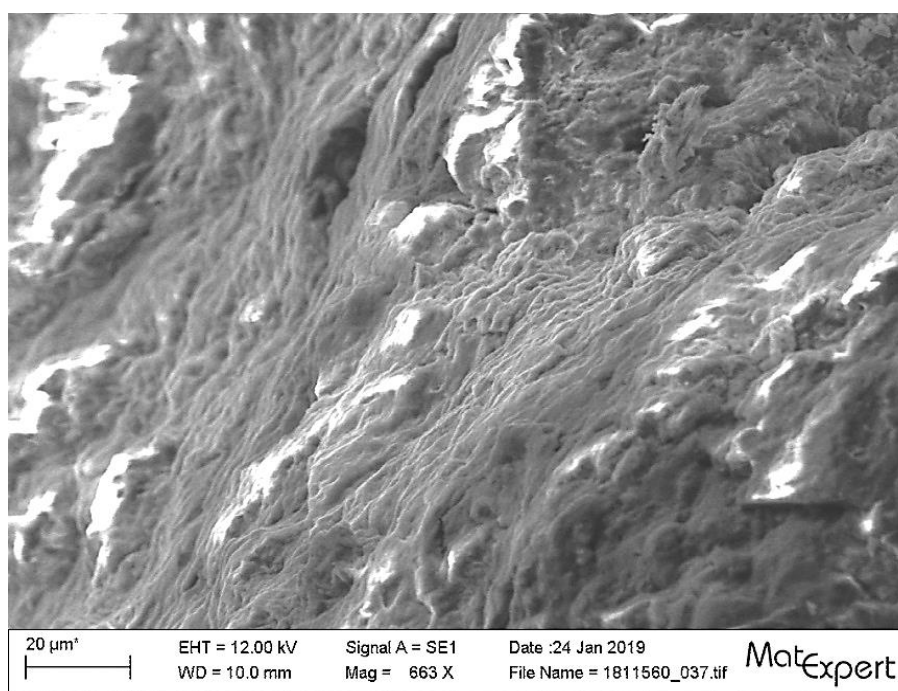


Figure 8: Fatigue fracture with typical striations.

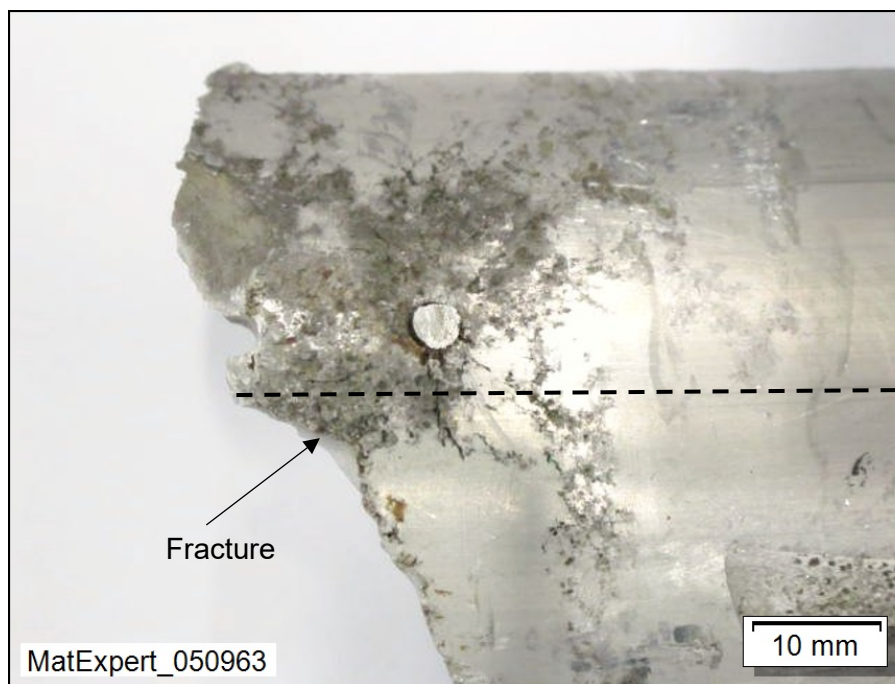


Figure 9: Point of corrosion with broken rivet. The black, dashed line indicates the position of the microsection.

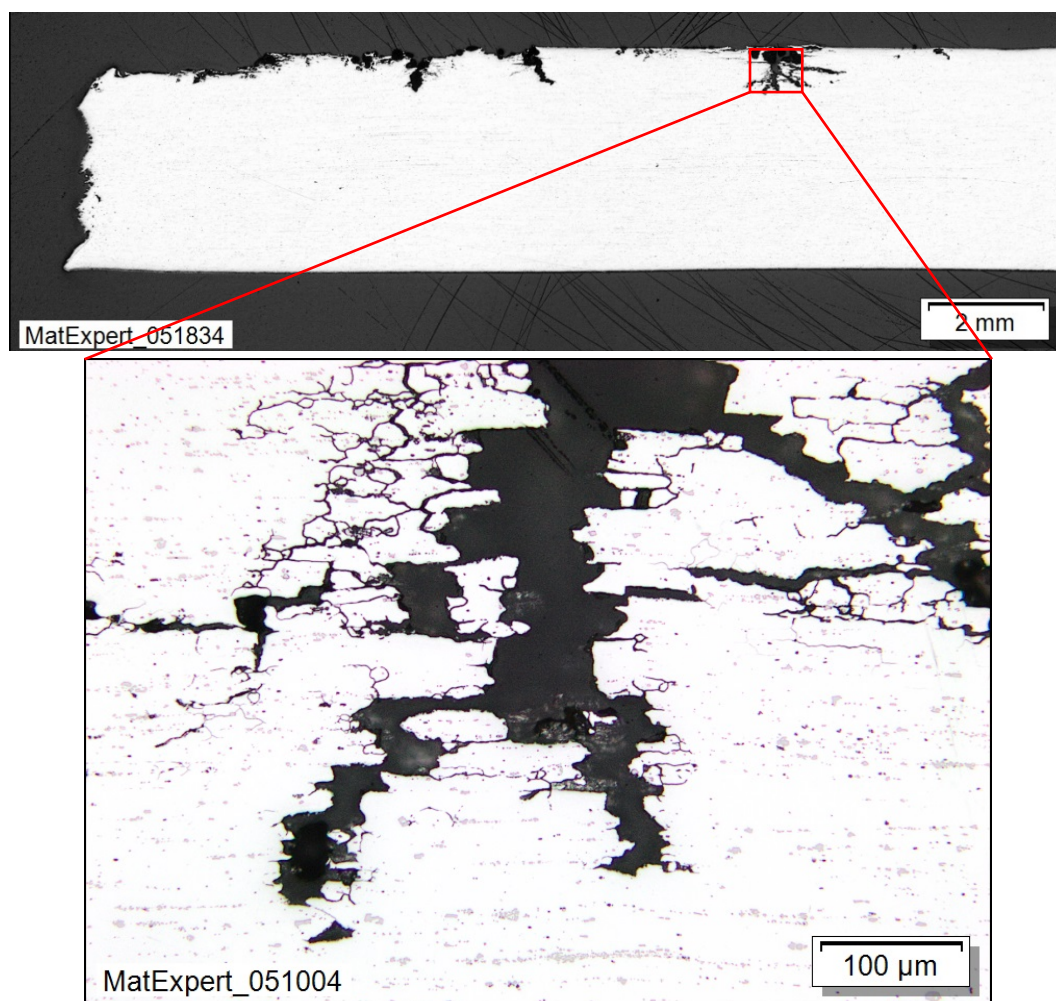


Figure 10: Wall thickness loss due to corrosion and intergranular corrosion.

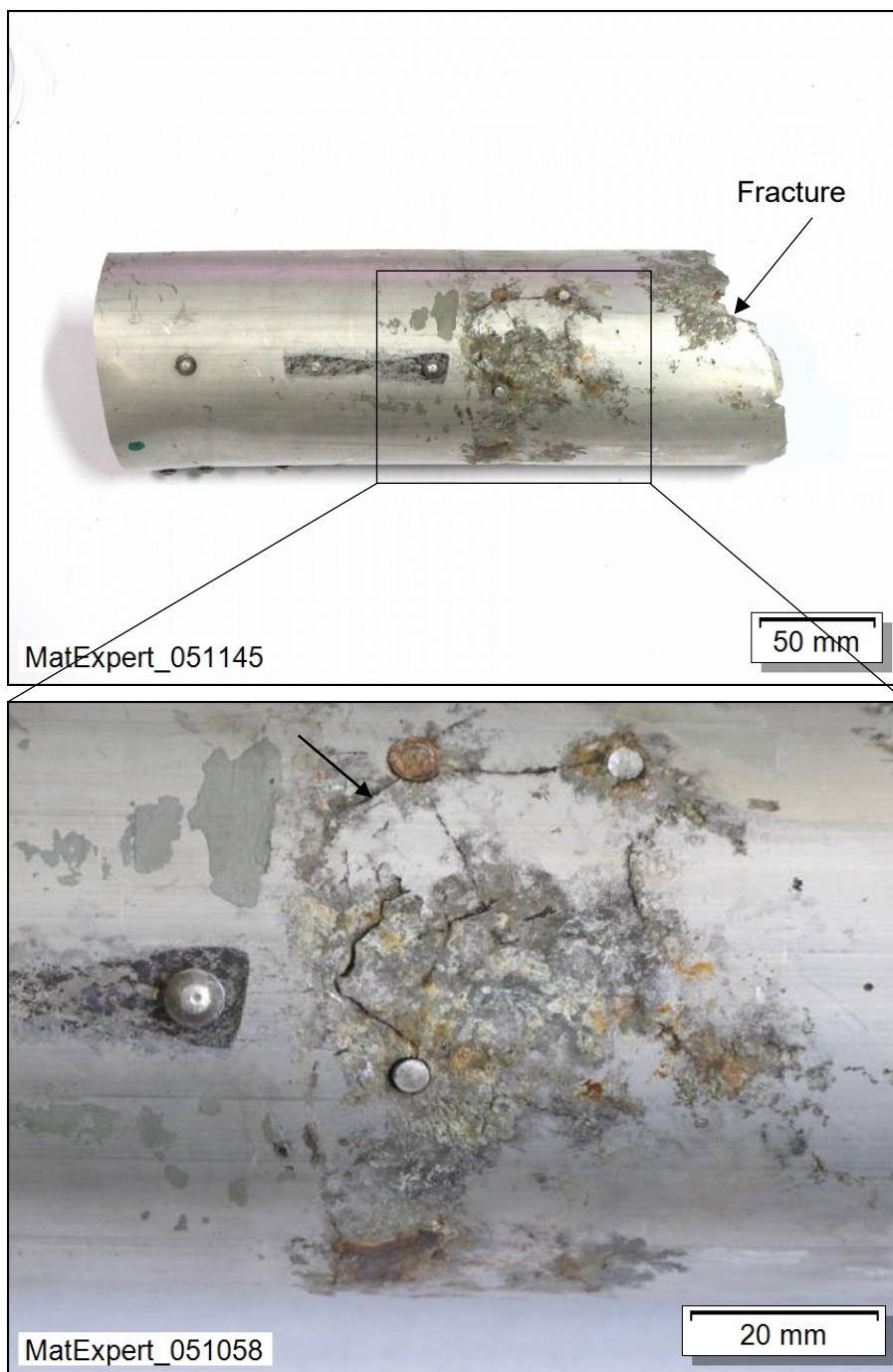


Figure 11: Exposed crack (arrow) under joint 89 on the lower spar section L1.

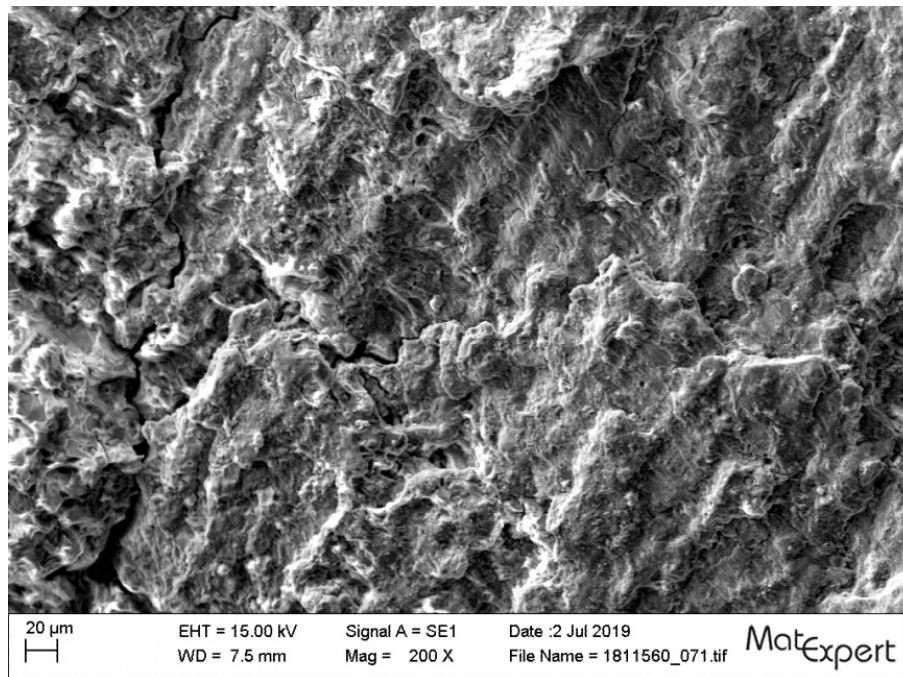


Figure 12: Close-up – crack surface in the exposed crack with fatigue fracture and intergranular cracks.

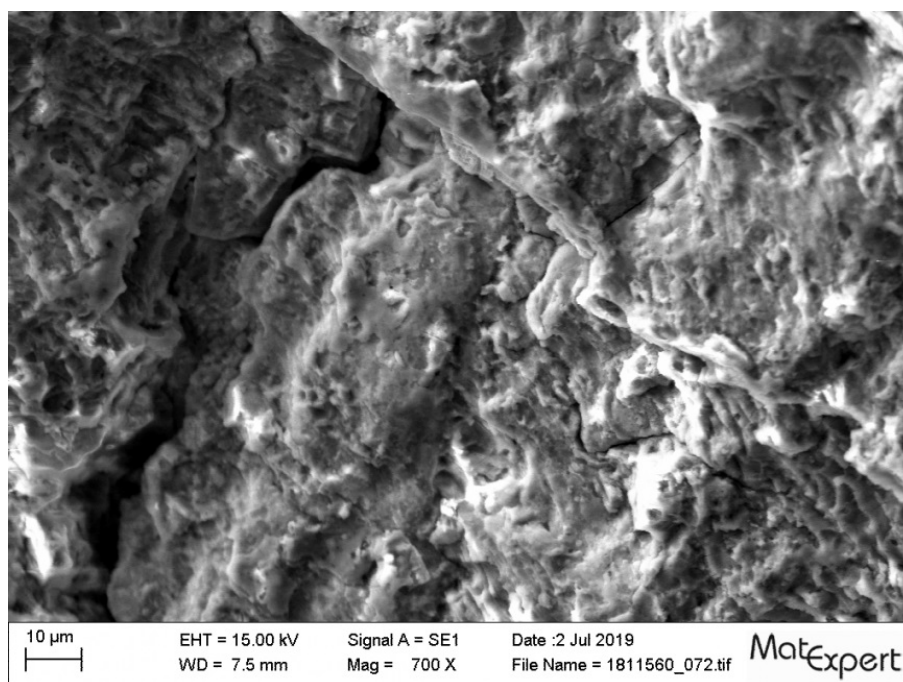


Figure 13: Magnified version of figure 12.

In the area where the panelling was riveted to the spars, damage similar to chafing can be seen (see figure 14). This type of wear attests that the panelling was no longer firmly attached to the spar and that the surface was severely damaged by the panelling's movement and by penetrating liquid (see figure 15). Besides general loss of material, intergranular cracks were also discovered (see figure 16). These cracks were mainly found near the rivet holes, and they can initiate fatigue cracks (see figure 17).

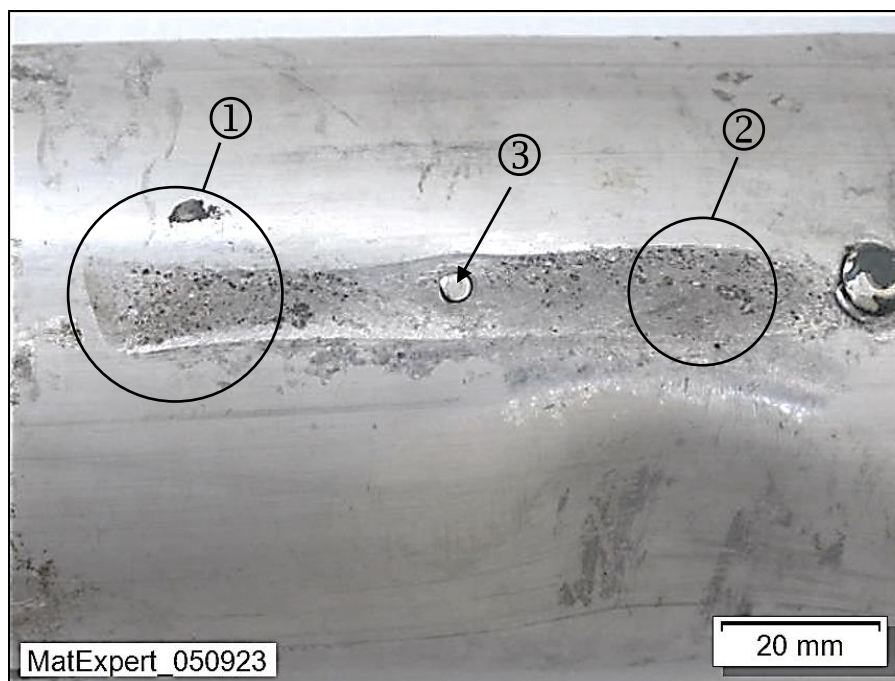


Figure 14: Wear on the lower spar L1 – number (1) see figure 15, number (2) see figure 16, number (3) see figure 17.

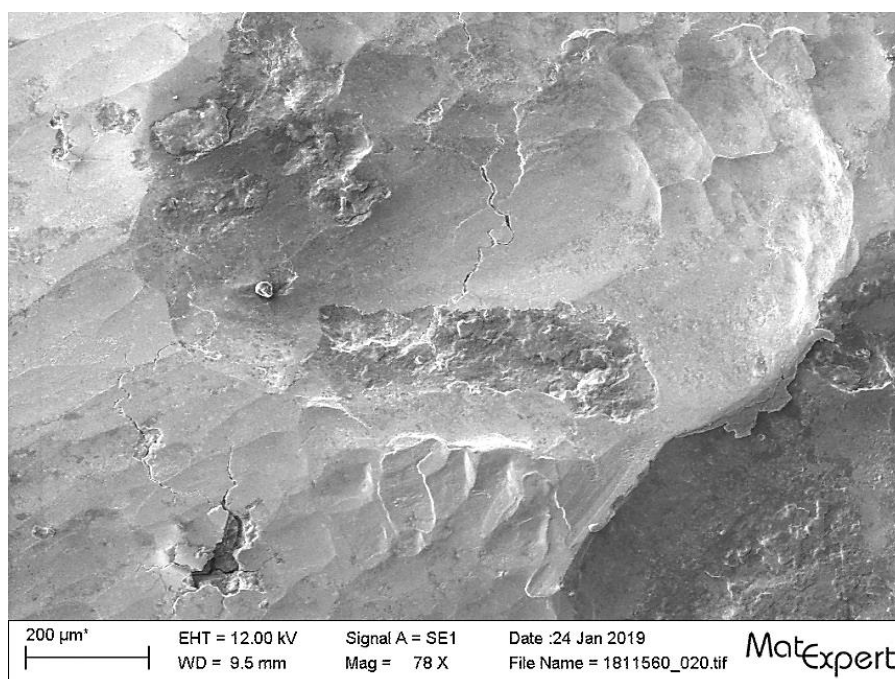


Figure 15: Impact wear on lower spar L1 (close-up of number (1) in figure 14).

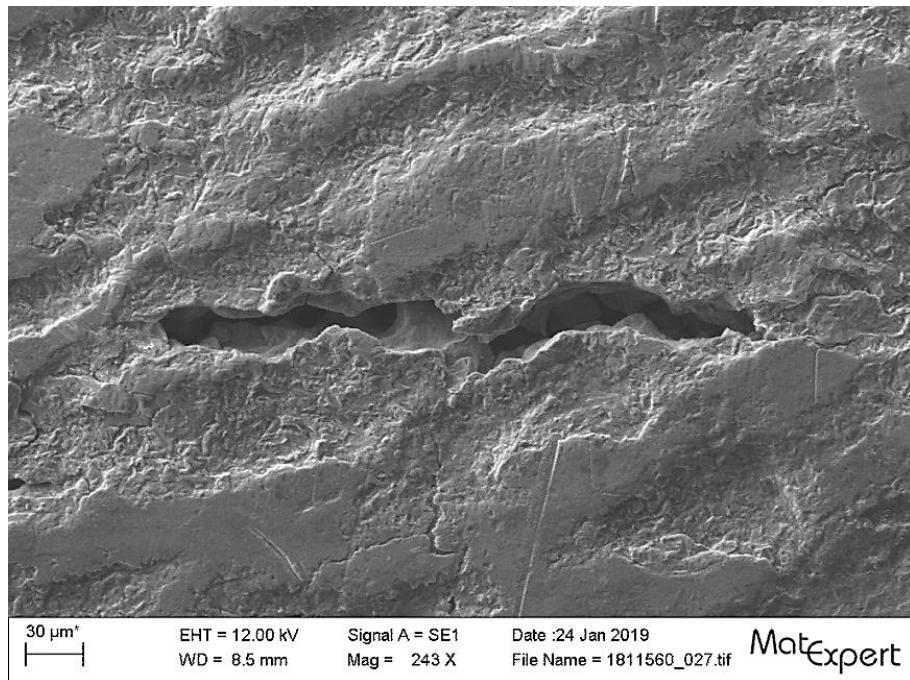


Figure 16: Incipient crack and wear due to erosion and cavitation (close-up of number (2) in figure 14).

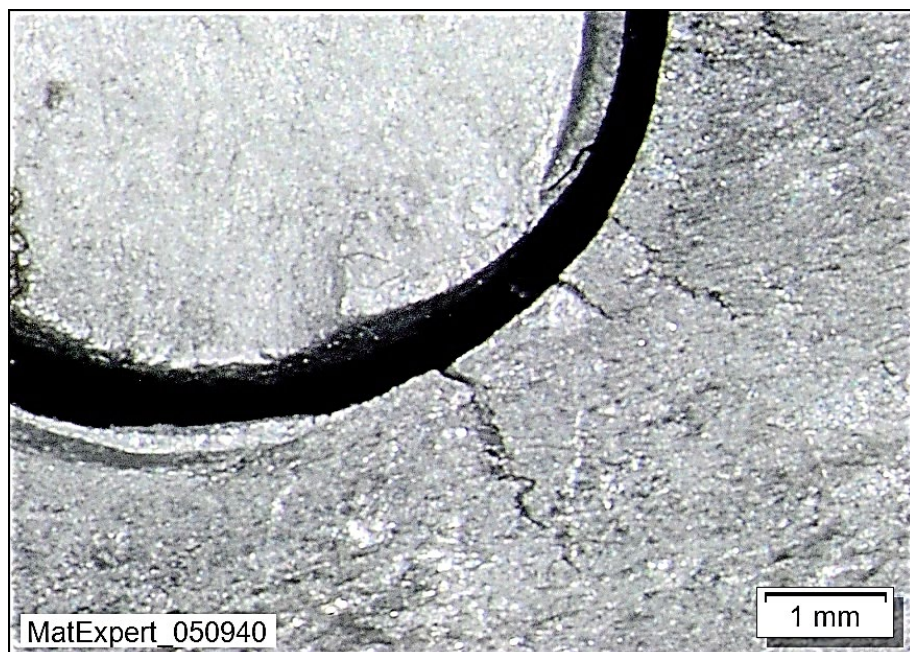


Figure 17: Intergranular incipient cracks at the rivet hole, crack lengths of up to 5 mm (close-up of number (3) in figure 14).

Upper spar section A showed a similar condition as lower spar section L1 at both joints. There are also several intergranular cracks, old rivet fractures and wear caused by the panelling.

The lower spar section 1Ru (see figure 18), cut from spar I near the right engine, exhibits pitting (see figure 19). This is the typical type of corrosion for a naturally aged structure. This type of corrosion also leads, among other things, to a localised loss of wall thickness. Wear caused by the panelling is also present on this spar section.

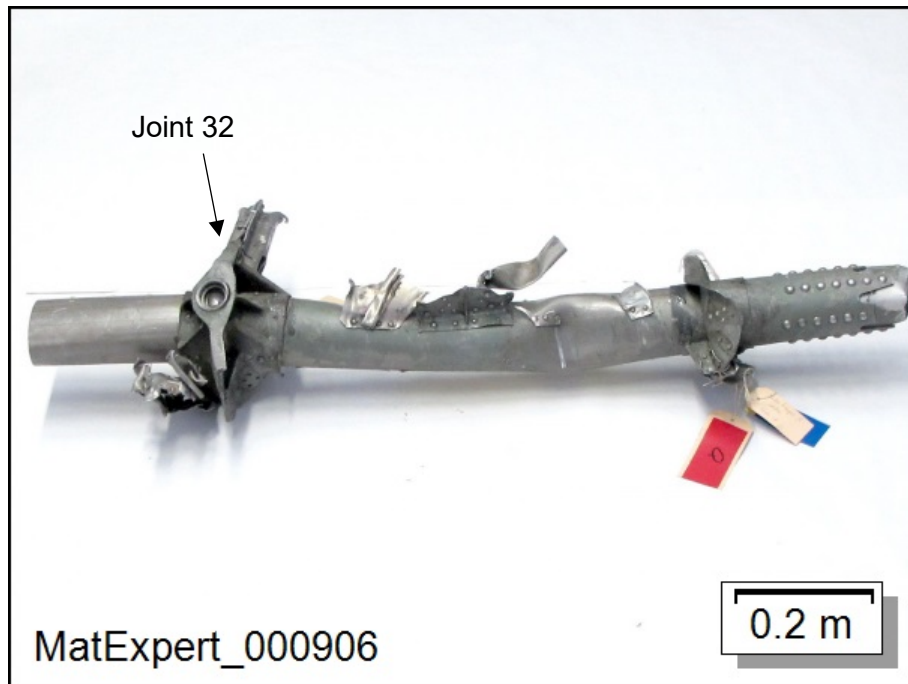


Figure 18: Lower spar section 1Ru.

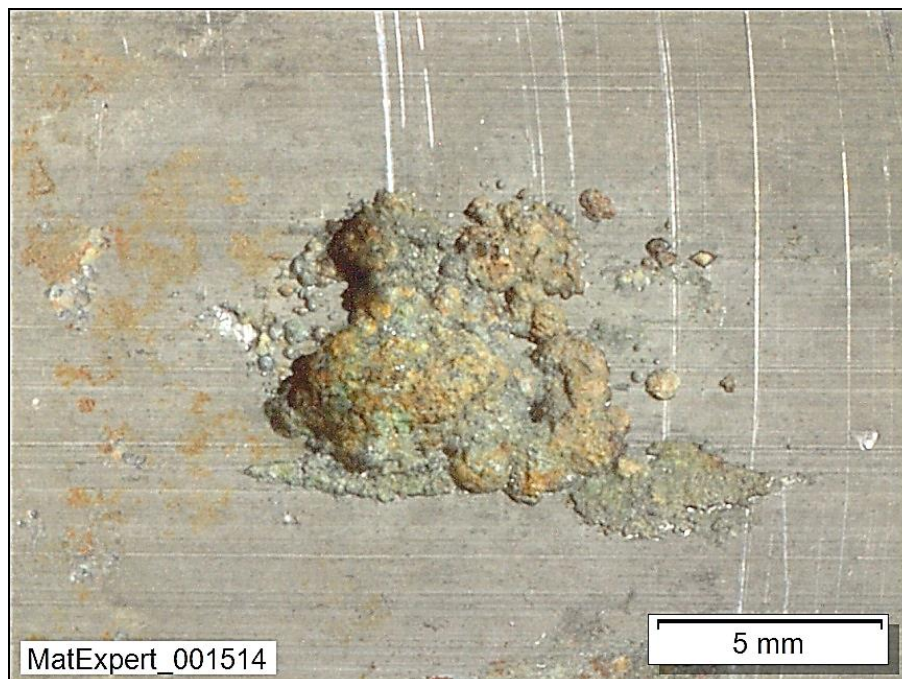


Figure 19: Close-up – pitting on the lower spar section 1Ru.

All of the spar sections analysed and the joints only exhibited remnants of anti-corrosion paint. The corrosion protection was therefore insufficient.

A1.16.3.2.3 Joints and rivets

Joint 89 mounted on the lower spar section L1 was twisted and displaced on the spar tube as a result of the accident. The joint is a welded steel construction. The inner tubing of joint 89, which was in direct contact with the lower spar, was made of a heat-treatable alloy steel. The inner tubing was un-heat-treated.

The inner tubing of the analysed joint exhibited corrosion with surface corrosion around the rivets (see figure 20).

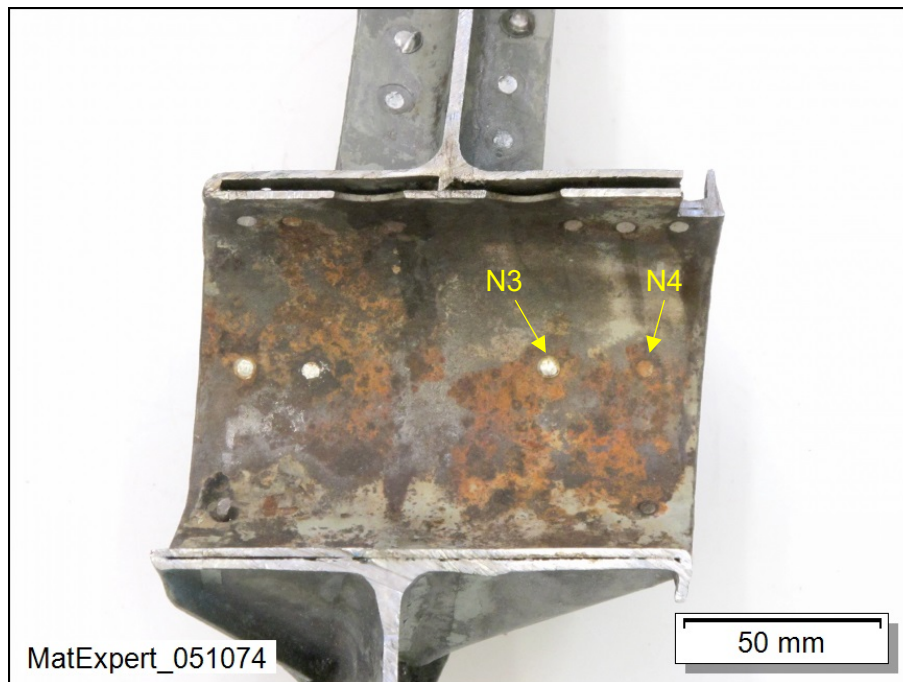


Figure 20: Cut open joint 89 with rivets N3 and N4.

Rivet fractures were discovered which clearly occurred before the accident (see figure 21). They can be easily distinguished from the shear fractures caused by the accident.



Figure 21: Close-up – broken rivet N4 with severe corrosion.

The fracture surfaces and the contact areas between the rivets and the joint and spar tube respectively were analysed. The rivets were examined metallographically as well as macro- and microfractographically.

The rivets consist of a wrought aluminium alloy (AlCuMg), which is very similar to the spar material.

Pitting and surface corrosion can be identified in the contact area between the rivets and both the joint and spar tube (see figure 22).

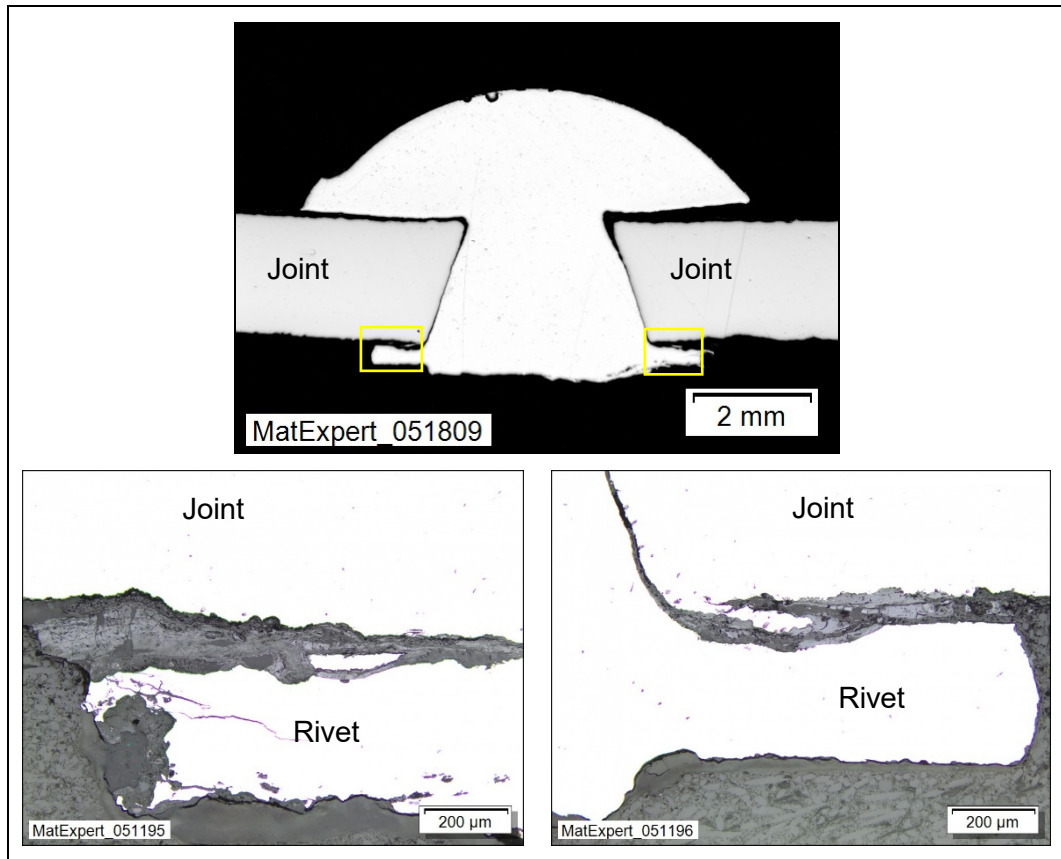


Figure 22: Cross section of rivet N3 – pitting and surface corrosion of sheet steel and aluminium rivets.

Fractures were found in the rivets which clearly occurred before the accident (see figures 23 to 25). Furthermore, intergranular corrosion was discovered (see figure 26). Fatigue and intergranular fractures were also discovered in some rivets. They can be easily distinguished from the shear fractures caused by the collision.

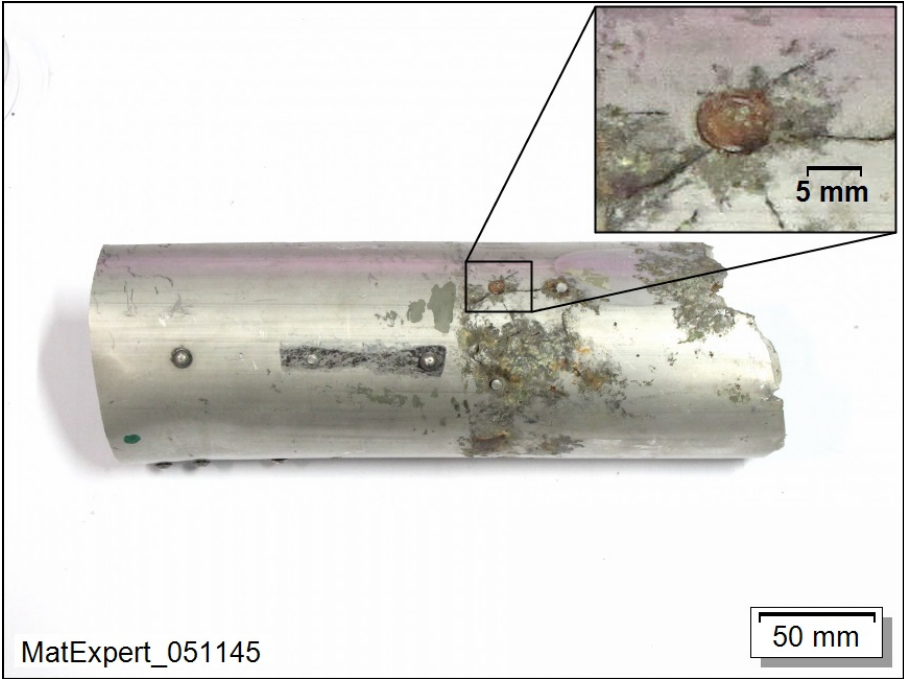


Figure 23: Spar section L1, after removing joint 89, with rivet N5.



Figure 24: Severely corroded rivet N5. The black dashed line indicates the position of the microsection and the arrow indicates the direction the microsection surface was viewed from.

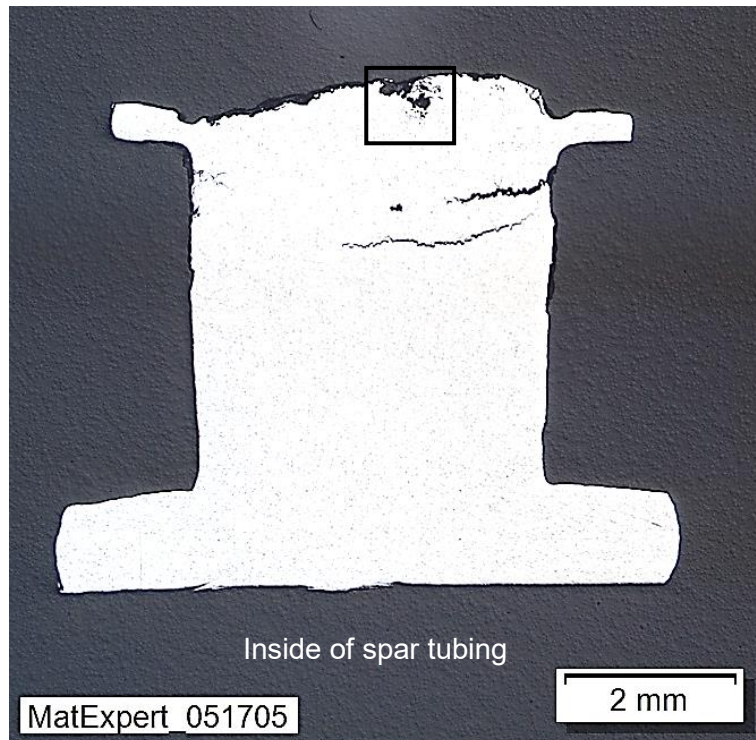


Figure 25: Cross section of broken rivet N5 with intergranular corrosion.

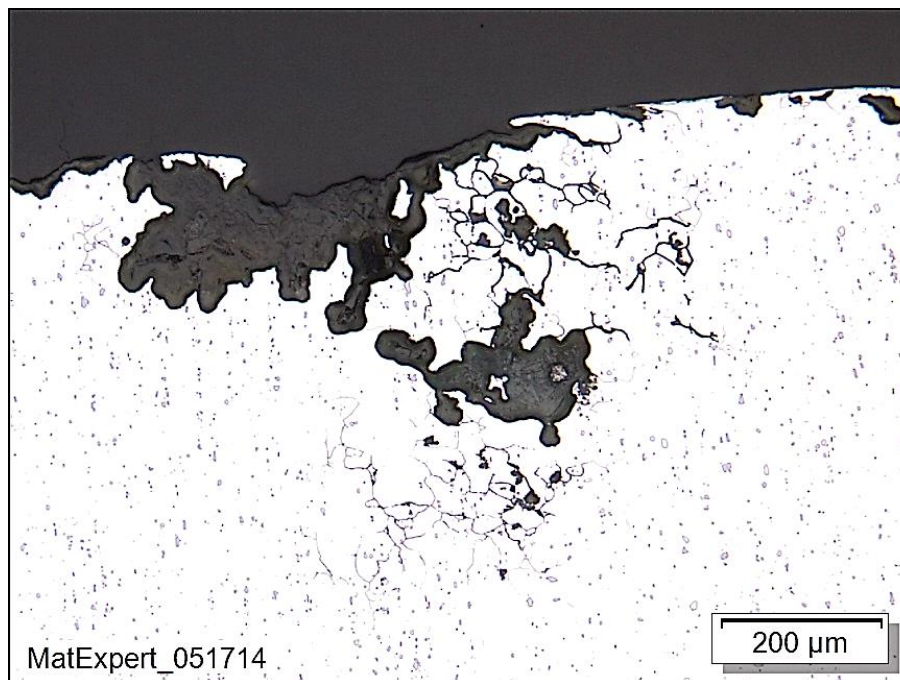


Figure 26: Close-up – intergranular corrosion on rivet N5.

Examination of spar section A (see figure 27) shows a similar condition for the joints as those on spar section L1. In the contact areas between the joints and the spar tube, severe corrosion and cracks, old rivet fractures, impact wear, erosion and cavitation were also found on the surface of the aluminium spar tube (see figures 28 to 32).

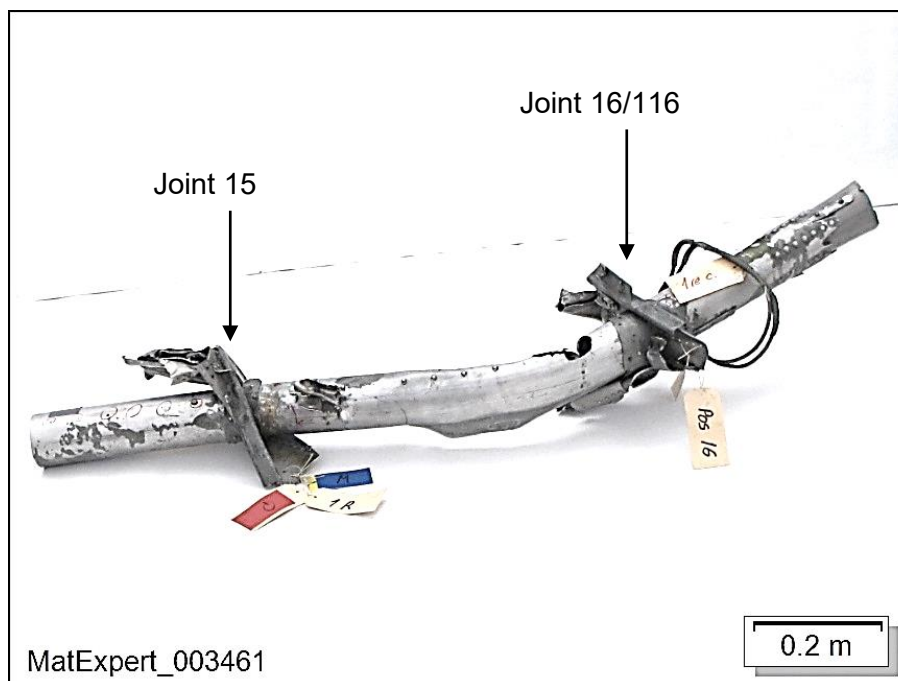


Figure 27: Spar section A.



Figure 28: Area around joint 15 – brittle cracking, partially intergranular.



Figure 29: Area around joint 15 – brittle cracking, partially intergranular.



Figure 30: Area around joint 15 – crack-like surface condition.



Figure 31: Close-up of figure 30 – start of a crack at the rivet hole (circled).



Figure 32: Area around joint 16/116 – pre-existing broken rivet and impact wear, erosion and cavitation on the spar tube.

A1.16.3.2.4 Panelling

The examined piece of sheet metal came from HB-HOT's wing panelling. The sheet thickness was 0.80 mm including an inner plating of 0.029 mm and an outer plating of 0.027 mm.

The sheet was made of a wrought aluminium alloy (AlCuMg). The core hardness was measured in microsection and was 123 HV1³. This corresponds to a hardened material. The plating, consisting of a material with a lower copper content, was applied to improve the level of protection from corrosion. There were areas of flaking anti-corrosion paint on both the inside and outside of the panelling.

A1.16.3.3 Engine mount

A1.16.3.3.1 Material analysis

The material used for the engine mount of the left and the centre engines has a low magnesium content, 0.44 % and 0.39 % respectively, and does not chemically correspond to the specified Duralumin Du42. The material structure of these two engine mounts is similar to cast aluminium and exhibits many intermetallic inclusions. Components with such a microstructure carry a high risk of fracturing. It is probable that the two engine mounts already exhibited these unfavourable material properties when new.

The right engine mount is made of an alloy that is chemically similar to the other two engine mounts, but has a magnesium content of 1.45 %. The structure is homogeneous and has good material properties. The machine-manufactured right engine mount was probably made of a rolled plate and therefore has a superior grain structure. The right engine mount was not broken, but plastically deformed.

A1.16.3.3.2 Fracture analysis

A fracture surface from the centre engine mount (see figure 33) was microfractographically analysed using SEM (see figure 34). The fracture was identified as a brittle, spontaneous fracture exhibiting a mixed fracture pattern of honeycomb, quasi-cleavage and intergranular fractures across a wide area (see figure 35). The intermetallic phases are clearly visible in the fracture pattern and are partially surrounded by roundish cavities. The localised 'terracing', which is a defect, is striking (see figure 36). On the fracture surface, a localised fatigue fracture-like formation can be seen (see figure 37).

³ Hardness test: Indentation of the material according to the Vickers test method.

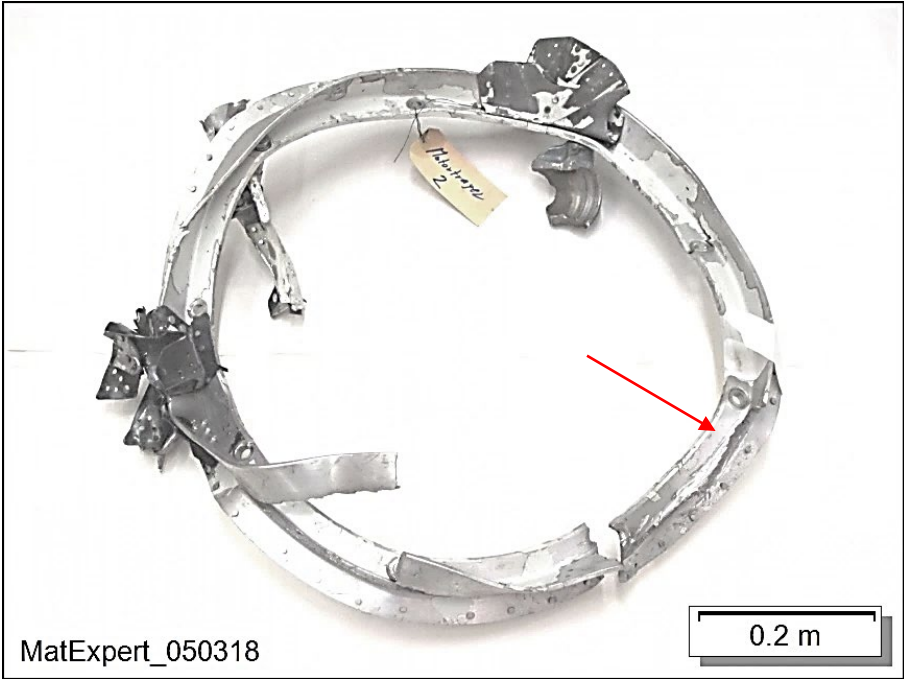


Figure 33: Severely deformed and broken centre engine mount. A part of the fracture surface on the engine mount (red arrow) was analysed.



Figure 34: Location of the analysed fracture surface (red circle).

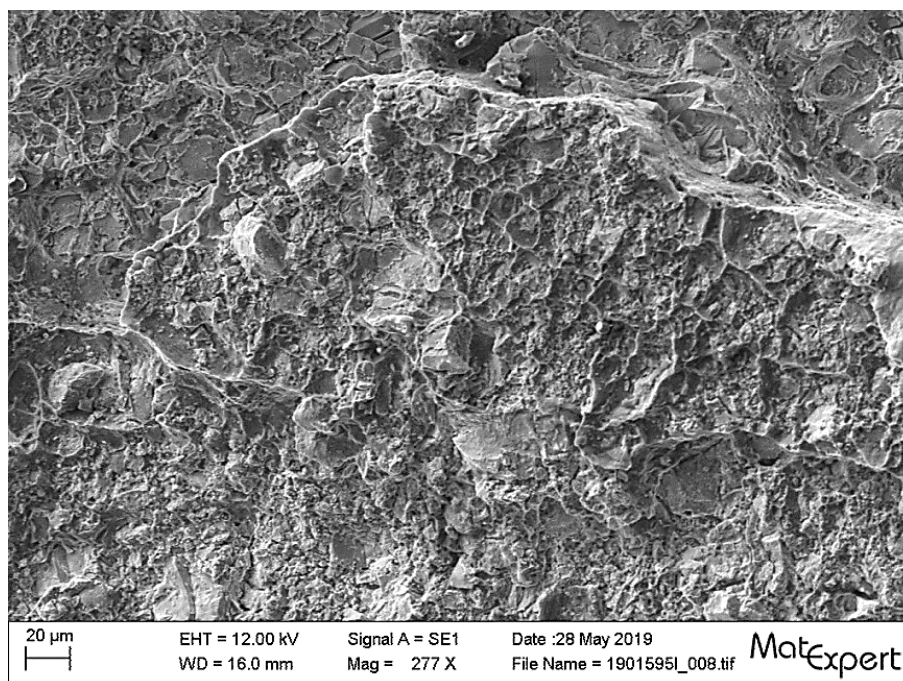


Figure 35: Mixed fracture featuring honeycomb and quasi-cleavage fractures.

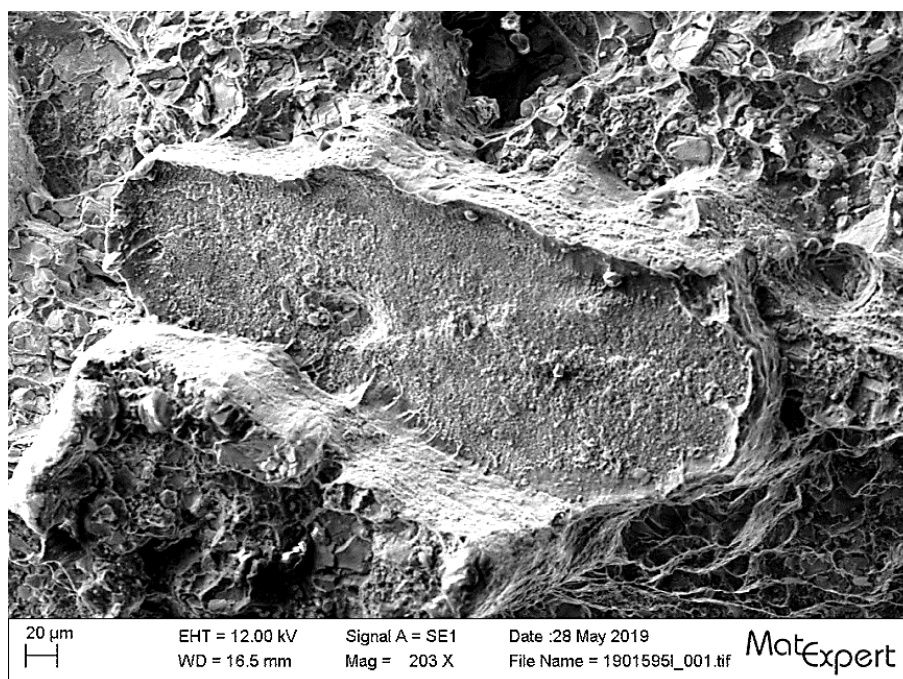


Figure 36: Defect in the form of a terrace, with oxide skin.

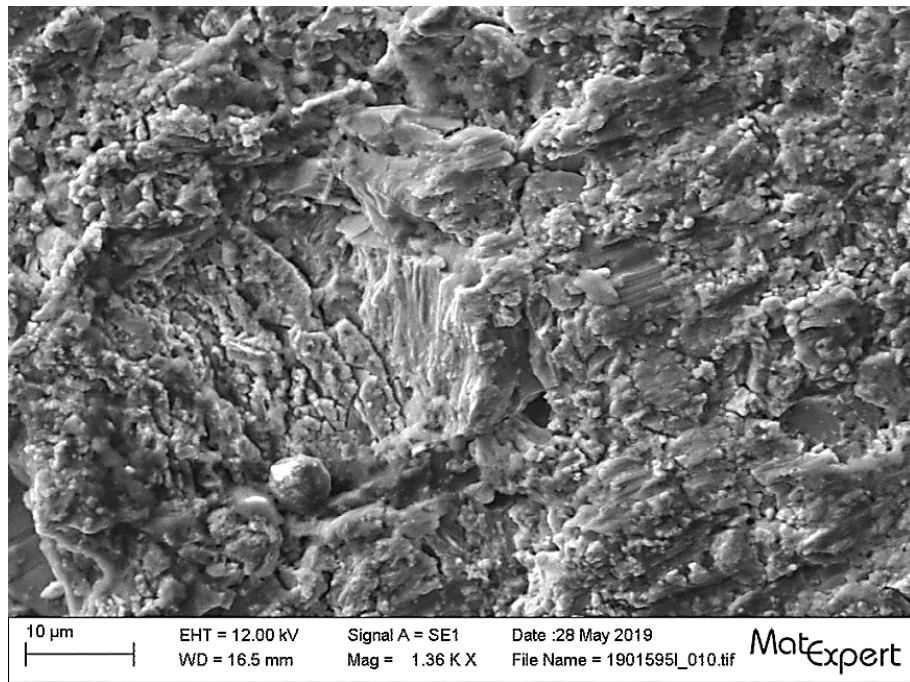


Figure 37: Fine, fatigue crack-like secondary cracks.

A1.16.3.3.3 Surface analysis

The surfaces of the three engine mounts were significantly different.

The centre engine mount is assumed to have been shot-peened. In addition, many small cracks can be seen on the surface (see figures 38 to 42). It is not possible to determine when these cracks were formed. The crack depth was not measured.

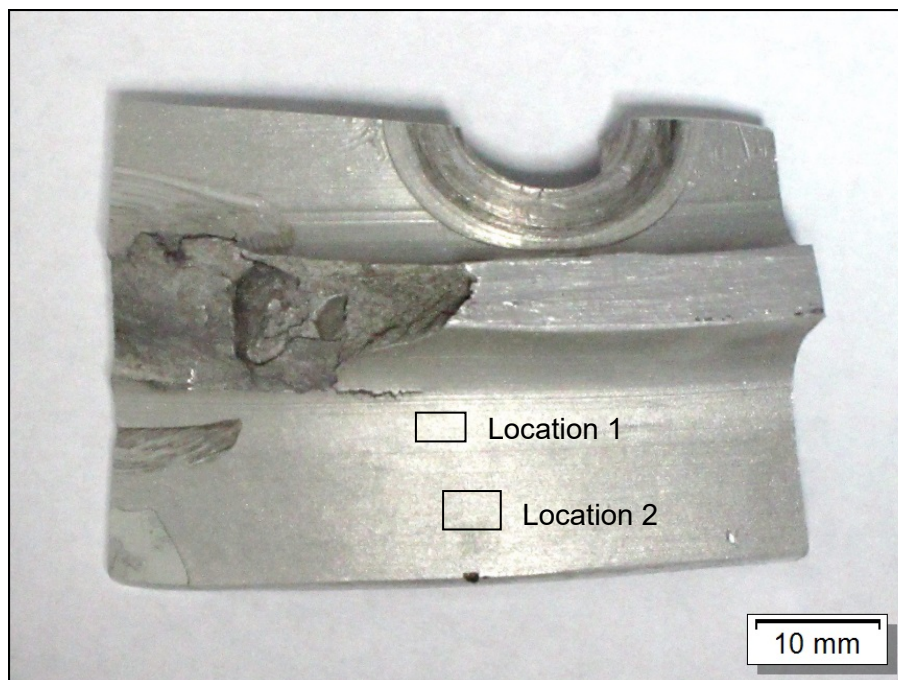


Figure 38: Segment of the centre engine mount – locations of the examined surfaces.

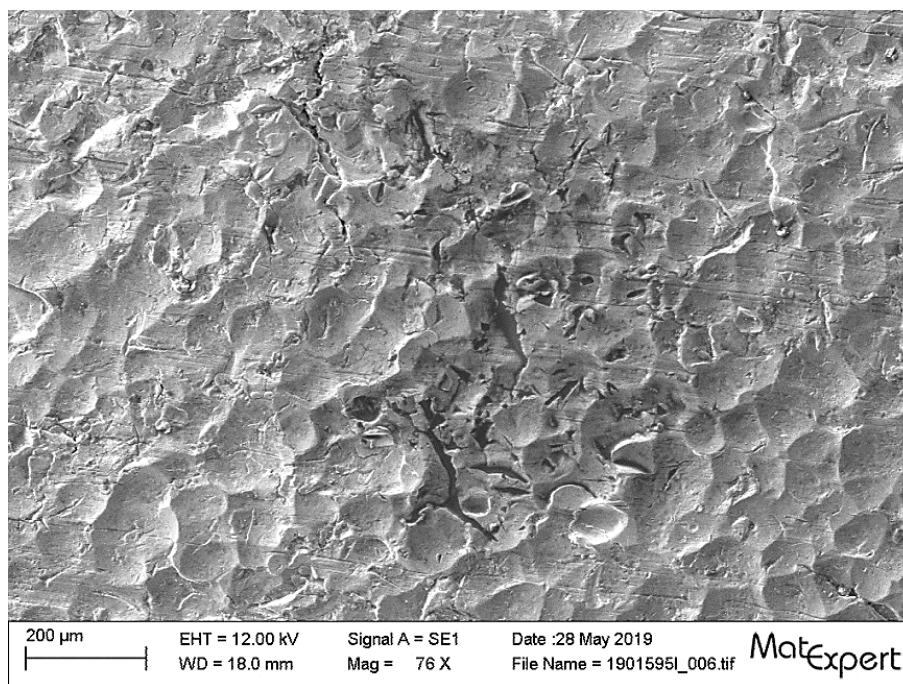


Figure 39: Close-up of location 1 – shot-peened surface with cracks.

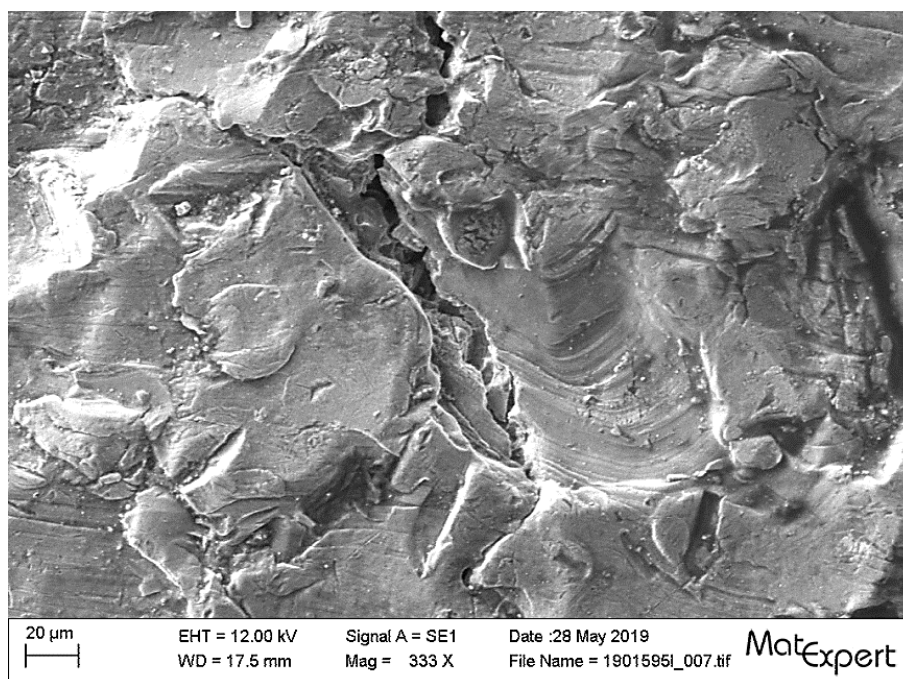


Figure 40: Magnified version of figure 39.

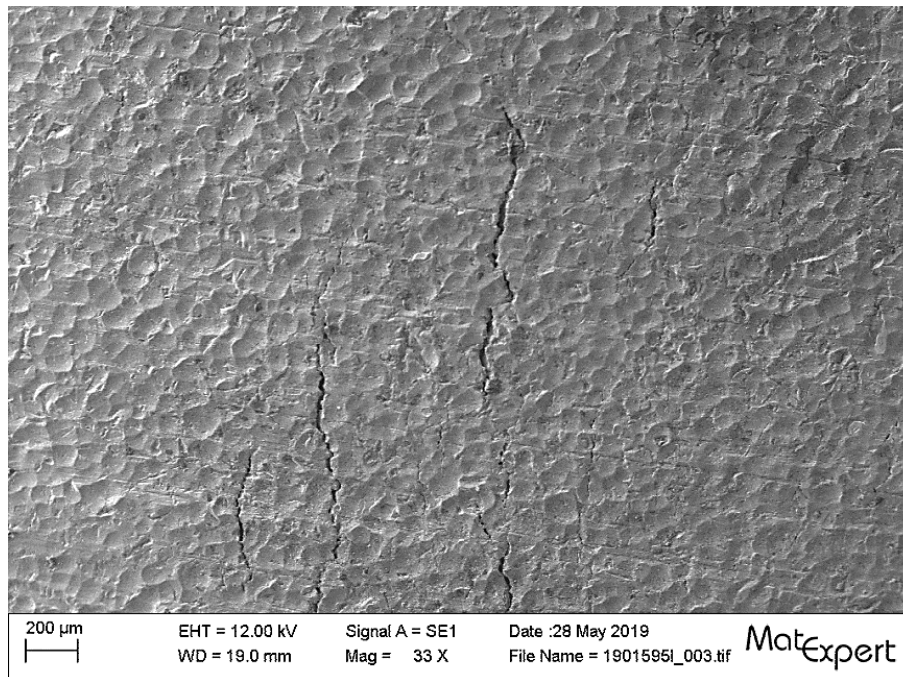


Figure 41: Centre engine mount, location 2 – shot-peened surface with cracks.

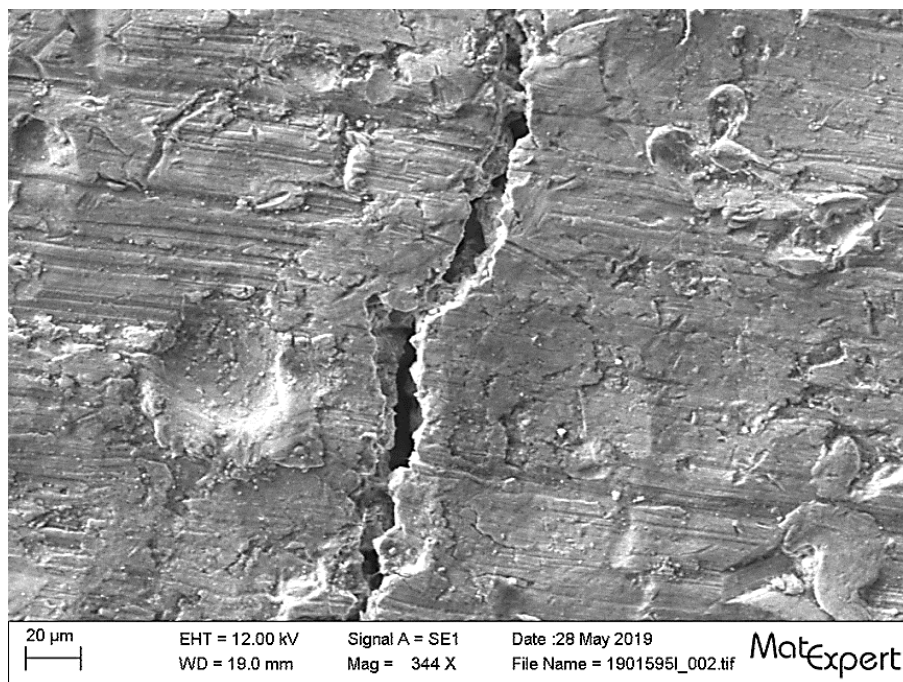


Figure 42: Magnified version of figure 41.

The distinct marks found on the surface of the right engine mount indicate that it was machined (see figure 43). No signs of shot peening and no surface cracks were found.

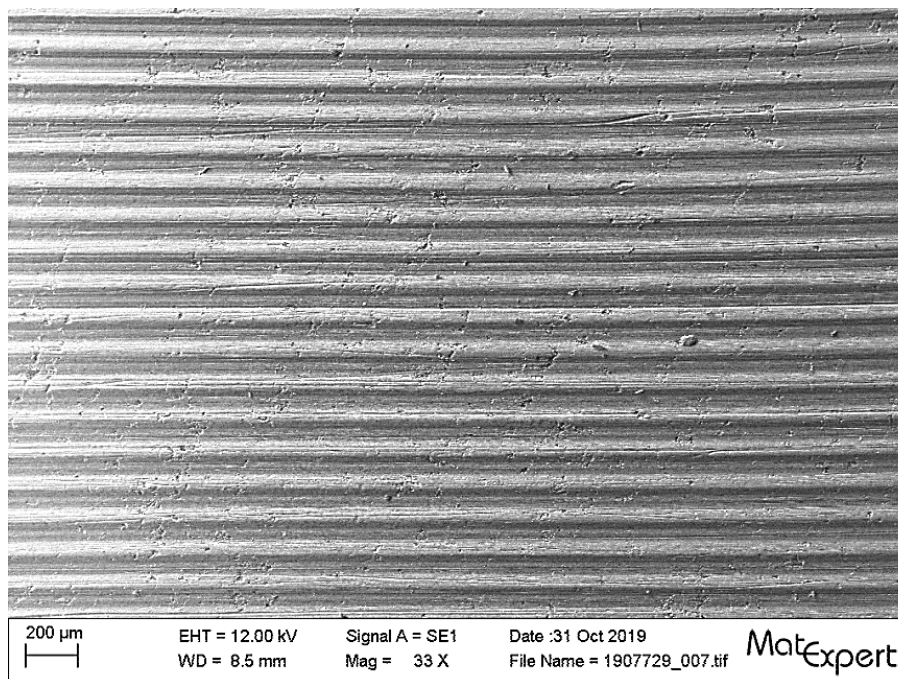


Figure 43: Right engine mount – existing, distinct machining marks (from turned surface).

There were no signs of shot peening on the left engine mount. Microscopic examination of the surface did not discover any microcracks. Based on the determined microstructure, it is conceivable that there are microcracks. However, a more elaborate examination method would be required to prove this.

A1.16.3.4 Engine components

A1.16.3.4.1 Cylinders

One cylinder from each of the three engines was metallurgically examined in the laboratory. The three cylinder barrels were sectioned and the structure of the cylinder wall was analysed. This revealed that all three cylinders were coated on the inside. The base material of the cylinder barrels, the type and thickness of the coatings and the Vickers hardness values were determined. One cylinder head was also analysed to determine the material used.

The examined cylinder from the left engine as well as that from the centre engine has been hard-chrome plated (see figure 44). The thickness of this plated surface is 0.121 and 0.123 mm respectively. It features peeling and has cracks covering the surface like a net, which can be seen with the naked eye. The cracks detected are typical for these kinds of coating and are a result of the process used. The chrome plating is extremely hard, the measured value HV0.3 is between 775 and 820.

The cylinder barrel is made of a medium-strength alloy steel. The HV10 hardness value measured for the cylinder material was 230 and 260 respectively. Before the centre engine's cylinder was chrome-plated, the cylinder's inner diameter was 156.12 mm.

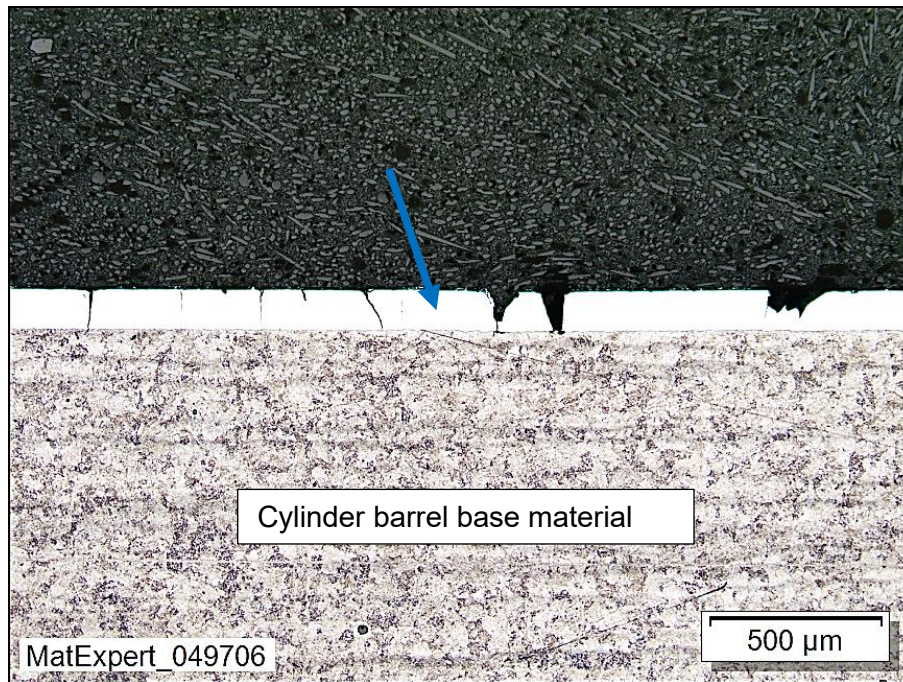


Figure 44: Microsection of the cylinder wall (left engine, cylinder 5) including hard-chrome plating (blue arrow), network of cracks and peeling.

The cylinder from the right engine was plated with a thermal sprayed coating consisting of two different materials (see figure 45). The surface of this plating was porous, cracked and partially discoloured red (see figures 46 and 71).

What is known as a bond coat was found on the substrate, which had been covered by a top coat that featured approximately the same level of thickness as the bond coat. The measured thickness of the bond coat was 0.135 mm and that of the top coat 0.165 mm. The hardness measurement HV0.3 of the bond coat was 160 and that of the top coat 340.

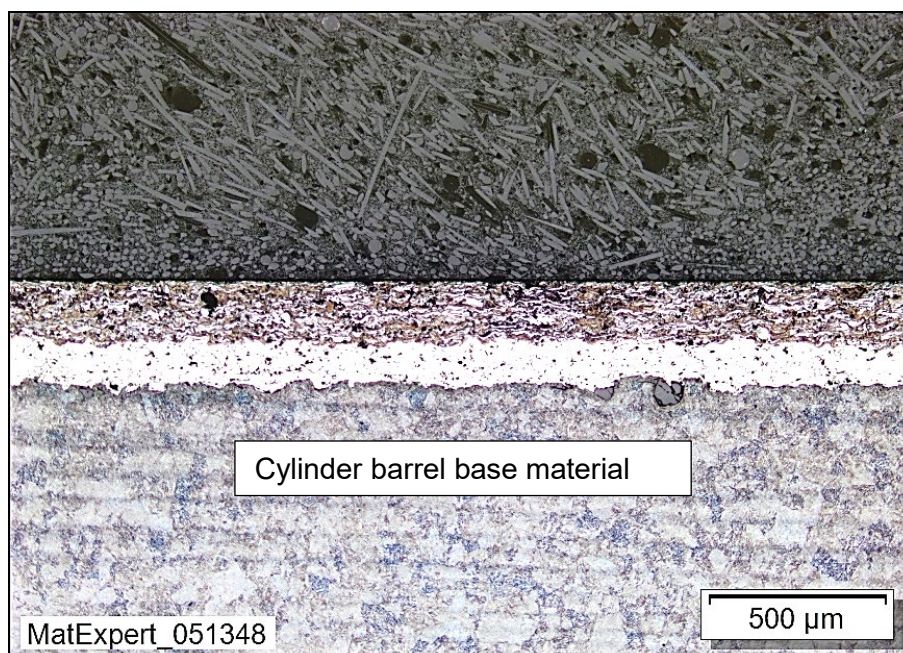


Figure 45: Microsection with two-layer spray coating (right engine, cylinder 1).

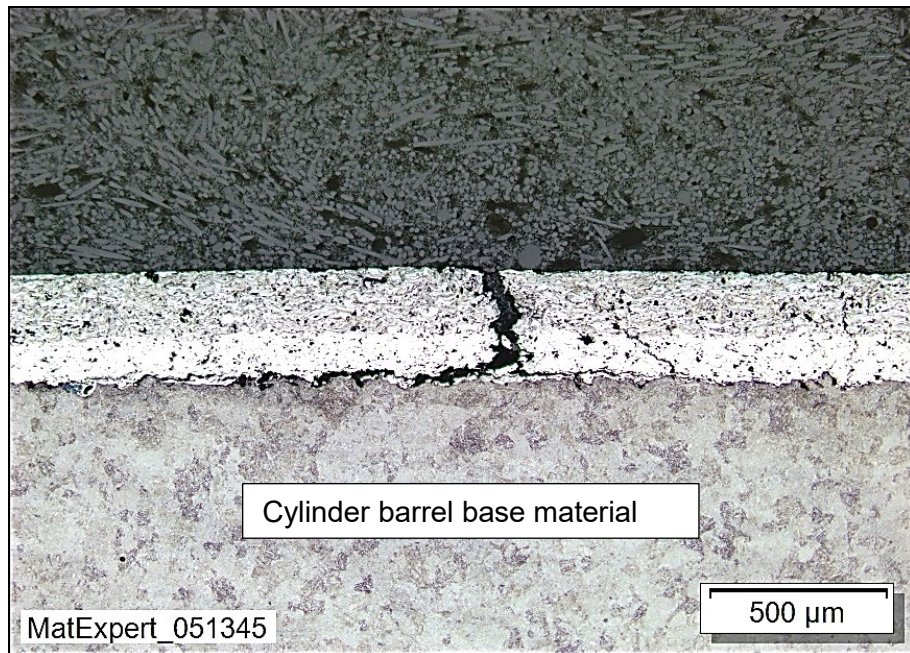


Figure 46: Crack in bond and top coat.

Prior to coating, the cylinder was honed to a diameter of 156.44 mm and the surface was abraded (see figure 47). Honing the cylinder to this diameter is not permitted according to the 1939 operating instructions supplied by the manufacturer of the BMW 132 A3 aircraft engine.

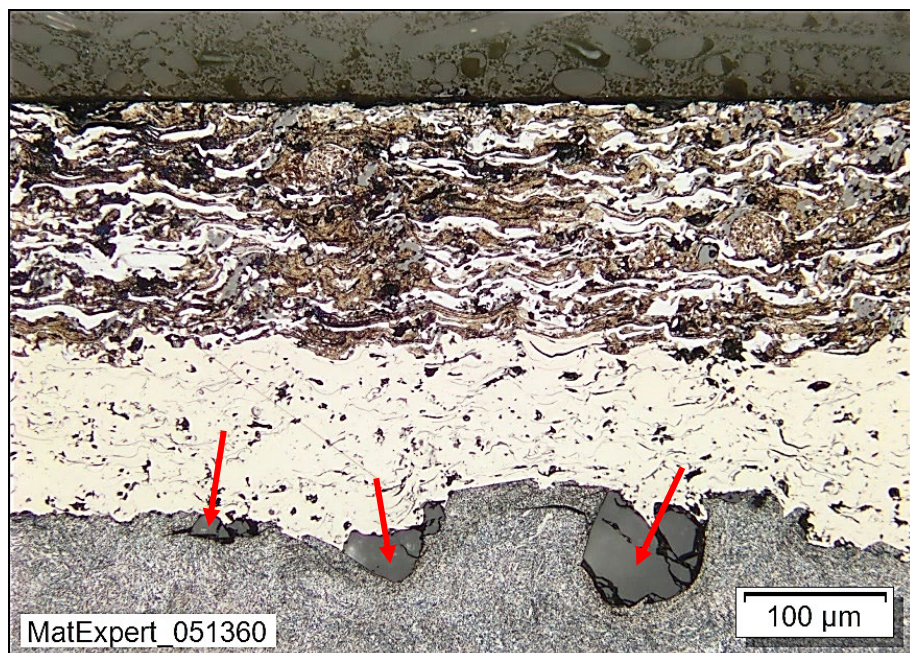


Figure 47: Microsection of the spray coatings with typical abrasive residues on the surface of the base material (red arrows).

The applied spray coatings were analysed for their chemical elements through micro-area analysis using EDX. The analysis was carried out on microsections.

The analytical values of the top coat correspond to a mixture of a low-alloy carbon steel and molybdenum (Mo). Boron (B) was also detected. The analysis of the

bond coat indicated an alloy of nickel (Ni) with aluminium (Al) and iron (Fe) i.e. an NiAlFe alloy.

The hardness of the base material for the cylinder from the right engine, measured according to HV10, was 225.

All examined cylinder barrel base materials correspond chemically to the requirements of the engine manufacturer.

The microstructures of all of the cylinder barrels have phase components (ferrite) which do not meet optimum tempering requirements. It is possible that these microstructures were created by long-term thermal stress.

The material used for the cylinder head complies with the specifications of the engine manufacturer. Casting defects in the form of shrinkage cavities are evident (see figure 48). The microstructure can be judged as typical for the alloy in question, but is more consistent with a brittle state.

Compared to modern materials, the alloy has a simple structure. The materials used to manufacture cylinder heads today are alloyed in such a way as to ensure high thermal shock resistance and long-term durability.

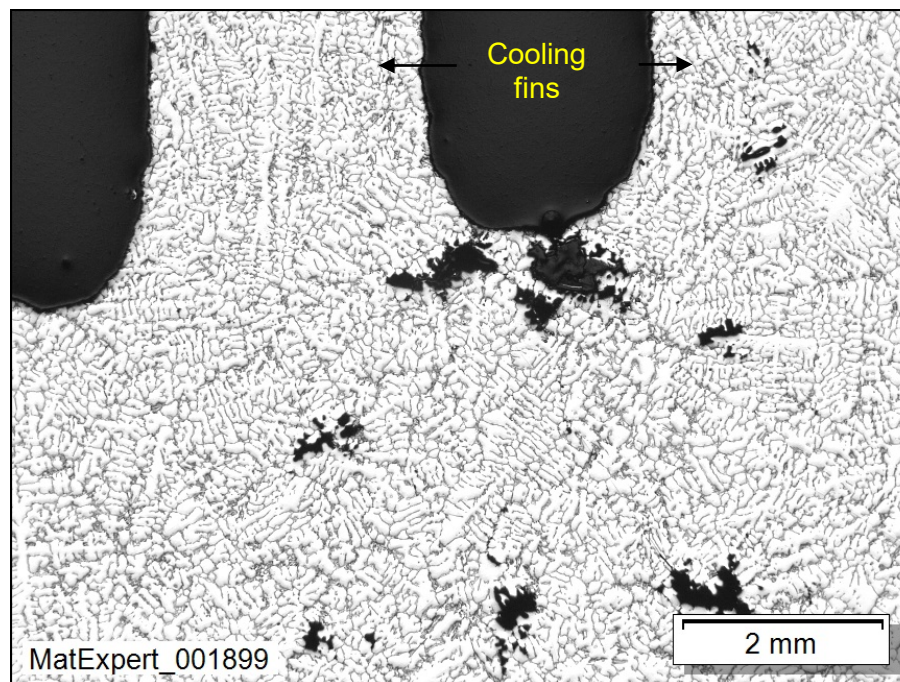


Figure 48: Microsection of the cylinder head's structure with solidification holes (left engine, cylinder 5).

A1.16.3.4.2 Propeller bearings

All of the ball bearings for the three propellers were metallurgically examined.

According to the chemical analyses, the material used for all inner and outer races is consistent with 100Cr6 steel used for common rolling bearings. The mechanical properties were determined using Rockwell hardness measurements on the end faces of the inner and outer races. The measured hardnesses are typical for this material when hardened and then tempered at low temperatures.

The fragments of the outer race from the ball bearing used on the centre engine underwent macro- and microfractographic analysis. A spherical impression can be seen in the area surrounding the origin of the fracture. Most of the fracture surfaces

exhibit an intergranular fracture with a low level of ductility, which indicates a certain level of brittleness to the material. The fracture was most likely caused by the accident.

The bearing tracks on the inner races of all three ball bearings and the bearing track on the outer race of the bearing from the centre engine were analysed using scanning electron microscopy. All of the tracks exhibit wear in the form of material chipping, pitting and mechanical indentations (see figures 49 to 53). The residues found were subjected to micro-area analyses using EDX, which revealed high oxygen content as is typical of iron oxide or iron hydroxide (see section A1.16.4.5.2).

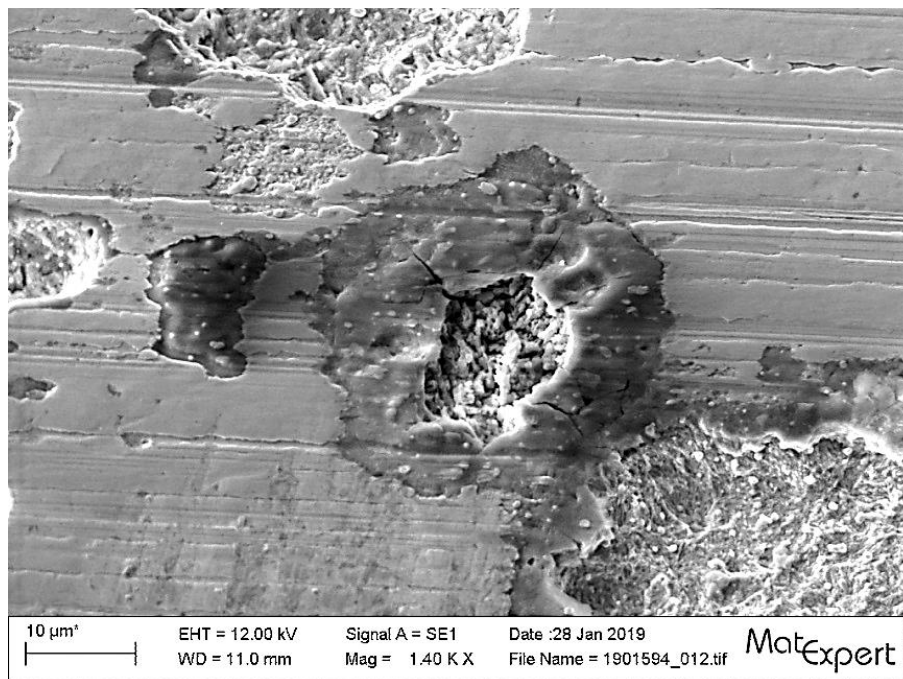


Figure 49: Ball bearing from the right engine, inner-race bearing track – material chipping and corrosive damage.

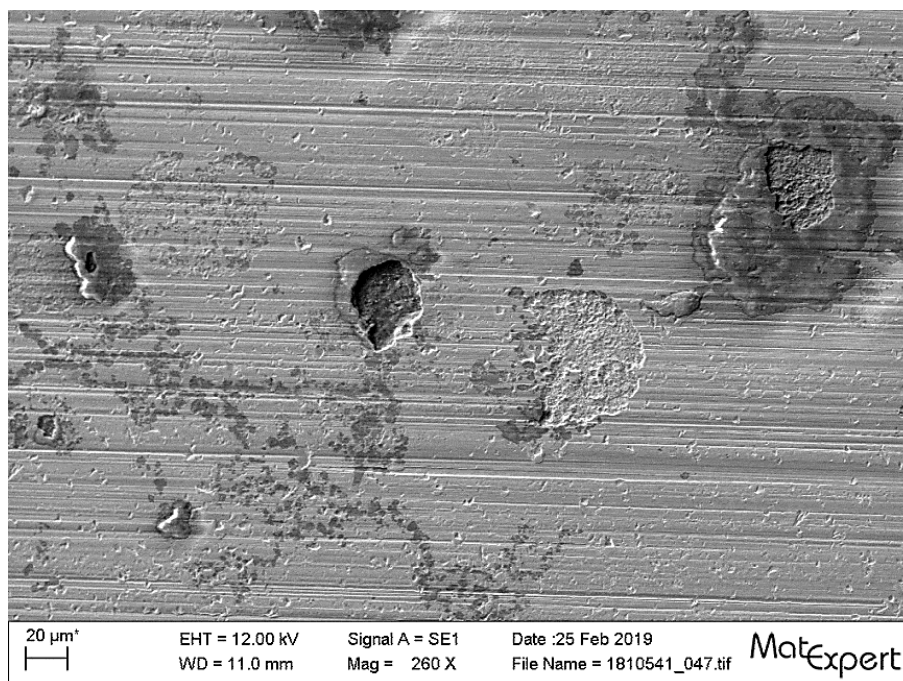


Figure 50: Ball bearing from the left engine, inner-race bearing track – material chipping, corrosion and minor pitting.

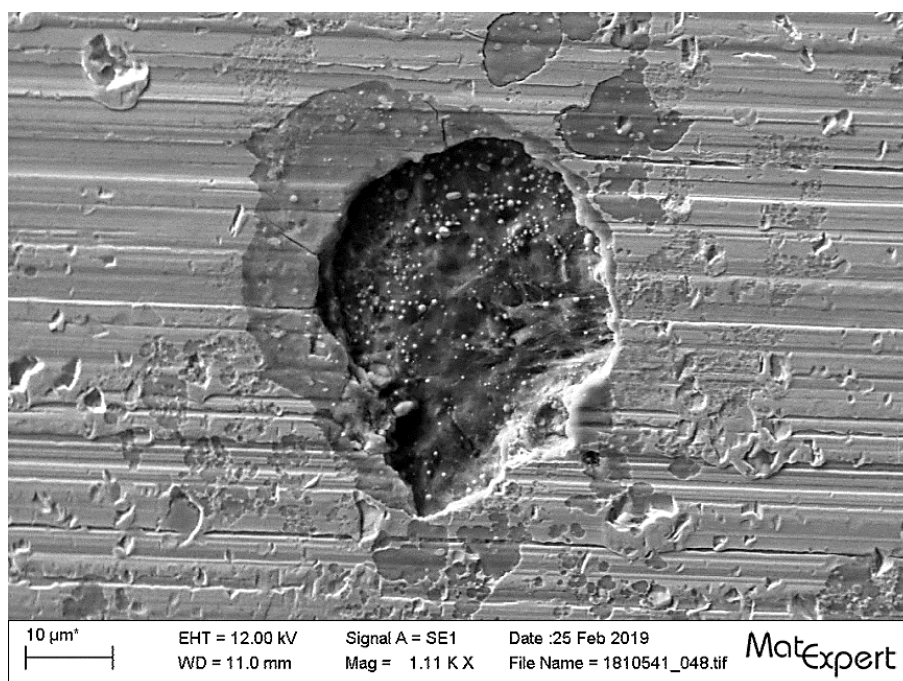


Figure 51: Close-up of figure 50.

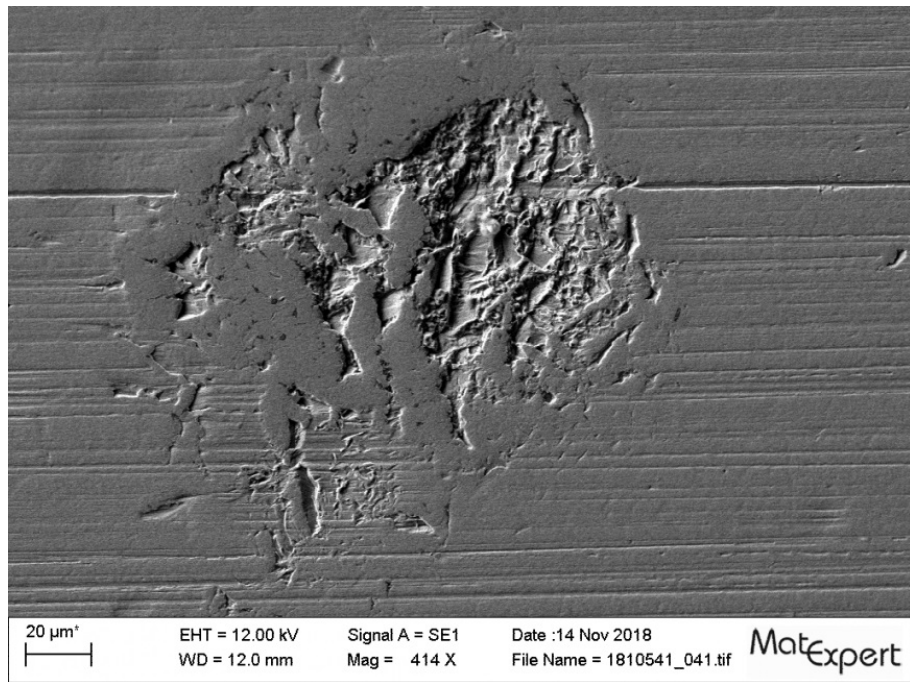


Figure 52: Ball bearing from the centre engine, outer-race bearing track – pitting, possibly due to foreign-body indentations.

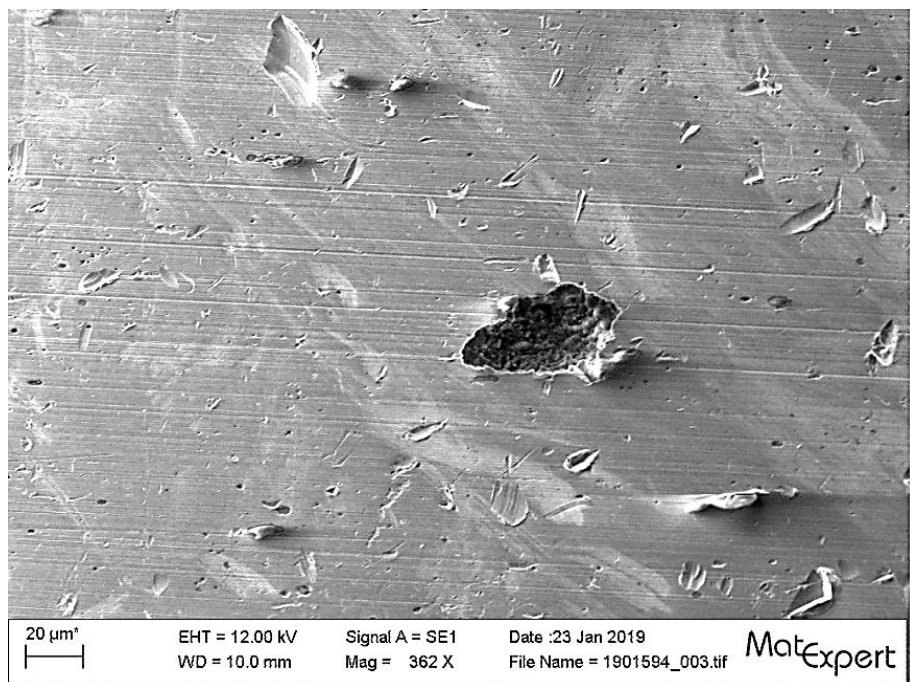


Figure 53: Ball bearing from the centre engine, inner-race bearing track – mechanical indentations, material chipping and pitting.

A1.16.3.4.3 Supercharger bearings

The supercharger bearing nos 3, 4 and 5 (see annex [A1.12](#)) from the left engine were metallurgically examined.

According to micro-area analysis, both races as well as the rollers from roller bearing no. 3 are made of 100Cr6 steel, which is often used for the production of rolling

bearings, and the roller cage is made of brass. The two races from ball bearing no. 4 are also made of 100Cr6.

The mechanical properties of the races from bearing nos 3 and 4 as well as the rollers were assessed using Vickers hardness measurements. The measured values correspond to usual values for a hardened material.

All the bearings examined exhibited corrosion and were tribologically⁴ damaged. On the bearing tracks and guide surfaces, evidence of material chipping, pitting, abrasive wear, intergranular cracks and flat-rolled corrosion was found (see figures 54 to 60). The inner and outer races from bearing nos 3 and 4 had become magnetised. This causes ferromagnetic particles such as any material abraded during use etc. to be attracted and damage the bearing tracks as well as the rolling elements of the bearings and severely interfere the tribological system.

The general condition of the bearings is poor, and the damage found indicates that the supercharger's bearings were at risk of sudden failure. This would lead to a loss of power and possibly to engine failure.

Bearing no. 5 displayed a similar picture.

The damage shows that the installed bearings did not meet requirements.

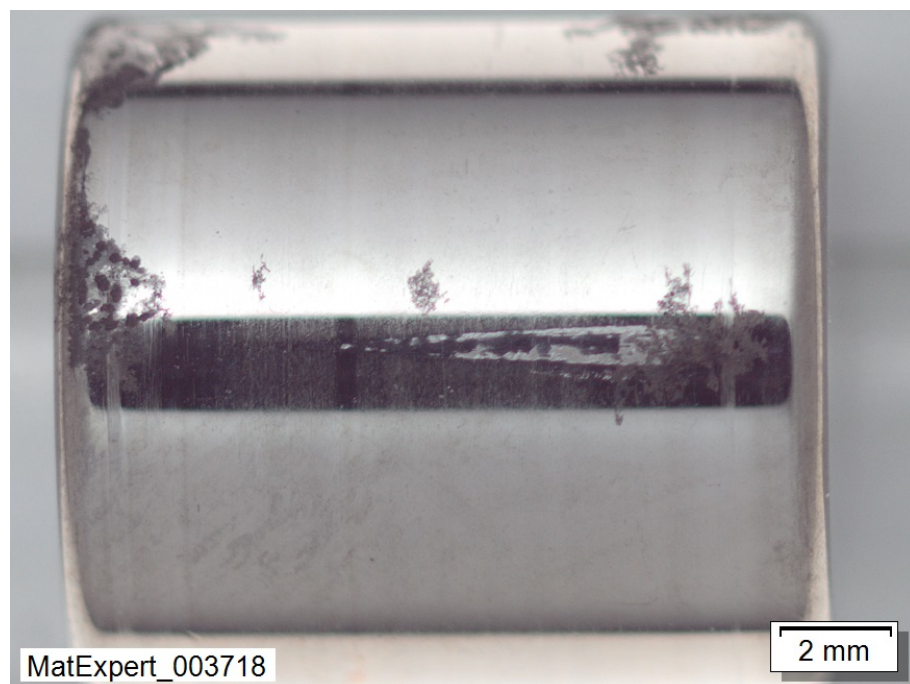


Figure 54: Bearing no. 3 – cylindrical roller with wear.

⁴ Tribology: The science of friction, wear and the lubrication of interacting surfaces in relative motion.

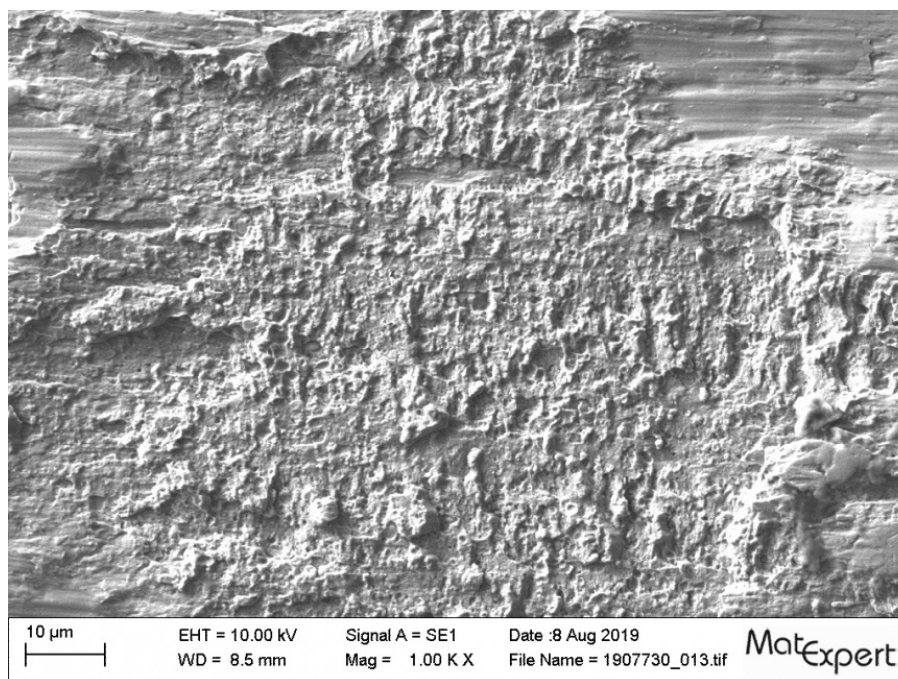


Figure 55: Close-up of the worn area – material chipping and cavitation.

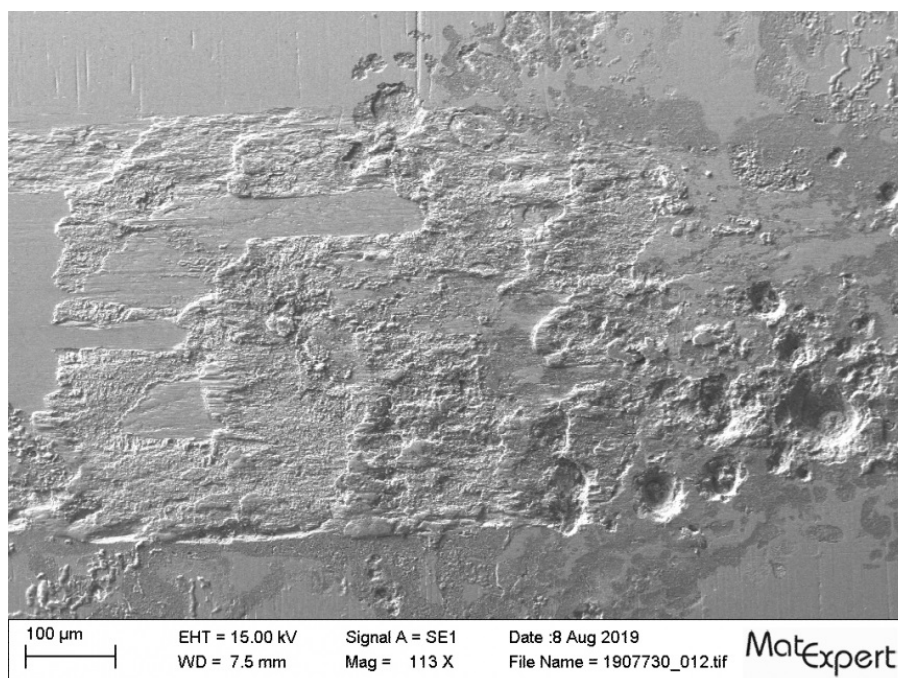


Figure 56: Close-up of the worn area – pitting.

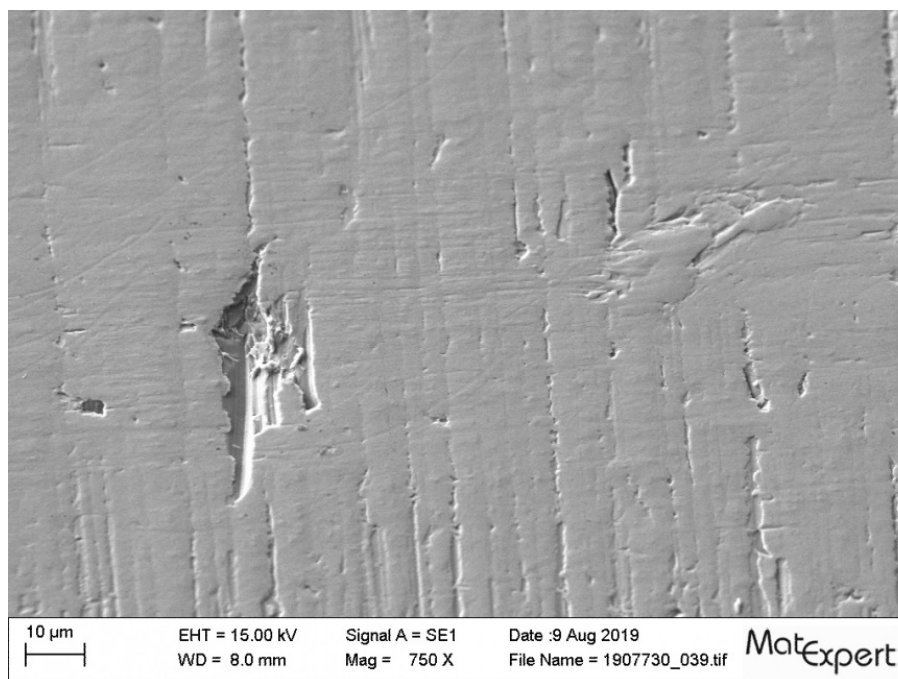


Figure 57: Bearing no. 3, outer-race bearing track – smoothed stop point and material build-up.

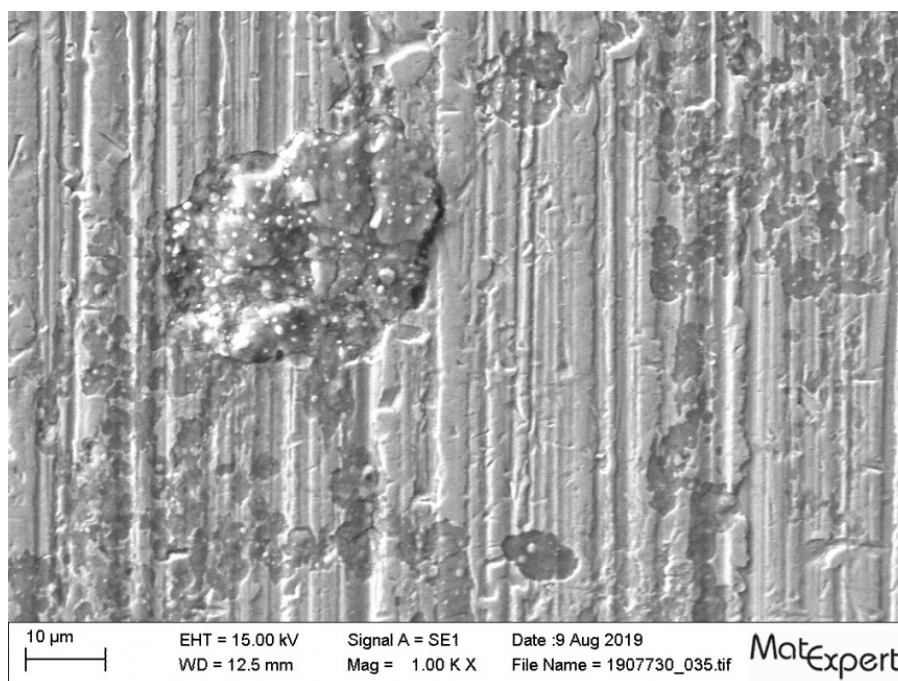


Figure 58: Bearing no. 3, outer-race bearing track – flat-rolled corrosion and abrasive wear.

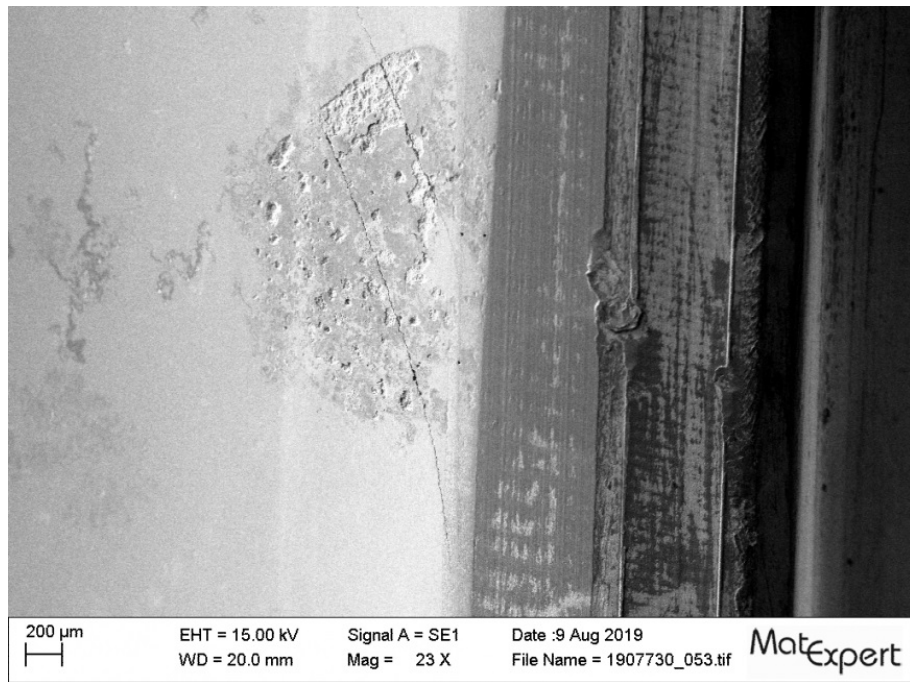


Figure 59: Bearing no. 4, outer-race bearing track – damage due to material chipping and cracks.

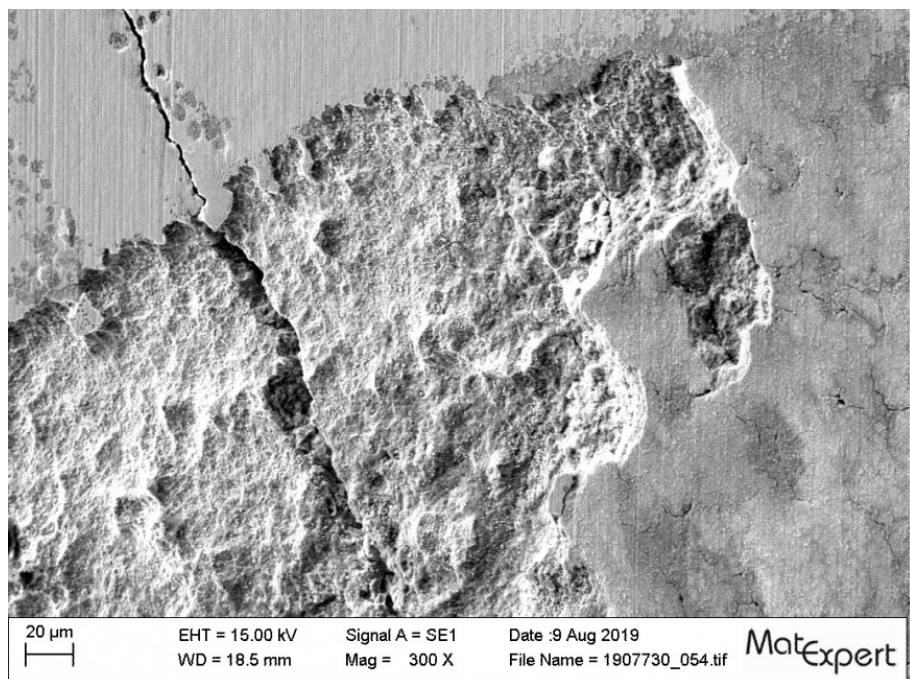


Figure 60: Close-up of figure 59.

A1.16.4 Corrosion analysis

A1.16.4.1 General

When exposed to a certain environment, such as a lack of surface protection, corrosion is able to penetrate Duralumin along the material's grain boundaries. This is known as intergranular corrosion. This phenomenon is also called intergranular

attack. This type of corrosion cannot be detected from the outside without appropriate aids, such as a microscope or scanning electron microscope. The ageing of the material due to exposure to heat increases the risk of intergranular corrosion.

When intergranular corrosion occurs, the static strength and fatigue strength are reduced. Depending on prior damage and loads, these strengths are significantly reduced.

Contact corrosion is a type of galvanic corrosion. This occurs, for example, when Duralumin comes into contact with steel and the two material surfaces are exposed to moisture. Contact corrosion often results in pitting.

Duralumin's susceptibility to corrosion was already well known during the production period of the Ju 52/3m g4e aircraft. For example, the susceptibility of AlCuMg alloys to intergranular corrosion was described in book 28 of "*Werkstoffkunde für den Flugzeug- und Motorenbau*" (a series of books on material science for aircraft and engine construction), published in 1937 (see figure 61).

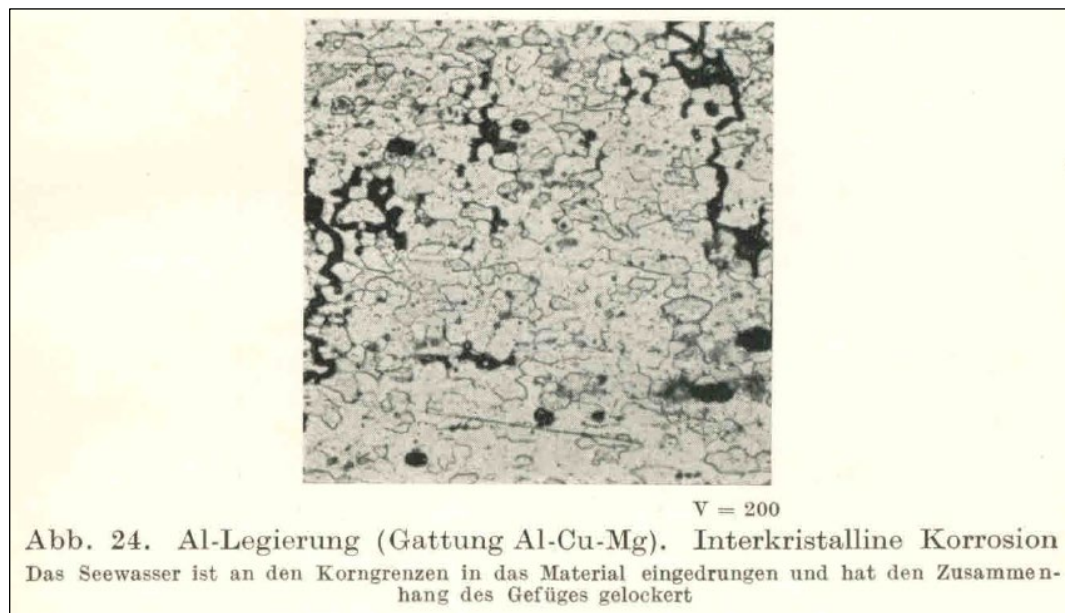


Figure 61: Illustration of an AlCuMg alloy with intergranular corrosion from book 28 of "*Werkstoffkunde für den Flugzeug- und Motorenbau*" by Ing. Cl. Böhne.

With the appropriate heat treatment, the examined AlCuMg alloy is not susceptible to intergranular corrosion when it is subjected to a corrosive environment but pitting usually occurs.

Intergranular corrosion is therefore not the typical form of corrosion, it only occurs under the following conditions:

- In the event of unfavourable heat treatment, e.g. quenching too slowly after solution heat treatment and/or artificial ageing;
- In the event of thermal stress after ageing;
- In the presence of a corrosive medium, such as combustion gases or condensation.

Stress corrosion cracking can occur in AlCuMg alloys under special circumstances. In addition, it is also possible for corrosion fatigue (a type of corrosion caused by a combination of conditions) to occur.

Intergranular corrosion causes cracks to form that give rise to the notch effect and can lead to the total failure of the component. Likewise, intergranular cracks form the ideal conditions for fatigue cracks to develop. This also applies to the connections between the steel joints and the aluminium spar tubes, which have been secured using rivets made of identical material (see figures 25 and 26).

Usually the aluminium alloy used is less corrosion-resistant than the steel used for the connecting joints. However, research has shown that the spar material is more corrosion-resistant when artificially aged, which explains the severe corrosion of the steel joint. Depending on the state of the microstructure, there are shifts in the corrosion potential between the pairing of aluminium and steel. Consequently it is possible that, when in an unfavourable structural state, the AlCuMg alloy creates an electrochemical environment that leads to the steel also corroding.

The material pairing of steel and an AlCuMg alloy is fundamentally problematic and this is accentuated in an aggressive environment. In this case, it is important to ensure that the metals are insulated from each other by a non-conductive material, e.g. by a coat of paint.

A1.16.4.2 Manufacturer's instructions regarding corrosion protection

In section 0, 'General', of the operating manual for the Ju 52/3m g4e aircraft, the manufacturer wrote the following regarding corrosion protection under 'Partial overhauls and major overhauls':

"Partial overhauls are to be carried out after approximately 300 operating hours.

[...]

Particular attention must be paid to the surface protection conforming with specifications.

Major overhauls are to be performed after approximately 1,500 operating hours.

For this, all larger parts, such as the outer wings, empennage, controls, engine parts, etc. are to be dismantled and thoroughly inspected; in addition, the surface protection and all equipment are to also be overhauled. Any necessary repairs are to be made so that the final condition of the aircraft is as close to factory-new as possible."

Furthermore, in the same section under 'Cleaning and Paint Care' the following instructions are given:

"At certain intervals, the entire coating must be carefully inspected inside and out for damaged areas, flaking, blistering and cracking, etc. caused by weathering. Any damage must be repaired in accordance with the information given in the 'Junkers Repair Instructions'."

In section 5, 'Surface protection', of the repair instructions (*Ausbesserungsanleitung*) for Junkers metal aircraft, the manufacturer provided the following information under 'Preliminary remarks':

"Surface protection (corrosion-proofing) is intended to protect the material against all kinds of corrosion and thus increase the service life of the aircraft.

[...]

In aircraft, corrosion is mainly caused by atmospheric influences (condensation), seawater and the electrical currents triggered when parts of different potential are connected (placed on top of each other).

The protection used must be easy to apply, durable, attractive and easy to repair or renew.

[...]

The decision as to whether the surface protection is to be repaired or renewed depends on whether or not sufficient protection is guaranteed during continued operation. Any increase in weight due to extensive paint application can also be a deciding factor. If the paint is not cracked or flaked off, it is usually not necessary to apply a new coat.

Before painting, the parts or areas concerned must be thoroughly cleaned with detergents (see 1a, 2a, 3a) as specified, avoiding sanding bare aluminium alloy with steel wool, sandpaper or wire brush as far as possible. The cleaned surfaces must be free of paint residues, oils, greases, dirt, scale, oxides, hand perspiration, etc.”

A1.16.4.3 Fuselage

The sheet metal of the cabin floor near the aft hinge of the cargo door exhibited cracks, pronounced intergranular corrosion and pitting. In parts, the sheet was affected all the way through (see figures 62 to 64).

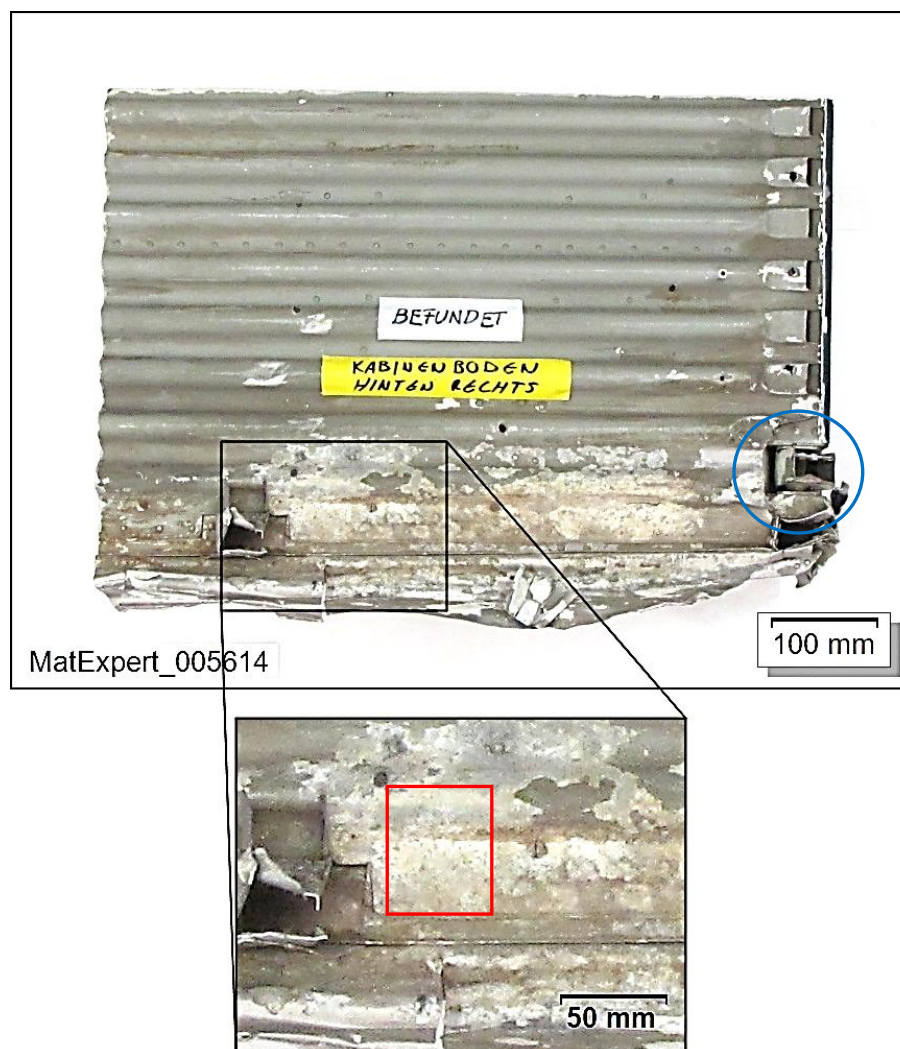


Figure 62: Corroded cabin floor from the aft right area (label text reads cabin floor, aft right). Samples were taken from the zone marked in red for the subsequent microsections. The blue circle marks the cargo door's aft hinge.

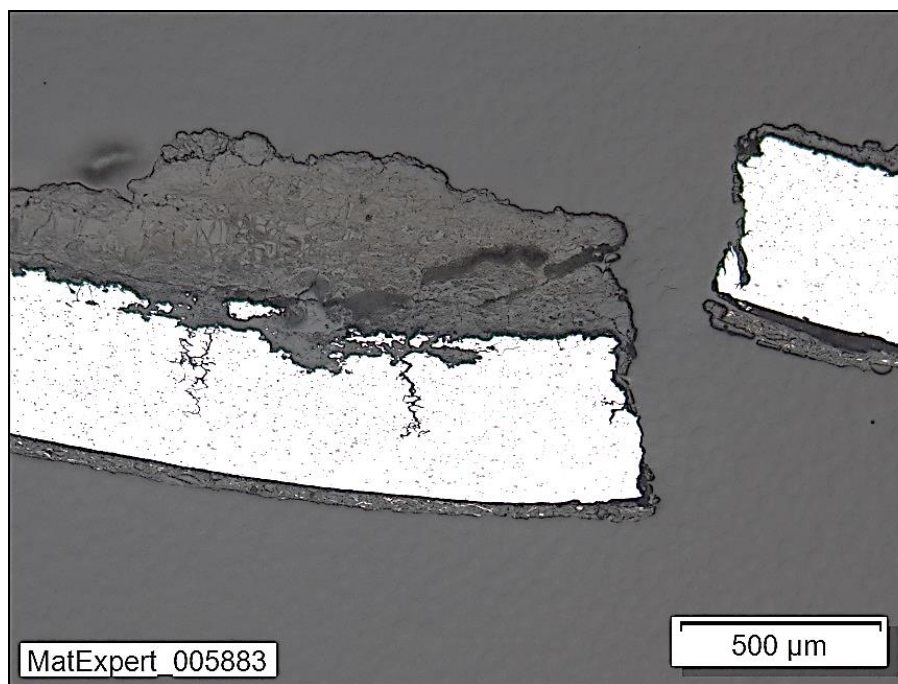


Figure 63: Microsection of the corroded sheet. Cracks with intergranular corrosion.

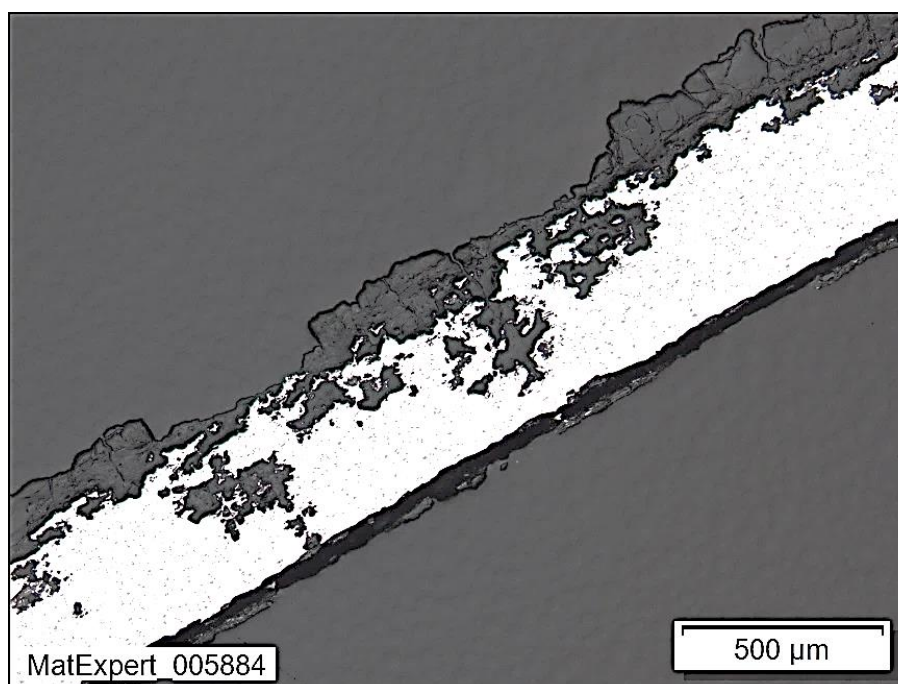


Figure 64: Microsection of the corroded zone; intergranular corrosion and pitting.

The hinge of the cargo door made of steel was severely corroded. Some of this corrosion was very advanced (see figure 65).



Figure 65: Severely corroded inner side of the cargo door hinge.

A1.16.4.4 Wing

Spar sections L1, L2u and 1Ru as well as the two joints from spar L1 were examined regarding corrosion in the laboratory. All examined spar sections corresponded chemically to hardened Duralumin Du44; the joints were made of steel. The lower spar sections and joints only exhibited remnants of the anti-corrosion paint. The corrosion protection was assessed to be insufficient.

Intergranular corrosion was found in lower spar section L1 (see figure 66), while on section 1Ru, pitting, as is common for this material, was found (see figures 67 and 68). The former only occurs when the material does not conform with the specifications and is the result of artificial ageing or thermal stress and grain boundary precipitation.

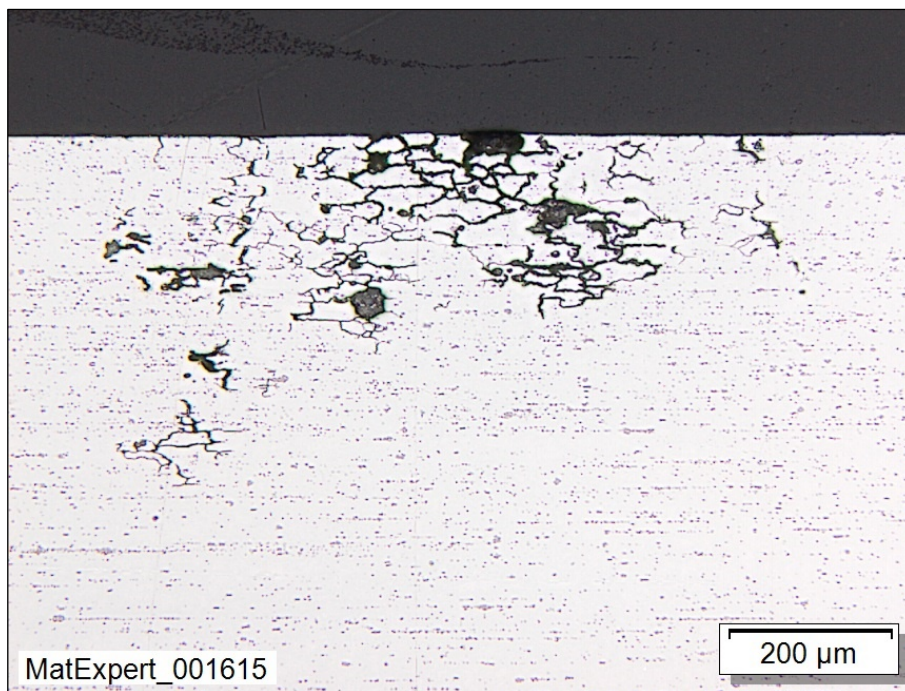


Figure 66: Microsection of lower spar L1 with intergranular corrosion.

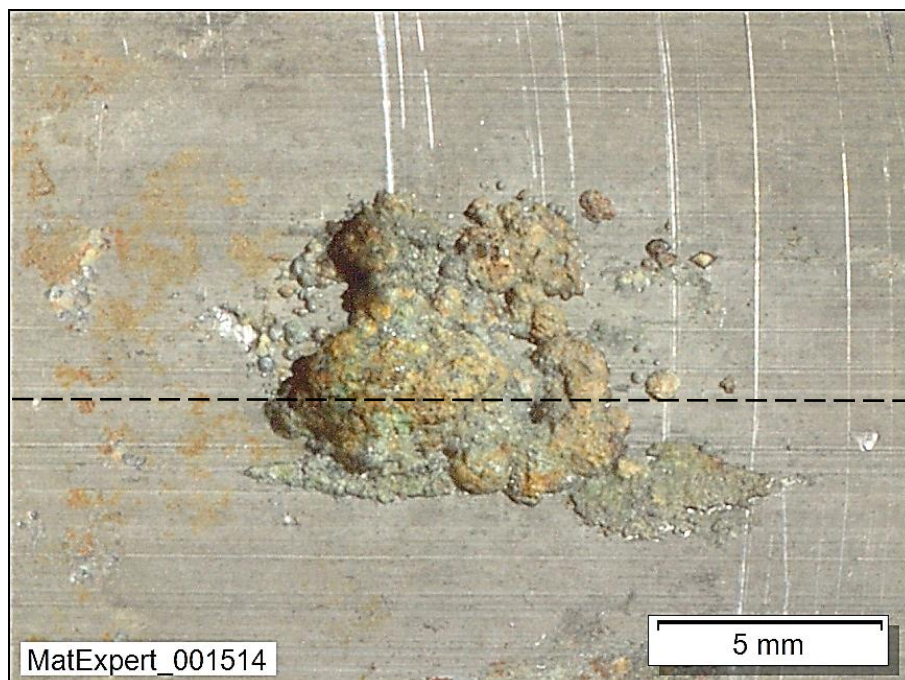


Figure 67: Pitting on spar section 1Ru (line of cross section, see figure 68).

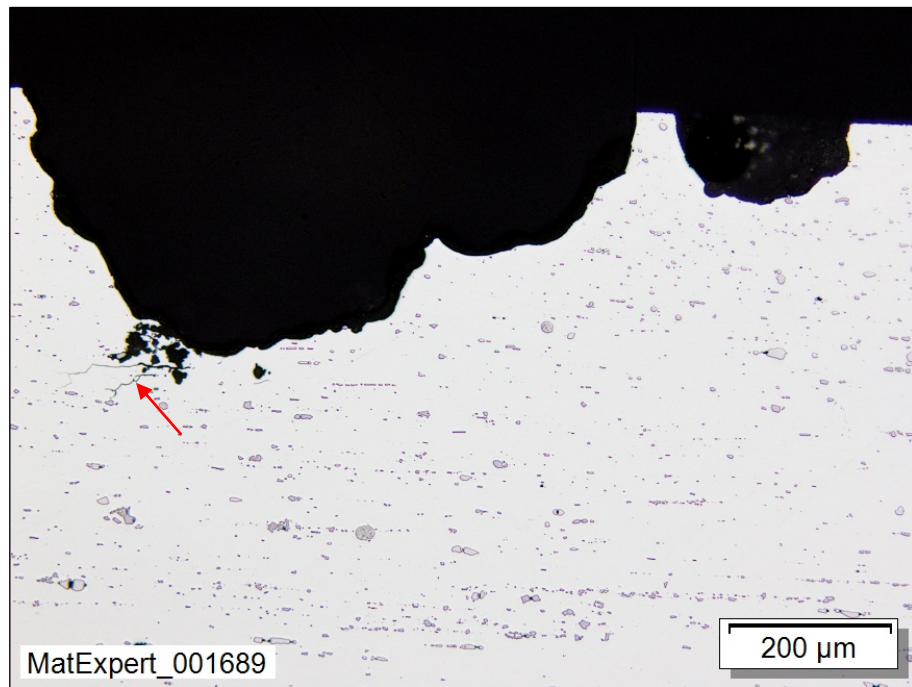


Figure 68: Microsection along the line as indicated in figure 67 with severe pitting and individual stress cracks (arrow).

Lower spar section L1 also exhibited intergranular corrosion outside of the point of contact between the spar and the joint. In some areas, signs of stress corrosion cracking were discovered. Likewise, some cracks exhibited areas that are typical of corrosion fatigue.

Joint 89 mounted on the left outer wing's lower spar L1 was examined for corrosion after being cut open. The joint is a welded steel construction. The inside, which was in contact with the aluminium spar, exhibited severe corrosion damage. Usually the aluminium alloy used is less corrosion-resistant than the steel used for the joints. However, research has shown that the material used for the lower spar is more corrosion-resistant when artificially aged, which explains the severe corrosion of the steel joint.

The corrosion isolated on spar section L1 mainly contained compounds of iron.

In the examined instance, given the position of the corroded lower spar section L1 in the left outer wing near the left engine, it is probable that the susceptibility only arose during operation as a result of heat from the engine. Engine exhaust gases are not only thermally problematic, but also contain reactive products or corrosion-promoting substances. Environmental conditions play a major role in this.

In addition to the contact surfaces between the joints and the spar, corrosion was found on the lower spar sections in the areas near the steel joints as well as in areas of wear caused by the panelling.

Examination revealed that the joints on upper spar section A exhibited a similar condition as those on lower spar section L1. Several intergranular cracks were also found.

The panelling was also examined in the laboratory for corrosion. Analyses using scanning electron microscopy show that the surface was partially covered with corrosion and exhibited corrosive damage (see figure 69). Metallographically, corrosion spots can be detected in some areas on the surface of the plating, underneath the coat of paint (see figure 70).

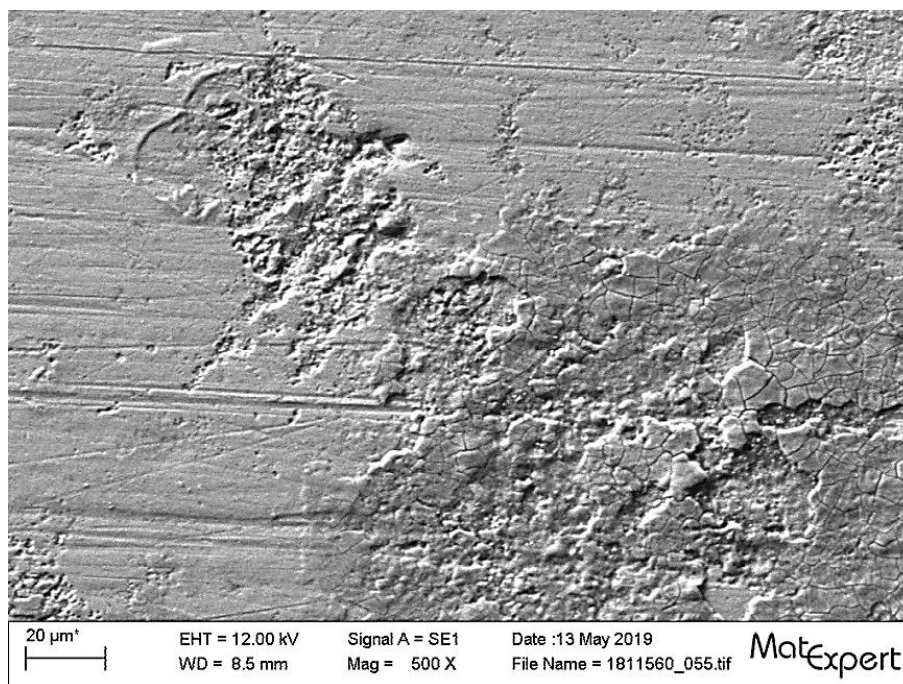


Figure 69: Outer surface with corrosion and corrosive damage.

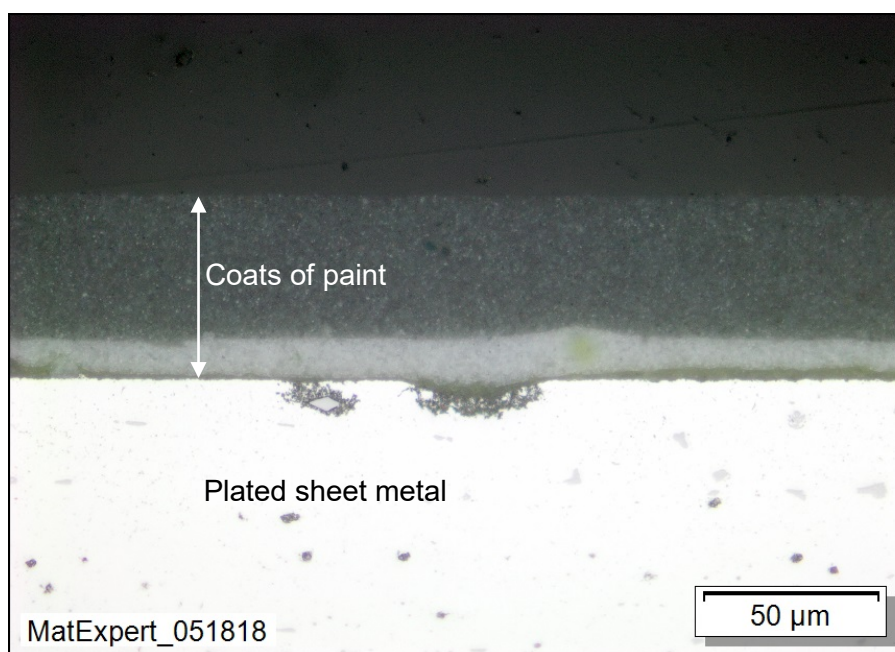


Figure 70: Microsection of corroded plated sheet metal under the layers of paint.

A1.16.4.5 Engine components

A1.16.4.5.1 Cylinder bores

Visual assessment revealed discolouration to the bore of several cylinders (see figure 71). Cylinder 1 from the right engine exhibited this discolouration and was subsequently examined in the laboratory for corrosion damage. This cylinder had been sourced from an engine that was recovered from wreckage located on a glacier. The coating to the bore of this cylinder consists of two different materials that were thermally sprayed onto the cylinder wall, which had been abraded by previous blasting (see section A1.16.3.4.1 and figure 72). Laboratory tests revealed that the top coating was open-pored and corroded in part.

This corrosion was identified as rust, which explains the red discolouration of the bore. The cause of the bond coat's detachment from the cylinder barrel (see figure 72) is indication of pre-existing corrosion damage.

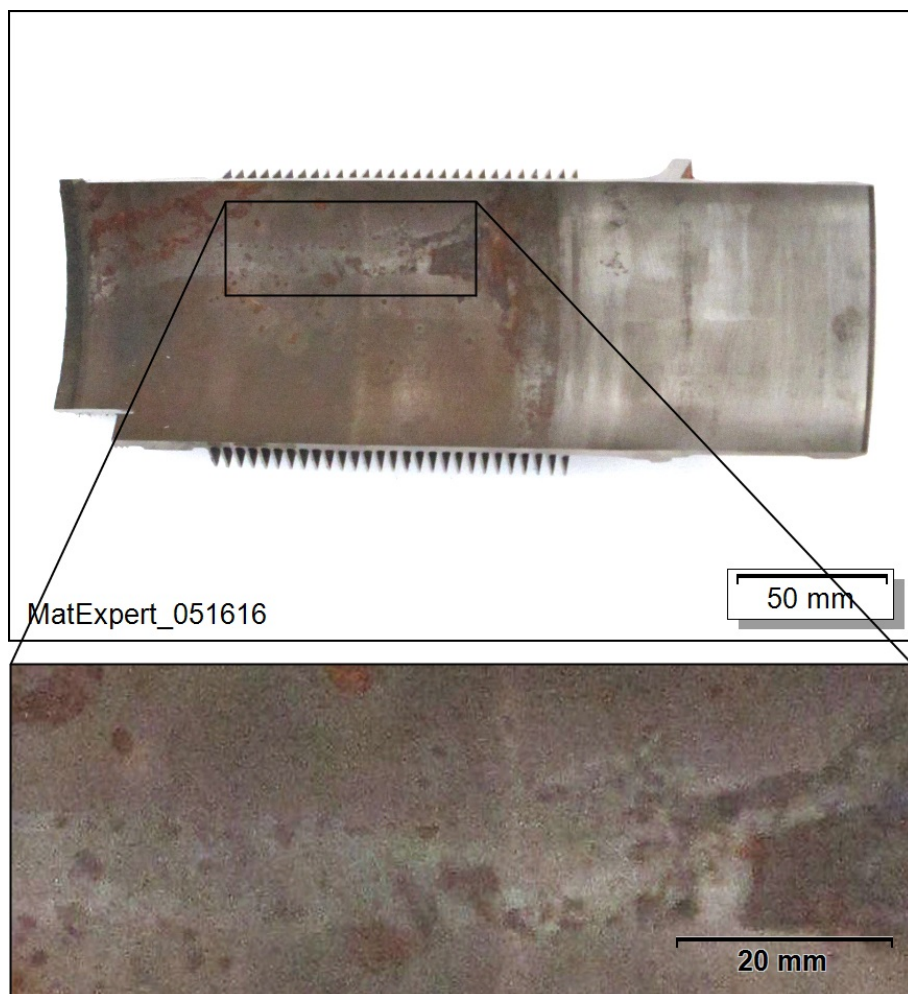


Figure 71: Right engine, bore of cylinder 1 – rusty surface.

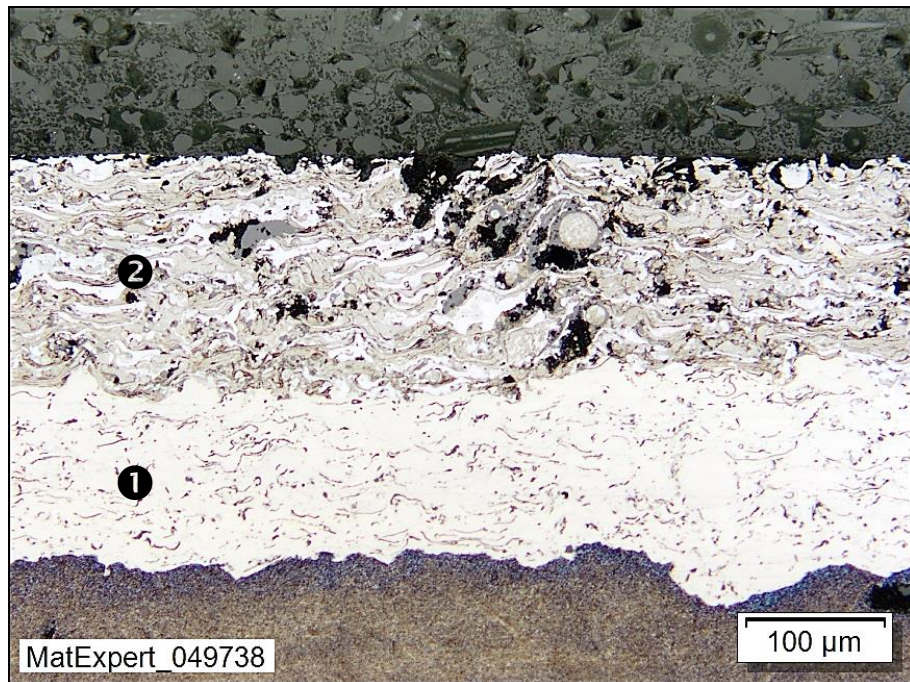


Figure 72: Close-up of the bore of cylinder 1 with two-layer thermal spray coating. Number (1) is the bond coat. Number (2) is the top coat, which is partially open-pored.

A1.16.4.5.2 Propeller bearings

The three propeller bearings were subjected to corrosion tests in the laboratory. For this purpose, the bearings were cut in half and the individual bearing components were analysed. All three bearings exhibited tribological and corrosive damage (see figures 73 to 75). As the corrosive damage to the bearing tracks and surfaces on the inner race fitting the shaft as well as on the outer race fitting the housing was found to have already existed for a long time prior to the accident, it has to be assumed that the corrosive damage caused the tribological damage to the bearings.

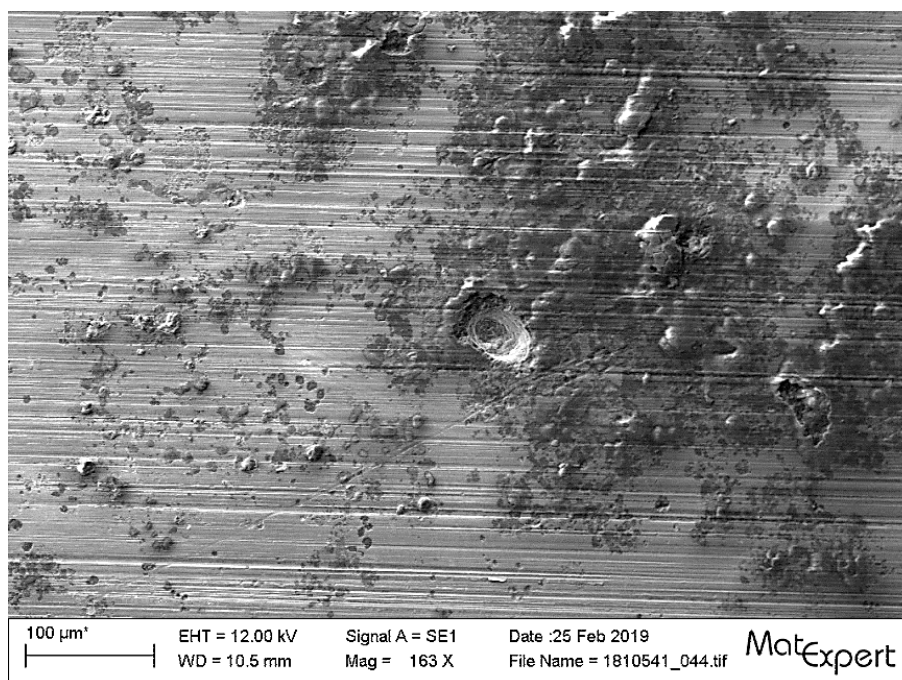


Figure 73: Ball bearing from the left engine, inner-race bearing track – corrosion.

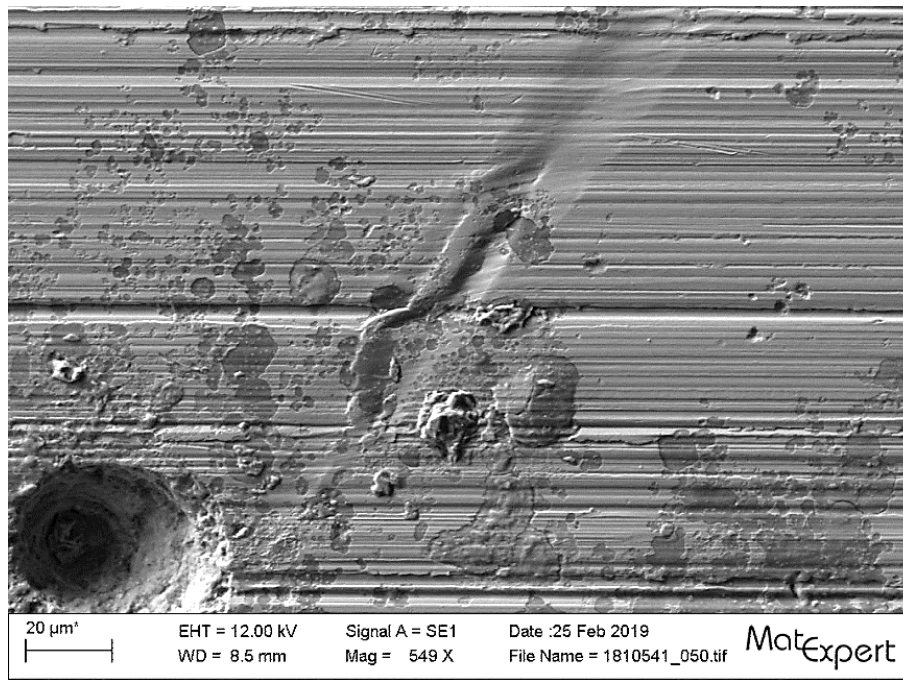


Figure 74: Ball bearing from the left engine, inner-race bearing track – pitting and indentation.

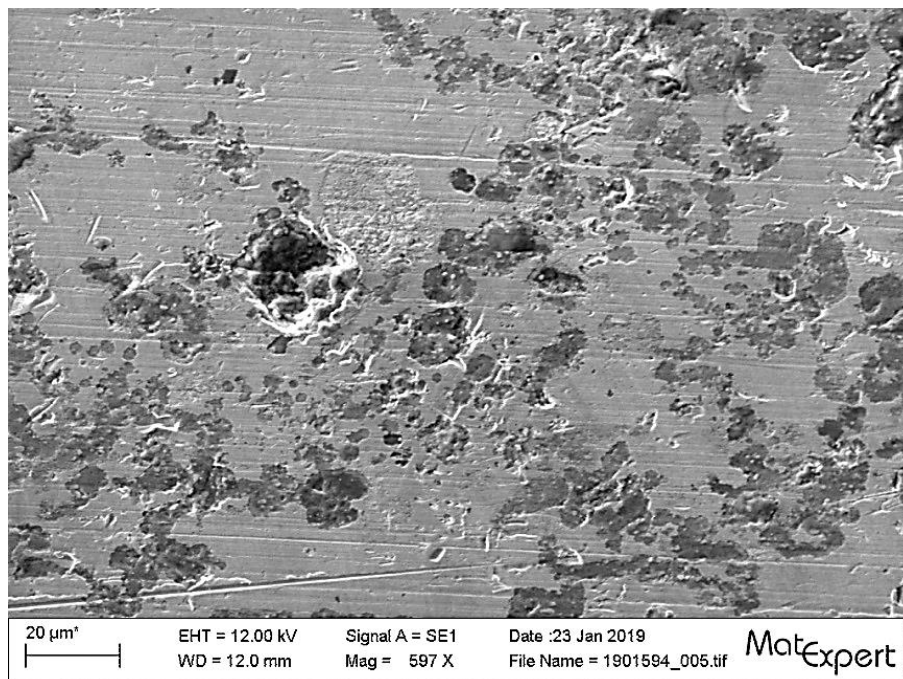


Figure 75: Ball bearing from the centre engine, inner-race bearing track – corrosion.

A1.16.4.5.3 Supercharger bearings

The corrosion tests in the laboratory for supercharger bearing nos 3, 4 and 5 (see annex [A1.12](#)) of the high-speed supercharger shaft from the left engine revealed the following results:

All three bearings were corroded. This corrosion was found on the end faces, the surfaces where the bearings were fitted as well as on the bearing tracks of the inner and outer races and the rolling elements (see figures 76 to 83).

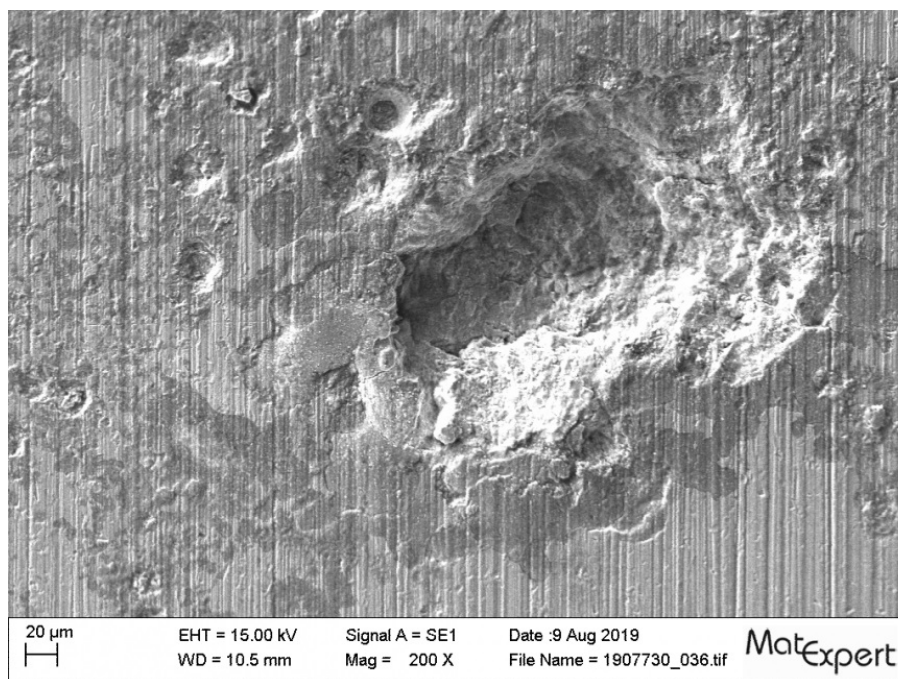


Figure 76: Bearing no. 3, outer-race bearing track – pitting.

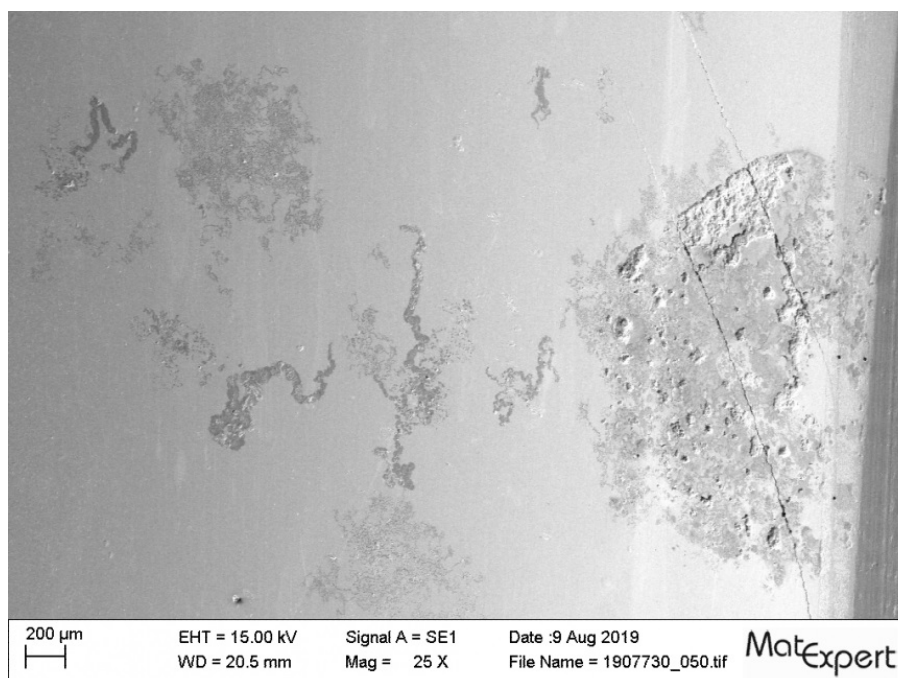


Figure 77: Bearing no. 4, outer-race bearing track – filiform corrosion and pitting with cracks.

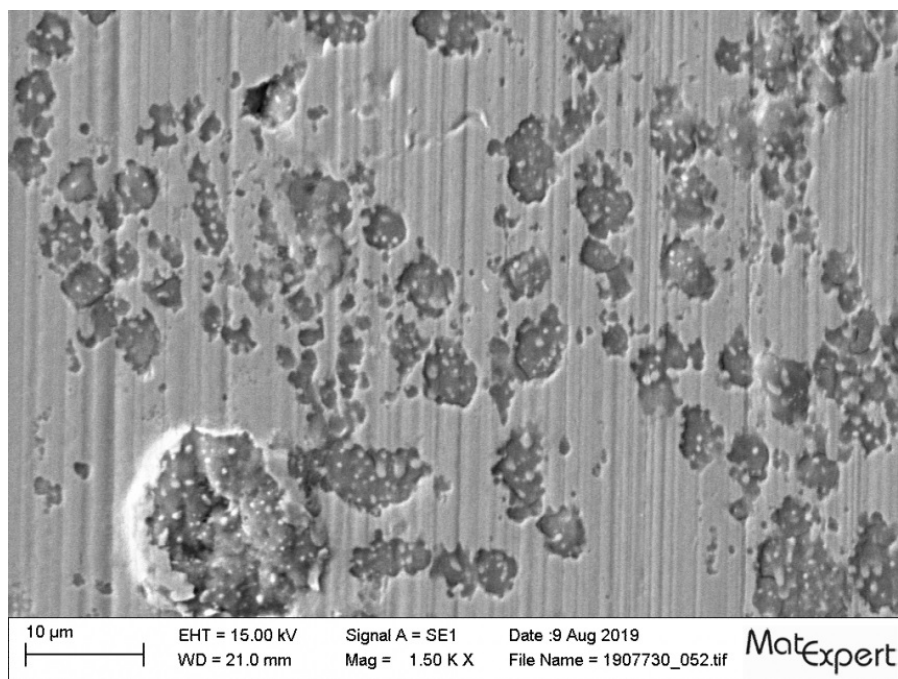


Figure 78: Close-up of figure 77.

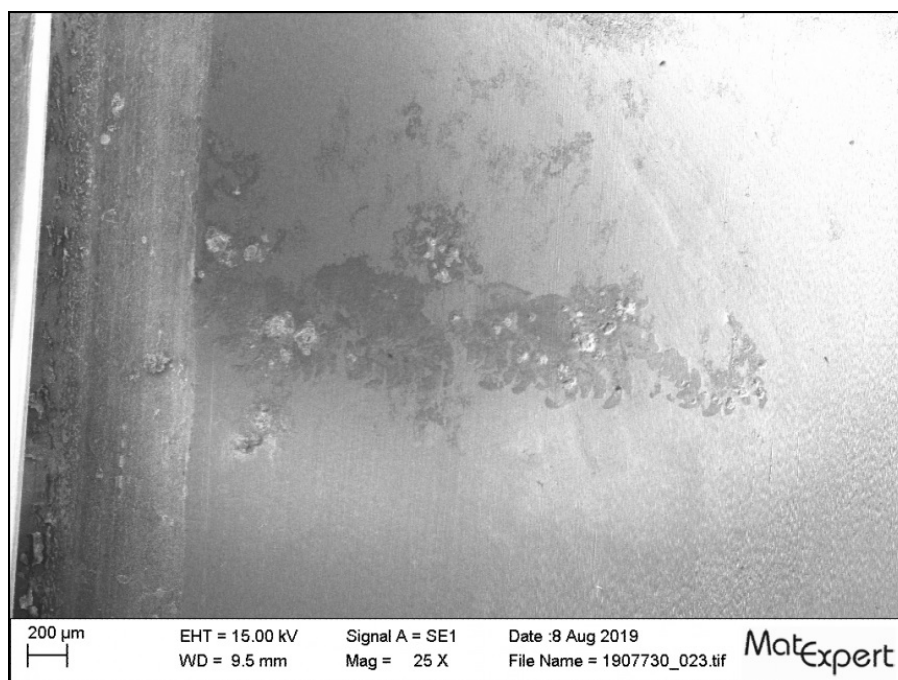


Figure 79: Bearing no. 3, inner-race bearing track – pitting and filiform corrosion.

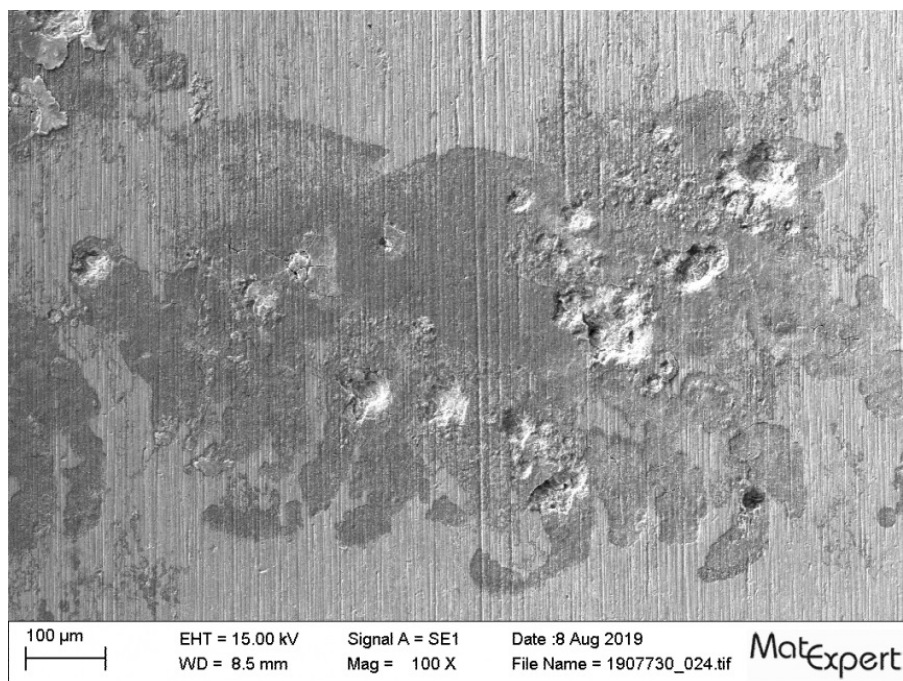


Figure 80: Close-up of figure 79.

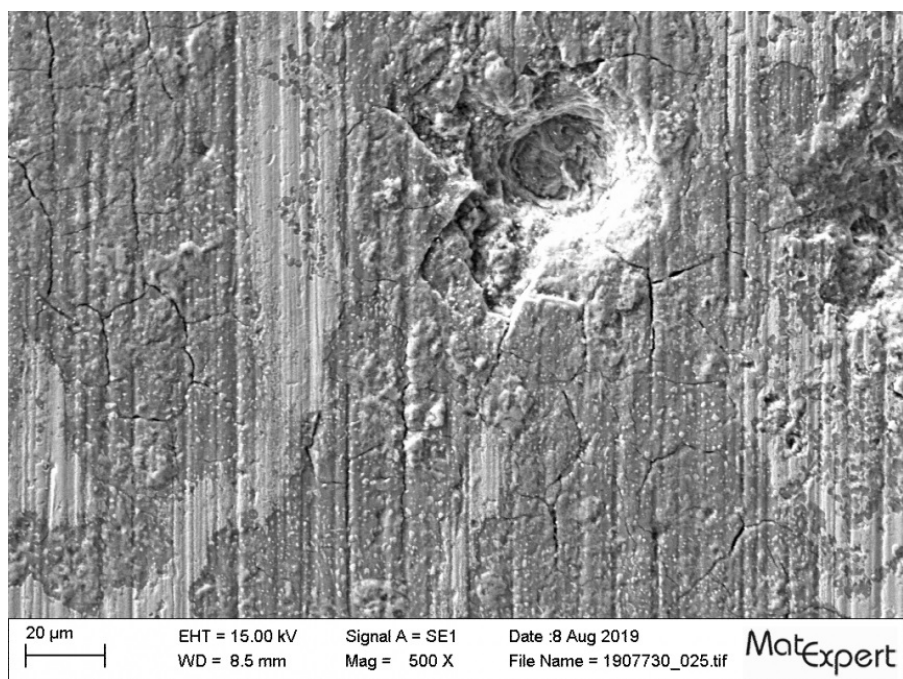


Figure 81: Close-up of figure 80 – stress cracks in the corrosion.

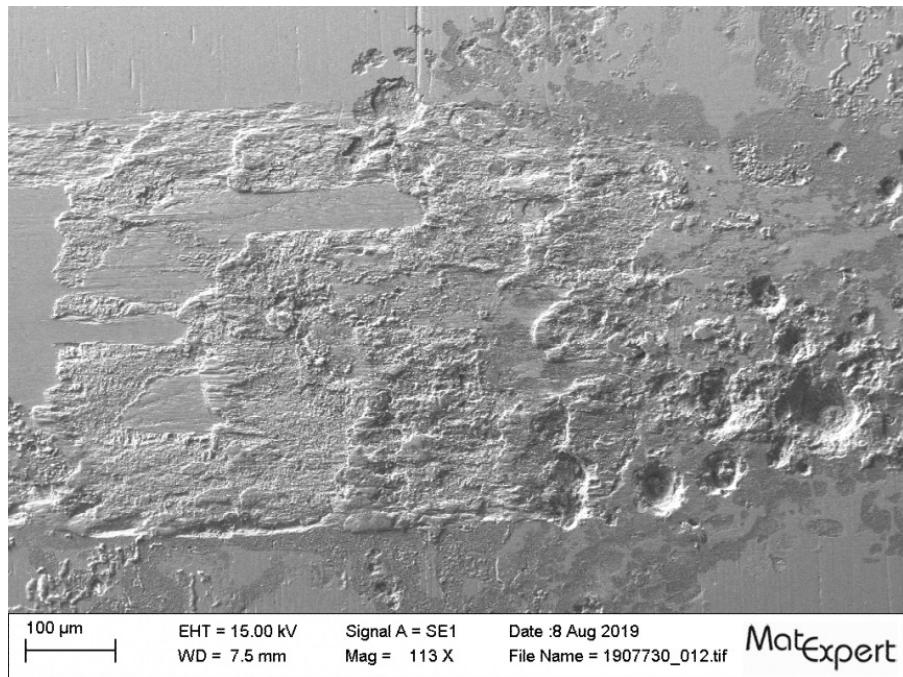


Figure 82: Bearing no. 3, cylindrical roller – pitting and corrosion.

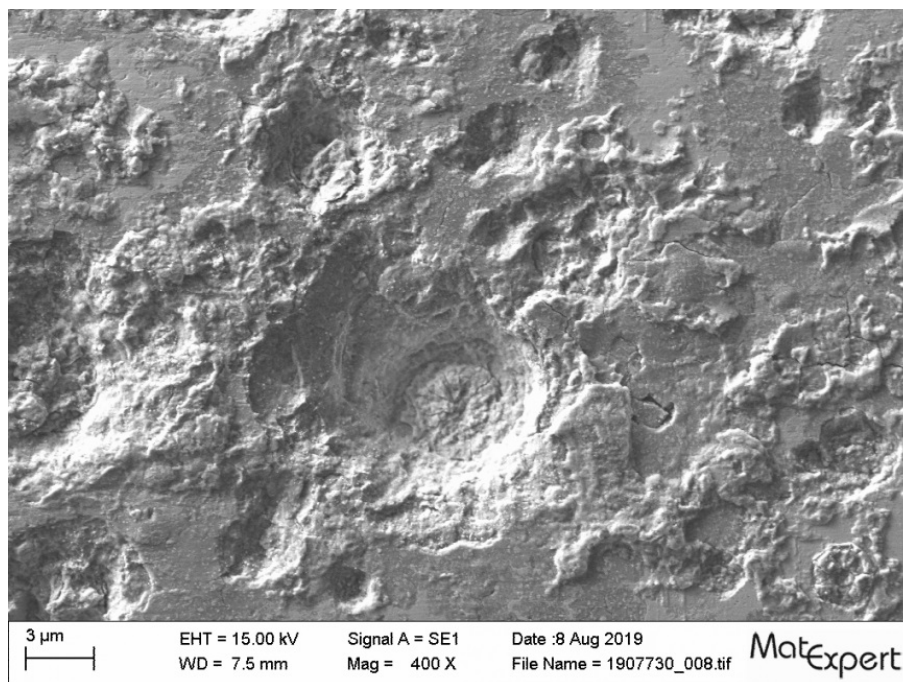


Figure 83: Close-up of figure 82.

Filiform corrosion and pitting were found on the bearing tracks and rolling elements. Flat-rolled corrosion was found on the bearing tracks. The corrosion mainly consisted of iron oxide and iron hydroxide. It was not possible to establish the cause of the corrosion, or rather the substance that caused it. However, in some places it was clearly evident that the corrosion spots were older and had been rolled over during operation.

In summary, the examinations revealed that all three bearings and their components were technically and functionally defective. Corrosion negatively affects the running behaviour and service life of rolling bearings.

A1.16.5 Forensic examinations

A1.16.5.1 Instruments

All instruments and indicator lights from the cockpit found after the accident were severely damaged. In some instances, only the dials remained. The instruments, warning lights and components of the engine control system that were able to help clarify the cause of the accident were examined by the Zurich Forensic Science Institute (FOR).

A1.16.5.1.1 Tachometers

All three tachometers were found as one unit. The lenses and the needles of the three instruments were no longer present. The instrument dials were removed and examined for needle markings (see figure 84).




Tachometer left engine	Tachometer centre engine	Tachometer right engine
		
<p>The needle's impact mark was located in the approximate range of 1,900 rpm. Further markings were found between 1,800 and 1,900 rpm.</p>	<p>The needle's impact mark was located in the approximate range of 1,800 rpm.</p>	<p>The needle's impact mark was located in the approximate range of 1,850 rpm.</p>

Figure 84: Tachometers for all three engines.

A1.16.5.1.2 Speed indicators

Of the two speed indicators, only the instrument dials, without needles, could be found. The two dials were examined for needle markings.

Dial 1:

The needle left scratch marks in the range of 200 km/h (see figure 85). The needle's counterweight left a notch above the letter 'k' of the km/h notation. The positioning of a comparable needle in line with the detected marks showed that the instrument needle should have indicated a value of approximately 202 km/h at the point of impact.



Figure 85: Speed indicator dial.

Dial 2:

Due to the numerous notch, grinding and abrasion marks that were found at various points on the dial and which were probably caused by parts of the instrument needle, it was not possible to come to a conclusion as to the instrument's actual indication at the time of the impact.

A1.16.5.1.3 Further examination of instruments

The display values at the time of the impact ascertained through further examination can be seen in table 1.

Examined instruments	Approximate indication
Fuel pressure indicator, left engine	4 psi
Fuel pressure indicator, centre engine	3.2 psi
Fuel pressure indicator, right engine	3.5 psi
Oil pressure indicator, left engine	85 psi
Oil pressure indicator, centre engine	80 psi
Oil pressure indicator, right engine	87 psi
Oil temp. input, left engine	65 °C
Oil temp. input, centre engine	indeterminable
Oil temp. input, right engine	65 °C
Oil temp. output, left engine	75 °C
Oil temp. output, centre engine	50 °C
Oil temp. output, right engine	85 °C
Voltmeter battery voltage	19–20 V

Table 1: Determined display values of the instruments examined.

A1.16.5.2 Warning lights

The cockpit was fitted with an 'oil low pressure' warning light for each engine. The forensic examination revealed that none of the three warning lights were lit at the time of the accident.

A1.16.5.3 Fuel valve battery

Forensic examination of the fuel valve battery revealed that, at the time of the accident, the fuel supply from the left- and right-hand fuel cells to the respective engines was selected.

A1.16.5.4 Engine control elements

A1.16.5.4.1 Full-throttle limiting mechanism

The control panel for main and high-altitude throttle regulation was severely damaged. The main throttle levers were deformed (see figure 86).



Figure 86: Deformed main throttle levers.

The three circled marks are located in the area where the limit stop bolts touch the front of the main throttle levers when in the 'on' position (see figure 87). Circled in red is the mark on the main throttle lever for the left engine, which was generated by the corresponding limit stop bolt (see figure 88). The direction of movement for the applied force is clearly visible in the image of the curved indentation, or notch.

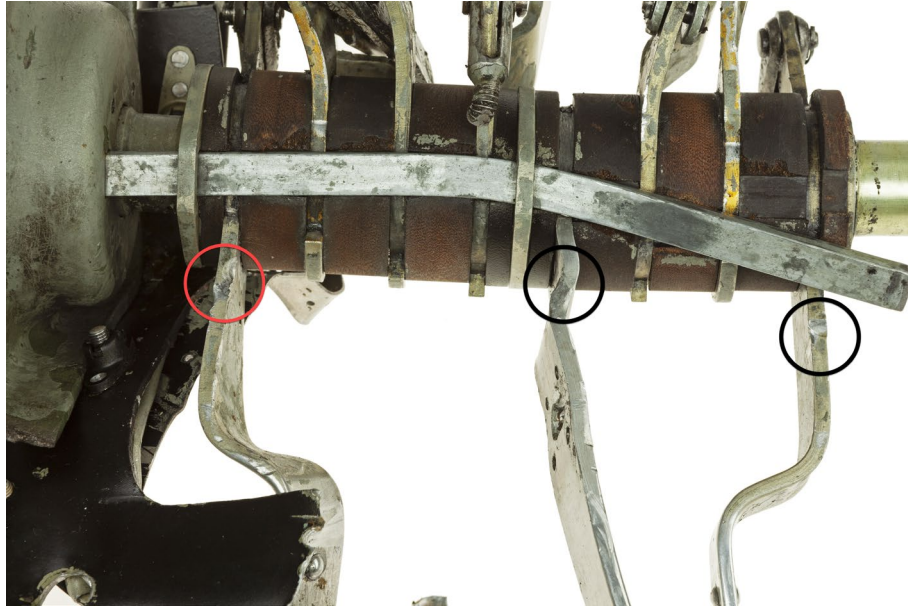


Figure 87: Front of the three main throttle levers with circled marks.

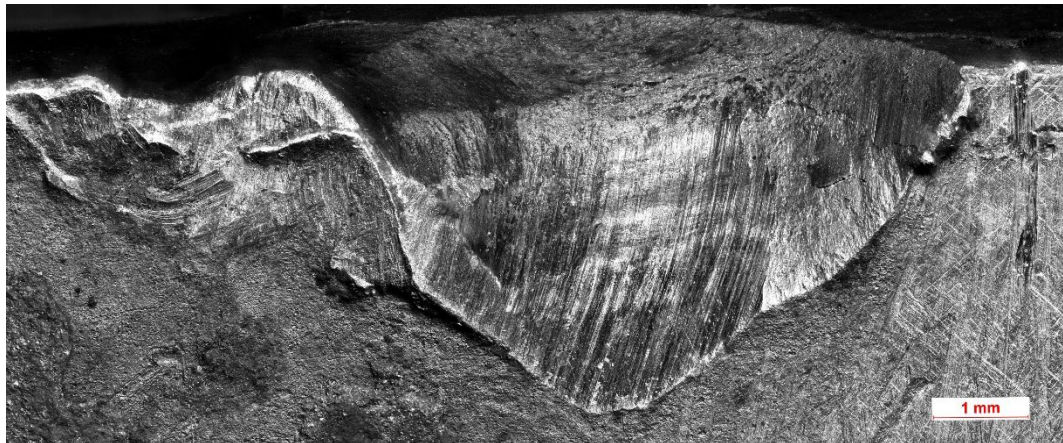


Figure 88: Notch mark on the main throttle lever for the left engine.

A fragment of the full-throttle limiting mechanism was found in the wreckage (see figure 89). On the limit stop bolt for the left engine, damage was found on 13 turns of the thread (see figure 90).

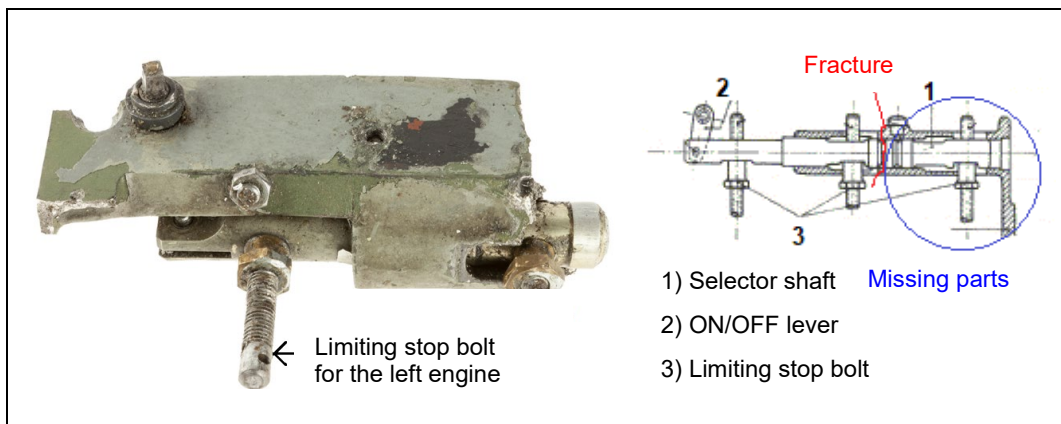


Figure 89: Fragment of the full-throttle limiting mechanism with limiting stop bolt for the left engine.

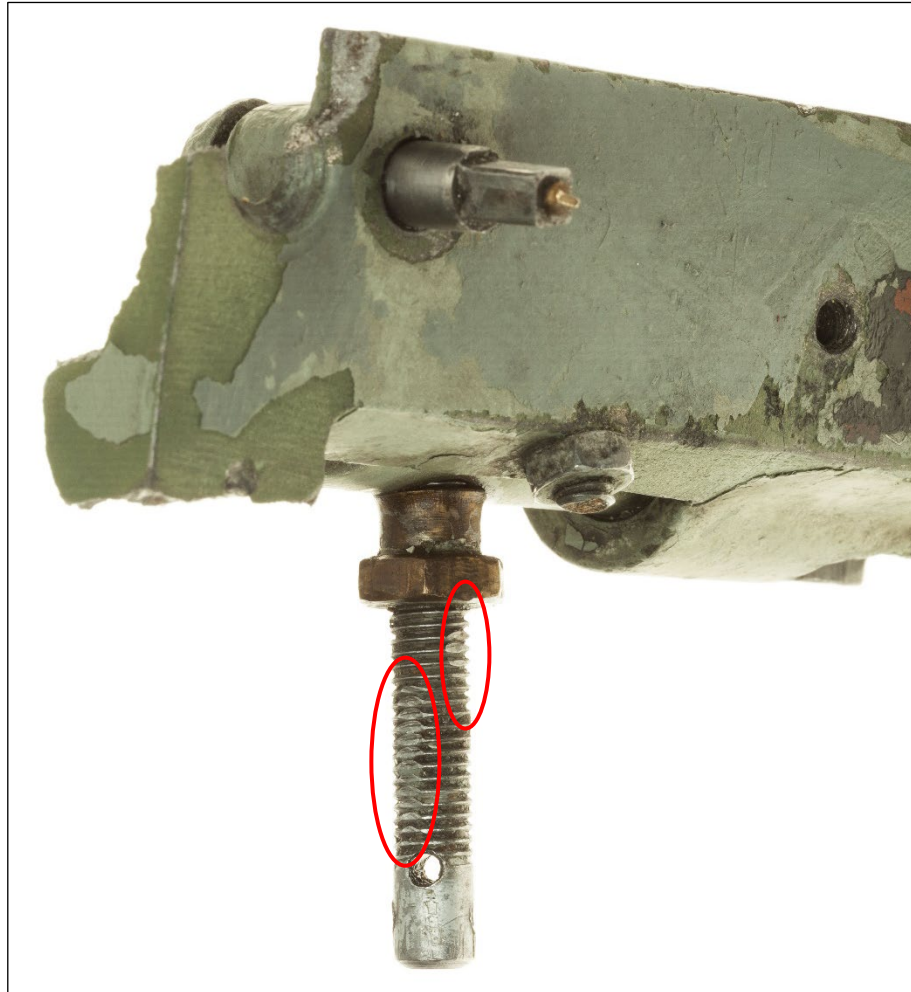


Figure 90: Limiting stop bolt for the left engine with damaged thread.

A1.16.5.4.2 Summary

These marks on the front of the main throttle levers and the damage on the thread of the limit stop bolt for the left engine could only have happened if the full-throttle limit had been set to 'on' at the time of the impact.

A1.16.5.5 Carburettors

The carburettors exhibited varying degrees of damage. With the carburettors for the left and the centre engines, the flange above the two butterfly valves was broken off (see figure 91).

The forensic analyses of the three carburettors focused on the positions of the butterfly valves and accelerator pumps at the time of the impact. The butterfly spindle is connected to the piston stroke rod in the accelerator pump via a linkage, ensuring these two elements move synchronously.

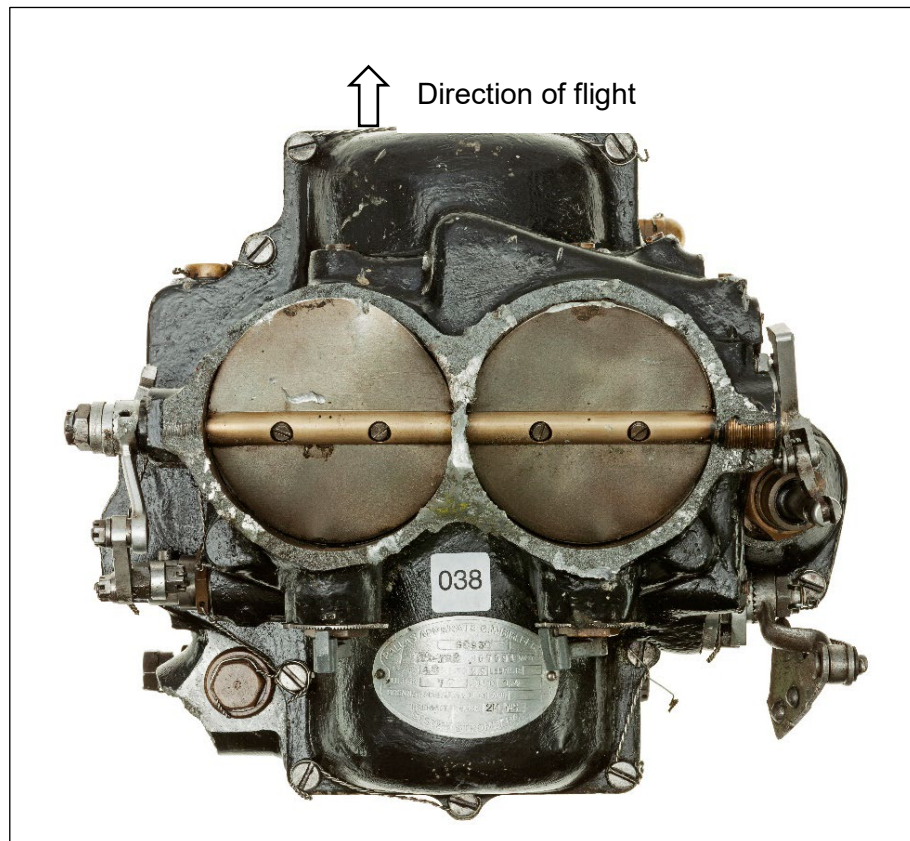


Figure 91: As an example, the carburettor for the centre engine is shown.

A1.16.5.5.1 Butterfly valves

Due to the arrangement of the carburettors on the engines, the butterfly spindles were positioned at 90 degrees to the direction of flight and the subsequent impact. The conditions for using witness marks on the butterfly valves to determine a potential last operating position were therefore unfavourable. In order to use any witness marks in this way, the butterfly valves would have had to have moved laterally in relation to the axial direction of the butterfly spindle and come into contact with the carburettor body.

Based on the lack of witness marks in the bores, it was not possible to determine exactly what position the butterfly valves were in at the time of the impact or immediately before it.

A1.16.5.5.2 Carburettor accelerator pumps

The accelerator-pump piston (see figure 92) is located at the top of the pump cylinder when the engine is idling. As the butterfly valve opens, the piston is pushed down by a connecting rod linked to a bell crank until it is at the bottom of the pump cylinder when the butterfly valve is fully open. As a result, the butterfly valve and the accelerator-pump piston run synchronously.

The maximum stroke for the piston in the pump cylinder is about 24 mm.



Figure 92: Accelerator-pump piston and pump cylinder.

A1.16.5.5.3 Accelerator-pump cylinder

The cylinders in the accelerator pumps were sectioned to allow the bores to be examined under a stereomicroscope. Abrasions that cannot be attributed to conventional wear caused by the piston movements during normal operation were visible on all of the bores (see figures 93 to 95). These abrasions do not run axially in a straight line, but are slightly curved or jagged.

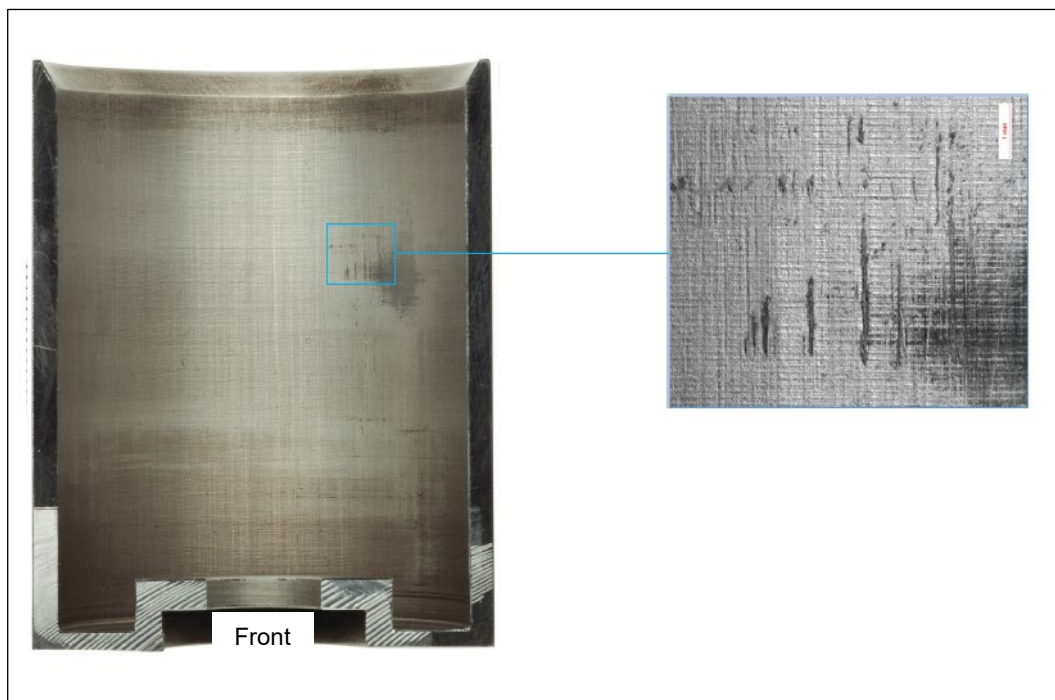


Figure 93: Abrasions in the pump cylinder from the carburettor for the left engine.



Figure 94: Abrasions in the pump cylinder from the carburettor for the centre engine.

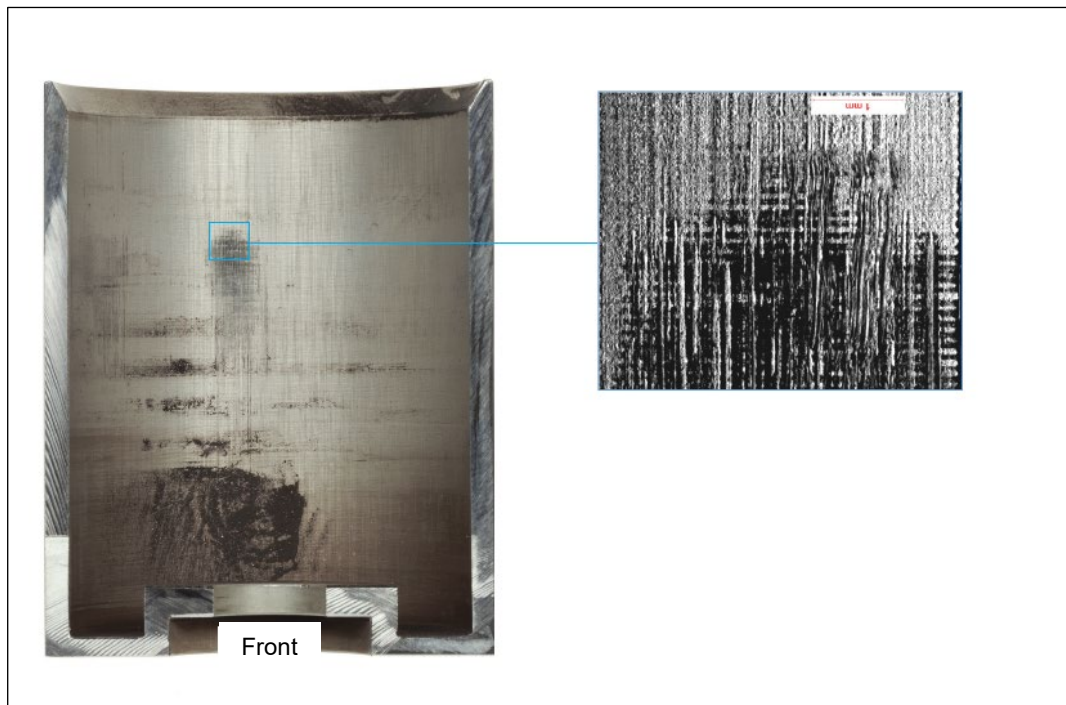


Figure 95: Abrasions in the pump cylinder from the carburettor for the right engine.

A1.16.5.5.4 Accelerator-pump piston

All three pistons were inspected for damage and other abnormalities under the stereomicroscope. This revealed that the chamfer at the lower end of the piston (see red arrow in figure 96) was not damaged on any of the pistons. However, all of the pistons exhibited signs of wear and abrasions on the chamfer where the upper end of the piston skirt (green arrow) transitions into the sealing ring. These abrasions can be plausibly attributed to the corresponding curved and jagged abrasions on the pump cylinder bores.

Below is an example of the marks on the accelerator-pump piston from the carburettor for the centre engine.



Figure 96: Accelerator-pump piston from the carburettor for the centre engine.

A1.16.5.5.5 Evaluation

A change in the throttle position during impact cannot be ruled out. As in this carburettor the butterfly spindle and the accelerator pump move synchronously due to levered connections, the position of the piston in the accelerator pump's cylinder could have changed immediately before the marks were made.

Due to this uncertainty, it is not possible to definitively reconstruct the butterfly valve positions.

A1.16.6 Summarised evaluation

A1.16.6.1 Material properties

A1.16.6.1.1 General

The Ju 52/3m g4e aircraft is a low-wing monoplane with an all-metal construction. Duralumin is the primary material used, important connecting pieces such as joints etc. are made of steel. The different metals were combined with each other and assembled into a structure using rivets made of Duralumin or steel. Corrugated panelling made of Duralumin was riveted to the airframe.

A1.16.6.1.2 Properties of Duralumin and corrosion protection

Duralumin is an alloy of aluminium with copper and magnesium that is high in strength and features good plastic elongation values. The favourable mechanical properties are achieved by thermal after-treatment and subsequent natural ageing.

The corrosion resistance properties of Duralumin are generally limited. It can be surmised that prolonged exposure to temperatures above 80 °C can make Duralumin more prone to corrosion. Thermal stress above 120 °C drastically increases the material's susceptibility to corrosion; this is referred to as a thermal ageing process. The corrosion penetrates the material along grain boundaries, which drastically reduces the strength of the material. Corrosion attack is intensified when the alloy is in contact with another metal, such as steel. The corrosion of the aluminium is difficult if not impossible to detect from the outside.

The aircraft manufacturer was aware that Duralumin is a very sensitive material in terms of its susceptibility to corrosion. For this reason, the manufacturer's instructions repeatedly refer to and stress the importance of intact corrosion protection (see section A1.16.4.2) and that after partial or major overhauls, the condition of the corrosion protection is to be as close to factory-new as possible. However, these instructions were not implemented by Ju-Air in their aircraft maintenance programme (AMP). Furthermore, a corrosion protection programme – as had been requested by FOCA – was not drawn up (see annex [A1.6](#)). Examination showed that the majority of the corrosion protection layer on the inside of the aircraft structure was no longer intact and corrosion was detected in many places.

For the above reasons, components made of Duralumin and parts in contact with Duralumin must therefore be provided with surface protection, such as a coat of paint. Intact surface protection effectively prevents corrosion from penetrating the Duralumin along grain boundaries and destroying the material.

Aluminium sheet can be effectively protected against corrosion using coats of paint and through plating. If there is a risk of contact corrosion, both of the parts in contact with each other must also be galvanically separated by using corrosion-prohibiting paint.

Scientific studies on the ageing and fatigue behaviour of Duralumin are scarce.

A1.16.6.2 Aircraft structure

The wing spars made of Duralumin were damaged by intergranular corrosion as well as pitting; the joints made of steel were rusted. The rivets, like the spars, also exhibited evidence of intergranular corrosion. Pitting and surface corrosion was identified in the contact area between the rivets and both the joint and spar tube. Fatigue fractures and intergranular fractures, which clearly occurred before the accident, were detected in the rivets and other structural parts.

The analysis of a spar fracture originally concealed by a joint showed a ductile spontaneous fracture and a fatigue fracture with typical striations. Extensive corrosion damage and further cracks were uncovered in the contact area between the joint and the spar tube. This corrosion was intergranular, resulting in a loss of wall thickness. One crack was an intergranular fracture with striations, i.e. a fatigue crack.

Cracks caused by intergranular corrosion were found mainly in the contact area between two layers of sheet metal and in the contact areas between the spar tubes made of Duralumin and the riveted-on steel joints as well as surrounding the rivets for fastening the panelling. Incipient cracks were found originating from the rivet holes in the spar tubes.

Intergranular cracks give rise to the notch effect and provide the ideal conditions for the initiation of fatigue cracks. This creates the risk of total failure of a component.

Corrosion damage and cracks running along the grain boundaries on important structural parts, such as the wing spars, the engine mounts and the fuselage spars could only be detected under the microscope or using SEM after dismantling the assemblies into their individual parts.

A1.16.6.3 Engines

In the examined cylinders that exhibited a net-like distribution of cracks, the bores were chrome-plated. This chrome plating is extremely hard, had cracks across the surface and exhibited peeling. The debris resulting from this peeling can find its way into the lubricating oil and cause serious damage to other engine parts, such as the bearings.

The examined cylinder with a red-discoloured bore had thermally sprayed-on bond and top coats. In places the top coat was open-pored, corroded and cracked or no longer bound to the underlying bond coat. This bore the risk that parts of the sprayed-on coatings could detach from the cylinder bore, which could have led to serious engine damage. The reconditioning of the cylinder walls according to this procedure was not covered by SB no. 1003.

The examined cylinders were honed to a diameter of 156.44 mm before coating. According to the 1939 operating instructions written by the manufacturer of the BMW 132 A3 aircraft engine, the cylinder is only permitted to be honed to a diameter of 155.90 mm. Unduly honing the cylinders to a diameter that is greater than stipulated by the manufacturer weakens the wall thickness of the cylinder barrel, creating a risk of engine failure.